

**NONCOHERENT MULTICARRIER  
COMMUNICATIONS AND MULTIUSER  
DETECTION**

**BY RAJNISH SINHA**

**A dissertation submitted to the  
Graduate School—New Brunswick  
Rutgers, The State University of New Jersey  
in partial fulfillment of the requirements  
for the degree of  
Doctor of Philosophy  
Graduate Program in Electrical and Computer Engineering**

**Written under the direction of**

**Professor Roy D. Yates**

**and approved by**

---

---

---

---

---

**New Brunswick, New Jersey**

**October, 2003**

© 2003

**Rajnish Sinha**

**ALL RIGHTS RESERVED**

## **ABSTRACT OF THE DISSERTATION**

# **Noncoherent Multicarrier Communications and Multiuser Detection**

**by Rajnish Sinha**

**Dissertation Director: Professor Roy D. Yates**

The Internet revolution has created the need for wireless technologies that can deliver data at high speeds in a spectrally efficient manner. However, supporting such high data rates with sufficient robustness to radio channel impairments requires careful selection of modulation techniques. Currently, the most suitable choice appears to be OFDM (Orthogonal Frequency Division Multiplexing). OFDM is currently being used in Europe for digital audio and video broadcasting. In the U.S., OFDM is being used by wireless LANs operating in the unlicensed bands and is also being considered as a serious candidate for fourth generation cellular systems.

In order to serve multiple users simultaneously, an OFDM based system would require a multiple access technology. One such access scheme called MC-MFSK (Multicarrier Multilevel Frequency Shift Keying) is proposed in this thesis. The MC-MFSK scheme is a new spread-spectrum, multiple-access scheme and it shares some of the advantages of both FH (Frequency-Hopping) and DS (Direct-Sequence) spread-spectrum systems,

while overcoming some of their disadvantages. The MC-MFSK scheme transmits a symbol in parallel over multiple sub-channels using OFDM and has the desirable properties of frequency diversity, near-far resistance, and multipath immunity. This thesis contends that the above benefits not only make MC-MFSK a simple yet competitive spread-spectrum technology but also make it a strong candidate for future high-speed wireless systems.

Systems operating in the unlicensed bands can experience rapidly changing, uncontrolled interference from other co-located systems. This rapid variation of the channel can make phase estimation, and hence coherent detection, extremely difficult if not impossible. Instead, noncoherent detection schemes may be more feasible in such scenarios. Since the proposed MC-MFSK scheme uses noncoherent detection, it can be an attractive alternative for the unlicensed bands as well.

This thesis also investigates the general area of noncoherent multiuser detection. Multiuser detectors are useful in jointly demodulating a superposition of signals received from different sources to yield improved performance. This thesis investigates noncoherent multiuser detection techniques that achieve near optimum performance while retaining reasonable complexity. A technique called *selective* filtering is proposed which exploits certain a priori information regarding a user's transmitted signal. It is shown that selective filtering offers improved performance over the noncoherent counterparts of the existing near-optimum multiuser detectors. Both deterministic as well as blind adaptive implementations of selective filtering are considered. Numerical comparisons are provided to demonstrate the near-optimum performance of the proposed detectors.

## Acknowledgements

I would like to thank my advisor Prof. Roy Yates for his invaluable advice, patience, and support during the work on this thesis. It has been a pleasure as well as a privilege to have had the opportunity to work with him.

I would like to thank my committee members Prof. David G. Daut, Prof. Christopher Rose, Prof. Narayan Mandayam, and Prof. Aylin Yener for providing valuable feedback on the thesis.

I would especially like to thank Prof. Aylin Yener for providing invaluable suggestions as a collaborator on the Multiuser Detection part of the thesis. I am also indebted to her for taking time out from her busy schedule at Pennsylvania State University and driving all the way to Rutgers to serve as an external member on my defense committee.

I would like to thank Prof. David Goodman of Brooklyn Polytechnic University and Prof. Jack Holtzman of Qualcomm Inc. for providing me with the opportunity to be a member of WINLAB back in 1992 when I was an undergraduate student. Their advice and support over the years has truly helped shape my career in wireless communications for the better.

Over the years at WINLAB, I have had the privilege of interacting with visitors and students from all over the world. I would like to thank all of them for the wonderful company they have provided me with. In particular, I would like to thank my friends Darshan Sonecha and Mark Wehle for their friendship and support over all these years.

I would also like to thank the staff at WINLAB, namely, Philomena Genatempo, Melissa

Gelfman, Noreen DeCarlo, Jeanne Sullivan, Ivan Seskar and Kevin Wine for their untiring efforts in making WINLAB the special place it is. I would also like to thank the graduate program secretary Barbara Klimkiewicz and the business manager Lynn Ruggiero for their support and assistance in both personal as well as administrative matters.

As the last few years of my thesis overlapped with a full-time job at Lucent Technologies, it was extremely challenging to manage both. This thesis would not have reached completion without the patience, understanding, and support of my supervisor Neil Bernstein, my mentor Mathew Thomas, and my colleague Arvind Mistry at Lucent Technologies. I would also like to thank my office mate Ashok Tikku for the many fruitful discussions we have had on topics related to my thesis.

I would like to thank my family members for providing encouragement and support during work on this thesis. I would like to thank my parents for the sacrifices they have made and for the inspiration and support they have provided throughout my life. Had they not instilled in me the value of higher education, I would not be writing this thesis today. Finally, I would like to thank my wife Shweta, without whose patience, understanding, support, and countless sacrifices, I would not have been able to venture this far.

# **Dedication**

To my teachers, family, and friends ...

# Table of Contents

<b>Abstract</b> . . . . .	ii
<b>Acknowledgements</b> . . . . .	iv
<b>Dedication</b> . . . . .	vi
<b>List of Tables</b> . . . . .	xi
<b>List of Figures</b> . . . . .	xii
<b>1. Introduction</b> . . . . .	1
1.1. Related Work . . . . .	8
1.1.1. MFSK Spread-Spectrum Multiple-Access Systems . . . . .	8
1.1.2. Noncoherent Multiuser Detection . . . . .	13
1.2. Thesis Overview . . . . .	15
1.3. New Results . . . . .	18
<b>2. Multicarrier MFSK: A Spread Spectrum Multiple Access Scheme for OFDM-based Systems</b> . . . . .	20
2.1. Introduction . . . . .	20
2.2. System Model . . . . .	21

2.3.	Review of FH Multilevel-FSK . . . . .	23
2.4.	MC-MFSK Decoder . . . . .	24
2.4.1.	Probability of Word Error . . . . .	26
2.5.	Performance in Rayleigh Fading Channels . . . . .	34
2.5.1.	Optimum Combining . . . . .	36
2.5.2.	Special Case of a Single User in a Rayleigh Fading Channel . . . . .	38
2.5.3.	Special Case of a Single User in an AWGN Channel . . . . .	39
2.6.	Selection of Detection Threshold . . . . .	40
2.6.1.	Threshold Selection for Soft Limiter . . . . .	41
2.6.2.	Threshold Selection for an Envelope Detector . . . . .	44
2.7.	Capacity of MC-MFSK and Comparison with FH-MFSK Systems . . . . .	49
2.8.	Near-Far Resistance of the MC-MFSK System . . . . .	53
2.9.	Chapter Summary . . . . .	54
<b>3.</b>	<b>Noncoherent Multiuser Communications: Multistage Detection and Selective Filtering . . . . .</b>	<b>56</b>
3.1.	Introduction . . . . .	56
3.2.	System Model and Optimal Detection . . . . .	57
3.3.	Non-Selective Detection . . . . .	59
3.3.1.	Prior Work . . . . .	60
3.3.2.	Constrained Noncoherent Multiuser Detection . . . . .	62
3.3.3.	Soft Interference Cancellation . . . . .	64

3.4.	Selective Filtering . . . . .	72
3.4.1.	Selective Decorrelation . . . . .	73
3.4.2.	Selective MMSE Detection . . . . .	74
3.4.3.	Selective Soft-IC . . . . .	78
3.4.4.	Selective Filtering with Successive Interference Suppression . . . . .	79
3.5.	Chapter Summary . . . . .	82
<b>4.</b>	<b>Conclusions . . . . .</b>	<b>85</b>
4.1.	Thesis Summary . . . . .	85
4.1.1.	The MC-MFSK Multiple-Access Scheme for OFDM-based Systems . . . . .	85
4.1.2.	Noncoherent Multiuser Detection . . . . .	86
<b>Appendix A.</b>	<b>. . . . .</b>	<b>88</b>
A.1.	Derivation of $P(\alpha_i = 0)$ . . . . .	88
A.2.	Distribution of $\rho$ . . . . .	90
A.2.1.	Binomial Approximation . . . . .	93
A.3.	Derivation of the Global Constrained Detector . . . . .	93
A.4.	Derivation of the Local Constrained Detector . . . . .	94
A.5.	Serial Soft-IC . . . . .	96
A.6.	Optimum Decision Rule for the Selective Decorrelator . . . . .	97
A.7.	Union Bound for the Selective Decorrelator . . . . .	99

<b>References</b> . . . . .	101
<b>Vita</b> . . . . .	106

## List of Tables

2.1. Simulated capacity and spectral efficiency comparisons of MC-MFSK and FH-MFSK systems in Rayleigh fading for $W/R_b = 128$ . . . . .	52
--	----

## List of Figures

1.1. Basic OFDM transmitter . . . . .	3
1.2. Basic OFDM receiver . . . . .	4
1.3. FH MFSK transmitter . . . . .	8
1.4. Multilevel FSK transmitter . . . . .	10
1.5. MC-MFSK transmitter . . . . .	11
1.6. Comparison of FSK-based transmission schemes . . . . .	12
1.7. An MC-MFSK communication system . . . . .	14
1.8. Noncoherent multiuser detector . . . . .	16
2.1. MC-MFSK transmitter . . . . .	22
2.2. An OFDM based transmitter for MC-MFSK . . . . .	24
2.3. An OFDM based receiver for MC-MFSK . . . . .	24
2.4. Comparison of system capacity obtained from simulations with the lower bound $K_{lb}$ . . . . .	32
2.5. Comparison of simulated $\eta_T$ with lower bound $\eta_T^*$ at $P_w = 10^{-3}$ . . . .	33
2.6. Optimum nonlinearity $G(R)$ for different combinations of total users $K$ and SNR/bit $\gamma_b$ . . . . .	37

2.7. Simulated WER for a single user at low SNRs in different channel conditions at $(L, M) = (20, 1328)$ . . . . .	40
2.8. Simulated WER versus detection threshold for the soft-limiter for $(K, L, M) = (25, 20, 1328)$ at $\gamma_b = 15\text{dB}$ . . . . .	41
2.9. Simulated WER versus average SNR/bit in a Rayleigh fading channel for $(K, L, M) = (25, 20, 1328)$ . . . . .	42
2.10. Simulated WER versus average $\gamma_b$ in a Rayleigh fading channel for a heavily loaded system for $(K, L, M) = (40, 20, 1328)$ . . . . .	43
2.11. Detection threshold $G(1)$ as a function of $\gamma_b$ for different number of total users $K$ . . . . .	44
2.12. PDFs corresponding to hypotheses $H_0$ and $H_1$ . . . . .	46
2.13. Comparison of $P_e$ and $\bar{P}_e$ for $(K, L, M) = (35, 25, 1328)$ . . . . .	47
2.14. Simulated MC-MFSK system capacity versus diversity factor $L$ in a Rayleigh fading channel with a soft-limiter for $M = 1328$ . . . . .	49
2.15. Simulated $K_{max}$ versus diversity factor ( $L$ for MC-MFSK and $\bar{L}$ for FH-MFSK) using envelope detectors for $W/R_b = 128$ and $\gamma_b = \infty$ dB . . .	50
2.16. Simulated $K_{max}$ versus diversity factor ( $L$ for MC-MFSK and $\bar{L}$ for FH-MFSK) in Rayleigh fading channels using envelope detectors for $W/R_b = 128$ and average $\gamma_b = 25\text{dB}$ . . . . .	51
2.17. Performance comparison of the different combiners in a Rayleigh fading channel with 9 equal-powered interferers. Desired user's SNR $\gamma_b = 10\text{dB}$ . . . . .	54
3.1. Comparison of various noncoherent detectors with $(K, M, N) = (2, 4, 20)$	65

3.2. Performance in the near-far scenario with $(K, M, N)=(2, 4, 20)$ . Desired user's SNR= 12dB . . . . .	66
3.3. Serial soft interference canceller (Soft-IC) . . . . .	68
3.4. Parallel soft interference canceller . . . . .	70
3.5. Comparison of soft-ICs in near-far scenario with $(K, M, N)=(2, 4, 20)$ . Desired user's SNR= 14dB . . . . .	72
3.6. Performance comparison of the MM-rule based selective decorrelator, the optimum decision rule, and the union bound . . . . .	75
3.7. Comparison of the convergence rates of the blind adaptive selective and non-selective MMSE filters with $(K, M, N)=(5, 4, 20)$ and variable step-size $\mu$ . . . . .	77
3.8. Comparison of the performance of the blind adaptive selective and non-selective MMSE filters with $(K, M, N)=(5, 4, 20)$ . . . . .	78
3.9. Comparison of selective and non-selective detectors in a lightly loaded system with $(K, M, N) = (2, 4, 20)$ . . . . .	80
3.10. Comparison of selective and non-selective detectors in a fully loaded system with $(K, M, N) = (5, 4, 20)$ . . . . .	81
3.11. Comparison of selective and non-selective detectors with higher processing gain $N = 64$ in a moderately loaded system with $(K, M, N) = (4, 8, 64)$ . . . . .	82
3.12. Comparison of selective and non-selective detectors with higher processing gain $N = 64$ in a fully loaded system with $(K, M, N)=(4, 16, 64)$	83
3.13. Performance of selective decorrelator with SIS with $(K, M, N)=(3, 4, 20)$ and desired user's SNR= 15dB . . . . .	84

A.1. Comparison of simulated value of  $P(\alpha_i = 0)$  with lower bound in (A.6) 89

# Chapter 1

## Introduction

Today, wireless communication has permeated all aspects of life through devices such as cellular phones, 802.11 based Wireless LANs, and Bluetooth, to name a few. Through these devices, users wish to have high-speed access to information anywhere at any-time. The challenge for communications engineers is to try and meet this demand with a constrained budget on system resources such as bandwidth and transmission power.

Two key components of any multiuser communication system are the *physical* and *media access control* (MAC) layers. In wireless communication systems, all the RF related signal processing and the transmission/reception of the actual signal take place at the physical layer. The MAC layer resides on top of the physical layer, and as the name suggests, it is responsible for efficiently controlling the transmissions of multiple users.

The MC-MFSK system proposed in this thesis is intended to serve as a MAC technology for an OFDM-based physical layer. In the following sections, we will discuss the benefits of OFDM and MFSK systems and then show the way in which the MC-MFSK system effectively combines the two.

In wireless systems where a receiver may receive signals from multiple users, multiuser detectors can be employed to jointly process the signals to improve performance. Since this thesis makes contributions in the area of noncoherent multiuser detection, an overview of multiuser detection will also be given in this chapter.

## OFDM Systems

Most wireless communication links are subjected to conditions in which the transmitted signal arrives at the receiver via multiple propagation paths at different delays [1]. The *multipath* phenomena arises in different ways depending upon the application. For example, in cellular radio it arises out of reflection and scattering from buildings, trees and other obstacles along the path. Signal multipath generally results in intersymbol interference (ISI) in digital communication systems. Moreover, the signal components arriving via the multiple propagation paths may add destructively resulting in a phenomenon called *fading*.

Typically, in single-carrier systems, equalizers are used to combat the channel distortion caused due to ISI. However, the complexity of the receiver increases as the span of the ISI increases. In a dispersive channel, to avoid ISI, the root-mean-square *delay spread*  $\sigma_c$  places a limit on the signaling rate  $R$ . A delay spread of  $\sigma_c$  corresponds to a *coherence bandwidth* of  $B_c \approx 1/\sigma_c$ . Thus, it is desired to have  $R < B_c$  in order to reduce susceptibility to ISI. In the time domain, this corresponds to having a signal time-period  $T > \sigma_c$ . Therefore, in a single-carrier system, after transmitting each pulse, the transmitter has to wait for at least  $\sigma_c$  time units before sending the next pulse. A multicarrier or parallel approach, on the other hand, splits the incoming data stream into parallel streams, thereby reducing the rate on each of the branches and making each branch less susceptible to delay spread [2]. Also, the data on each branch is transmitted on mutually orthogonal frequency channels.

OFDM is a physical layer technology that implements the multicarrier modulation scheme. Initially, the implementation of OFDM was prohibitively complex due to the requirement of a bank of analog oscillators [3–5]. However, advances in signal processing have now made it a viable technology, and today, OFDM can be implemented by using IFFT/FFT operations. In OFDM, the frequency channels are allowed

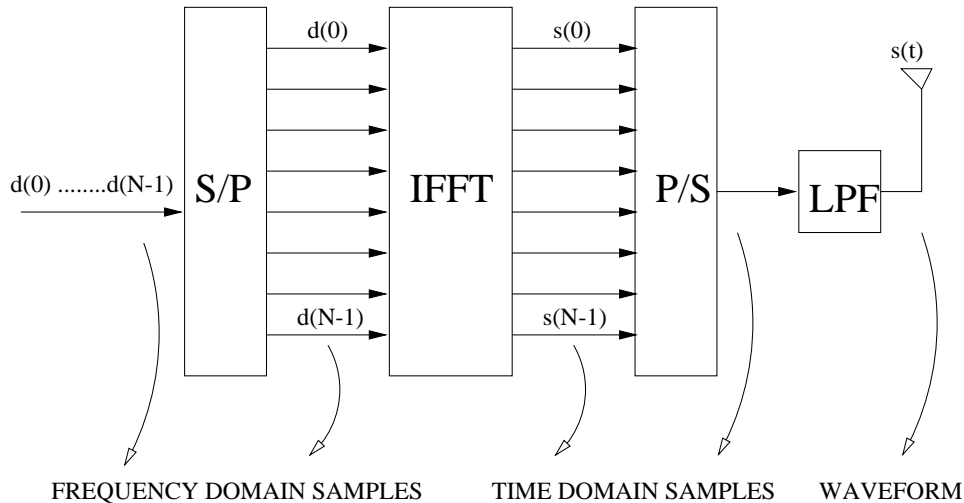


Figure 1.1: Basic OFDM transmitter

to overlap partially while still maintaining orthogonality, which allows for higher *spectral efficiency*. Consequently, in contrast to the majority of wireless technologies in use today, OFDM is capable of providing high data rates on a wireless channel without succumbing to ISI problems.

An OFDM-based transmitter transmits multiple symbols in parallel over a channel as shown in Figure 1.1. For a set of  $N$  samples  $d(0), \dots, d(N-1)$ , the sampled version of the OFDM signal  $s(t)$  can be written as

$$s(m) = \text{Re} \left[ \sum_{n=0}^{N-1} d(n) e^{j \frac{2\pi}{N} nm} \right] \quad m = 0, \dots, N-1. \quad (1.1)$$

Thus, the resulting sequence  $s(m)$  is seen as the real part of the IFFT of the sequence  $d(n)$ . Although (1.1) could have written as an FFT equation, it is more desirable to think of the samples  $d(n)$  as being in the frequency domain. That is why most of the OFDM implementations show an IFFT operation in the transmitter and an FFT in the receiver, as shown in Figure 1.2. In order to serve multiple users efficiently, an OFDM-based system would require a multiple-access technology. The MC-MFSK spread-spectrum technique serves this purpose.

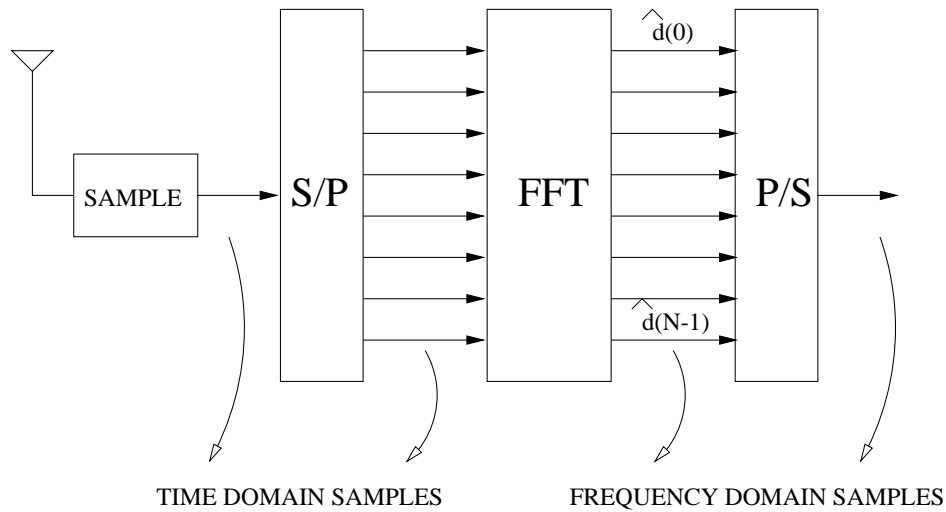


Figure 1.2: Basic OFDM receiver

### Spread-Spectrum Multiple Access

Since the proposed MC-MFSK system is a spread-spectrum based multiple-access scheme, we first briefly discuss the merits of spread-spectrum technology. Spread-spectrum technology has become the technology of choice for commercial systems operating in both the licensed [6] as well as the unlicensed spectrum [7,8]. The key properties of this technology that make it desirable are as follows: First, spread-spectrum signals are effective in combatting and suppressing certain types of interference that arise in wireless channels. Second, the pseudo-randomness inherent in the design of spread-spectrum signals enables these systems to achieve a high degree of security. Third, a frequency-reuse factor of one allows for easy planning and deployment of spread-spectrum based systems. Among the different implementations of this technology, the most popular are FH and DS spread-spectrum systems [9]. The proposed MC-MFSK scheme shares some of the advantages of both FH and DS spread-spectrum systems, while overcoming some of their disadvantages.

The MC-MFSK scheme is partly motivated by a variant of an  $M$ -ary FSK based FH system. In this section, we discuss an  $M$ -ary FSK based FH system, and then later, in Section 1.1.1, explain the connection between this scheme and the MC-MFSK system.

In an  $M$ -ary FSK based modulation scheme, the modulator selects one of  $M$  frequencies corresponding to the transmission of  $\log_2 M$  bits. The resulting  $M$ -ary FSK signal is translated in frequency by an amount that is determined by the output of a frequency synthesizer which is in turn driven by a PN generator [1]. The receiver has an identical PN generator synchronized with the transmitter. The PN generator drives a frequency synthesizer, the output of which is mixed with the received signal to remove the pseudo-random frequency translation introduced by the transmitter. Once the signal is at baseband, it is passed through an  $M$ -ary FSK demodulator to recover the desired  $\log_2 M$  bits. It is difficult to maintain phase coherence both in the synthesis of the frequencies used in the hopping pattern as well as in the propagation of the signal over the channel as the signal is hopped over multiple frequencies. Consequently,  $M$ -ary FSK modulation with noncoherent detection is usually employed with FH spread spectrum systems.

### **Multuser Detection**

In multiple-access systems, multuser detectors can be used to exploit the structure of the received signals to improve system performance. In this section, we first develop a general framework for multuser detection and then discuss the special cases of *linear* modulation with *coherent* detection and *nonlinear* modulation with *noncoherent* detection.

Consider a  $K$ -user system where user  $k$  transmits message  $m_k$  (drawn from an arbitrary finite alphabet  $\mathcal{A}$ ) by transmitting a signal  $s_k(t; m_k)$ ,  $t \in [0, T]$ . Denote the phase shift associated with user  $k$  as  $e^{j\phi_k}$ . Then, assuming that the signals of the  $K$  users are received synchronously, the receiver observes a sum of the users' signals embedded in noise  $n(t)$ , i.e.,

$$r(t) = \sum_{k=1}^K e^{j\phi_k} s_k(t; m_k) + n(t). \quad (1.2)$$

Denote  $\mathbf{m} = [m_1 \cdots m_K]^\top$  and  $\phi = [\phi_1 \cdots \phi_K]^\top$ . If the noise  $n(t)$  is white and Gaussian

then, the optimal decision rule in the maximum-likelihood (ML) sense is to select the set of symbols and phases  $(\mathbf{m}, \phi)$  corresponding to the signals that resemble most closely (in the mean-square sense) the received waveform  $r(t)$  [10, 11], i.e.

$$(\hat{\mathbf{m}}, \hat{\phi}) = \arg \min_{\mathbf{m} \in \mathcal{A}^K} \min_{\phi} \left\| r(t) - \sum_{k=1}^K e^{j\phi_k} s_k(t; m_k) \right\| \quad (1.3)$$

where  $(\hat{\mathbf{m}}, \hat{\phi})$  is the estimate of  $(\mathbf{m}, \phi)$ . Next, we consider some special cases.

### • Linear Modulation with Coherent Detection

Linear modulation pertains to the case where the signal  $s_k(t; m_k)$  is a linear function of the message symbol  $m_k$ , for example,

$$s_k(t; m_k) = m_k s_k(t) \quad k = 1, \dots, K. \quad (1.4)$$

We define

$$y_k = \int_0^T s_k(t) r(t) \quad k = 1, \dots, K \quad (1.5)$$

$$R_{ij} = \int_0^T s_i(t) s_j(t) \quad (1.6)$$

where  $R_{ij}$  is the  $i$ th row,  $j$ th column element of a matrix  $\mathbf{R}$ .

Coherent detection assumes knowledge of the phase vector  $\phi$ . Therefore, for linear modulation with coherent detection, (1.3) reduces to [11]

$$\hat{\mathbf{m}} = \arg \max_{\mathbf{m} \in \mathcal{A}^K} 2\mathbf{m}^\top \mathbf{y} - \mathbf{m}^\top \mathbf{R} \mathbf{m}. \quad (1.7)$$

The maximization in (1.7) is a combinatorial optimization problem and no algorithm is known whose computational complexity is polynomial in the number of users [10]. This has motivated the development of less complex suboptimal detectors such as the decorrelator, MMSE detector and soft interference cancellers [11]. Reference [12] constructs an insightful, nonlinear-programming based approach to the optimum multiuser detection problem in (1.7) and shows that the popular suboptimal multiuser detectors

proposed in the literature can be derived as solutions to relaxations of the problem in (1.7).

- **Nonlinear Modulation with Noncoherent Detection**

Nonlinear modulation with noncoherent detection is often necessary when phase estimation is difficult due to rapid changes in the channel conditions [1]. A popular example of nonlinear modulation is  $M$ -ary FSK. In this case,  $m_k \in \mathcal{A} = \{0, \dots, M-1\}$  and  $s_k(t; m_k)$  is not a linear function of  $m_k$ . Hence,  $s_k(t; m_k)$  cannot be directly written in the form shown in (1.4). However, using the approach of [13], the  $K$ -user channel employing  $M$ -ary nonlinear modulation can be written as an  $MK$ -user pseudo-linearly modulated channel, where the data of the different “users” are dependent. If we define [11]

$$\bar{\phi}_{M(k-1)+j} = \phi_k \quad (1.8)$$

$$\bar{b}_{M(k-1)+j} = \begin{cases} 1 & j = m_k \\ 0 & \text{otherwise} \end{cases} \quad (1.9)$$

$$\bar{s}_{M(k-1)+j}(t) = s_k(t; j) \quad (1.10)$$

then, (1.2) can be written in the linear form

$$r(t) = \sum_{n=1}^{MK} \bar{b}_n e^{j\bar{\phi}_n} \bar{s}_n(t) + n(t). \quad (1.11)$$

The linear representation allows the use of popular linear multiuser detectors such as the decorrelator and the MMSE receiver.

As in the linear modulation case, the implementation of the optimal detector for the received signal in (1.11) also requires an exhaustive search over possible vectors  $\bar{\mathbf{b}} = [\bar{b}_1 \cdots \bar{b}_{MK}]^\top$ . Further, since the phases are not known in the present scenario, the problem becomes even more complex. In this thesis, in order to obtain suboptimal noncoherent detectors with reasonable complexity, we *relax* the constraint set of the ML

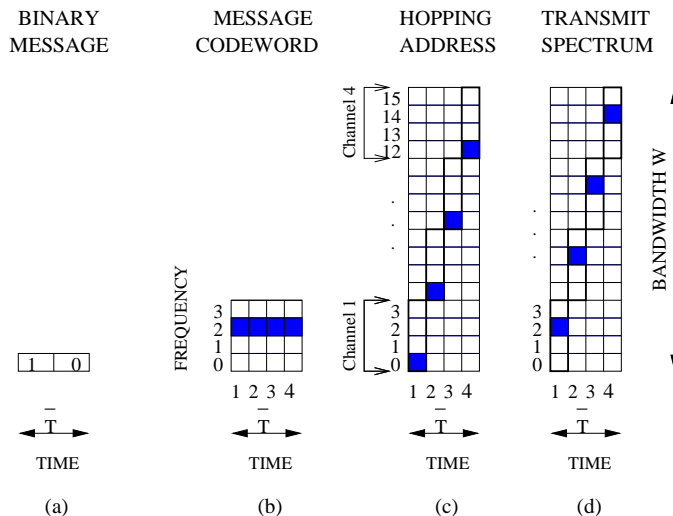


Figure 1.3: FH MFSK transmitter

noncoherent multiuser detection problem. This approach is similar to the linear modulation counterparts considered in [12, 14, 15]. Other approaches in the literature will be discussed in the next section and in Chapter 3.

## 1.1 Related Work

### 1.1.1 MFSK Spread-Spectrum Multiple-Access Systems

Since the MC-MFSK system is motivated by another FH-based system, we first explore this relationship in a little more detail.

The most popular implementation of the FH spread-spectrum system is the  $M$ -ary Frequency Shift Keyed system which is also known as the *conventional* FH-MFSK system [16–18]. At the FH-MFSK transmitter,  $\log_2 \bar{M}$  bits form a message  $m \in \{0, \dots, \bar{M} - 1\}$ . Message  $m$  is mapped to the transmission of a tone on sub-channel  $m$ . For the FH-MFSK system, the total duration of the  $\log_2 \bar{M}$ -bit message will be referred to as the *signaling-interval* and will be denoted by  $\bar{T}$ .

Ideally, in a single-user, error-free environment, the transmitter would transmit a single

tone on sub-channel  $m$  for a duration of  $\bar{T}$  secs and the receiver would be able to decode the message reliably. However, in non-ideal channel conditions, the transmitter may need to employ both time and frequency diversity to increase the probability of correct reception. An example is shown in Figure 1.3. In Figure 1.3(a), a two-bit message ‘1 0’ is transmitted as a tone on sub-channel  $m = 2$  (shown as shaded boxes in Figure 1.3(b)). The total signaling interval  $\bar{T}$  is kept the same as that of the two-bit message. To achieve time diversity, the signaling interval  $\bar{T}$  is divided into  $\bar{L}$  intervals known as *hopping-intervals* and the tone on sub-channel  $m$  is repeated over the  $\bar{L}$  hopping-intervals. In the example,  $\bar{L} = 4$ .

Figures 1.3(c) and (d) illustrate the way in which frequency diversity is achieved. The entire system bandwidth  $W$  is partitioned into  $N = 4$  orthogonal *channels*, with each channel comprising  $\bar{M} = 4$  orthogonal *sub-channels* (in this example, we have chosen  $\bar{L} = \bar{M} = N = 4$ ; they do not have to be the same). During each of the  $\bar{L} = 4$  hopping-intervals, a channel is chosen pseudo-randomly in accordance with a hopping-address  $\mathbf{f} = [f_1 \cdots f_{\bar{L}}]^\top$  as shown in Figure 1.3(c). Then, as shown in Figure 1.3(d), during the  $l$ th hopping-interval, a tone is transmitted on sub-channel  $\bar{M}(f_l - 1) + m$ ,  $l = \{1, \dots, \bar{L}\}$ . In our example,  $\bar{M}(f_l - 1) + m = 4(f_l - 1) + 2$ , and since  $\mathbf{f} = [1 \ 2 \ 3 \ 4]^\top$ , the tones are transmitted on sub-channels  $[2 \ 6 \ 10 \ 14]^\top$ . The transmitted tones are represented by the shaded boxes in the figure.

The receiver knows the hopping address  $\mathbf{f}$  and can therefore translate the signal back to baseband as in Figure 1.3(c). However, since the receiver does not know the sub-channel on which the tone was transmitted, it performs threshold detection on all the  $\bar{M}$  sub-channels over the  $\bar{L}$  hopping-intervals. The receiver then adds up the  $\bar{L}$  entries in each of the  $\bar{M}$  sub-channels (rows in Figure 1.3(c)) and then selects the index of the sub-channel with the maximum entries as the desired message. In the presence of noise and/or multiuser interference, there may be significant energy on the undesired sub-channels as well which could potentially lead to decoding errors.

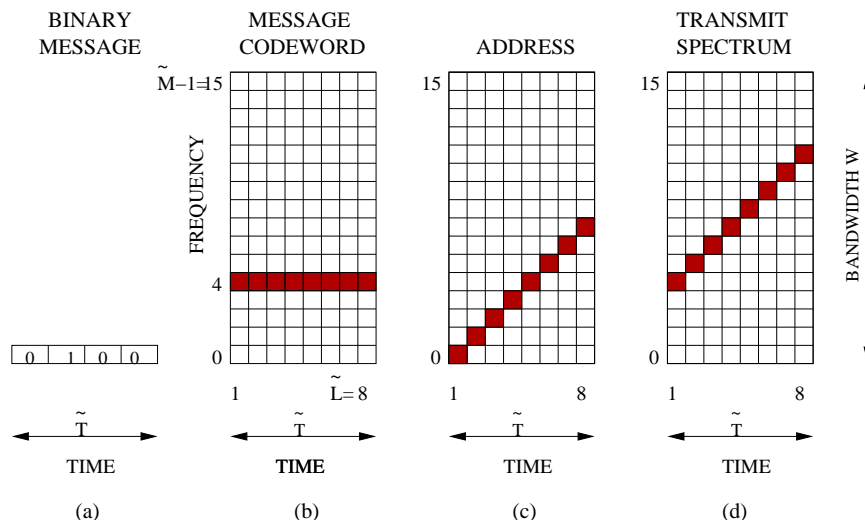


Figure 1.4: Multilevel FSK transmitter

In the FH-MFSK system, since each hopping-interval is of length  $\bar{T}/\bar{L}$ , the sub-channel spacing is assumed to be  $\bar{L}/\bar{T}$  Hz. Since there are a total of  $\bar{M}\bar{N}$  sub-channels in a bandwidth of  $W$  Hz,  $W = \bar{L}\bar{M}\bar{N}/\bar{T}$  Hz. Also, by definition,  $R_b = \log_2 \bar{M}/\bar{T}$  bits/sec. If  $W$  and  $R_b$  are assumed to be fixed, the spectral efficiency of a user defined as  $R_b/W$  bits/sec/Hz is also a constant and can be written as

$$\eta = \frac{R_b}{W} = \frac{\log_2 \bar{M}}{\bar{L}\bar{M}\bar{N}} \quad [\text{bits/sec/Hz}]. \quad (1.12)$$

In the example in Figure 1.3, we chose  $\eta = 1/32$  and  $\bar{L} = N = 4$  which yielded  $\bar{M} = 4$ .

A variation of FH-MFSK with  $N = 1$  was proposed in [19] and termed FH Multilevel-FSK. Here, the system bandwidth comprises of just one channel ( $N = 1$ ), but with a far greater number of sub-channels  $\tilde{M}$  than the FH-MFSK system. In this case,

$$\eta = \frac{R_b}{W} = \frac{\log_2 \tilde{M}}{\tilde{L}\tilde{M}} \quad [\text{bits/sec/Hz}]. \quad (1.13)$$

Figure 1.4 shows an example with  $\eta = 1/32$ ,  $\tilde{L} = 8$ ,  $\tilde{M} = 16$ , and  $\log_2 \tilde{M} = 4$  bits-per-message. Although the signaling mechanism is similar to that of FH-MFSK, since there is only one channel, tones are transmitted on a pseudo-randomly chosen sub-channel during each of the  $\tilde{L}$  hopping-intervals. The signaling interval for FH Multilevel-FSK will be denoted by  $\tilde{T}$ . Since we have assumed that the bit-rate  $R_b$  is constant, so is the

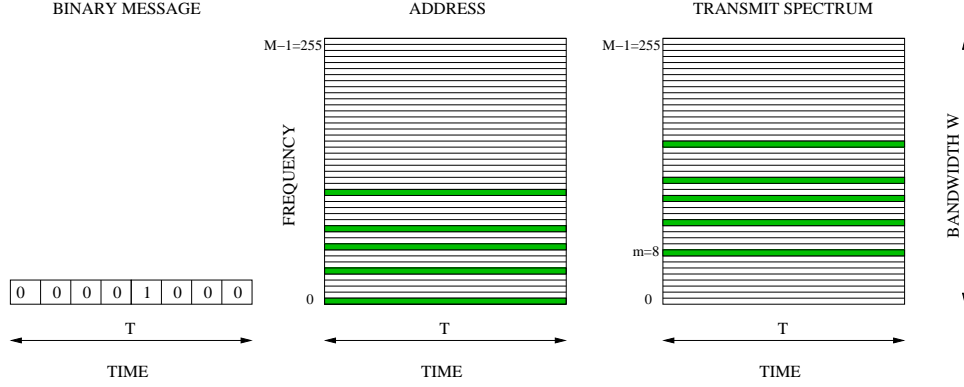


Figure 1.5: MC-MFSK transmitter

bit-duration  $T_b = 1/R_b$ . Therefore, the four-bit message in Figure 1.4 is transmitted in  $\tilde{T} = 4T_b$  secs as opposed to the  $\bar{T} = 2T_b$  secs taken by the two-bit message in Figure 1.3. This highlights the fact that the signaling interval in the two cases can be different depending upon the chosen system parameters.

In the example in Figure 1.4, the message ‘0 1 0 0’ is transmitted as a sequence of  $\tilde{L} = 8$  tones. The message codeword is denoted by  $m \cdot \mathbf{1}$  where  $\mathbf{1}$  is a vector of ones of length  $\tilde{L}$ . In the example, the message codeword is  $[4 \ 4 \ 4 \ 4 \ 4 \ 4 \ 4 \ 4]^\top$ . The address vector is denoted by a length  $\tilde{L}$  vector  $\tilde{\mathbf{a}}$  with elements  $\tilde{a}[l] \in \{0, \dots, \tilde{M} - 1\}$ . In the example shown in Figure 1.4(c),  $\tilde{\mathbf{a}} = [0 \ 1 \ 2 \ 3 \ 4 \ 5 \ 6 \ 7]^\top$ . The transmitted signal associated with message  $m$  is obtained as  $\tilde{\mathbf{s}}_m = (m \cdot \mathbf{1}) \oplus \tilde{\mathbf{a}}$ , where  $\oplus$  represents vector addition modulo  $\tilde{M}$ . The receiver uses the same algorithm as that used by the FH-MFSK system discussed above. Since its inception, Multilevel-FSK has been studied by several researchers [20–23]. It has been shown that Multilevel-FSK is capable of offering a higher capacity than conventional  $M$ -ary FSK based systems [23, 24].

The MC-MFSK scheme proposed in this thesis is partly motivated by the FH Multilevel-FSK system. As in FH Multilevel-FSK, the transmitted signal in MC-MFSK is also  $\tilde{\mathbf{s}}_m = (m \cdot \mathbf{1}) \oplus \tilde{\mathbf{a}}$ , where  $m \in \{0, \dots, M - 1\}$  and the vectors are of length  $L$ . However, in contrast to the FH-MFSK and FH Multilevel-FSK schemes considered above, in the

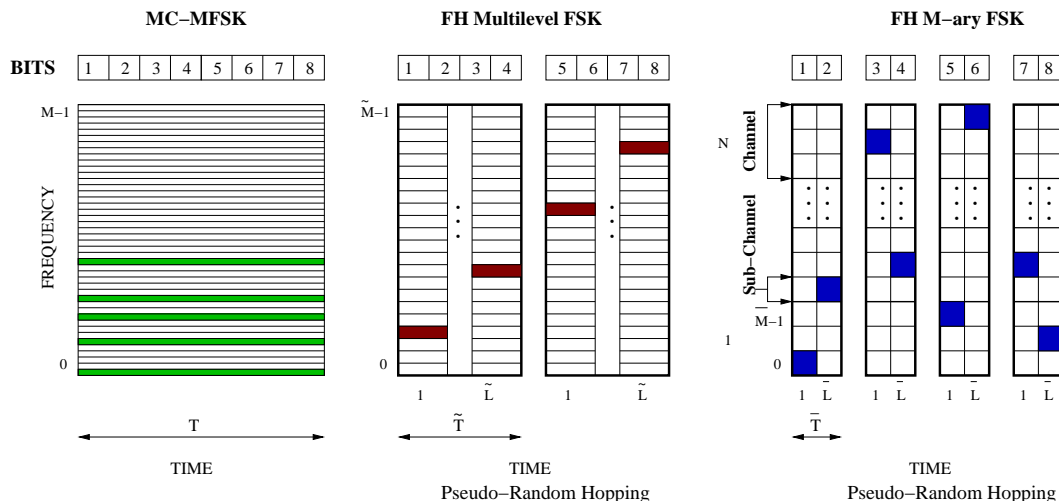


Figure 1.6: Comparison of FSK-based transmission schemes

MC-MFSK system, the elements of the address vector  $\tilde{\mathbf{a}}$ , and hence  $\tilde{\mathbf{s}}_m$ , represent *parallel* tones shown as shaded boxes in Figure 1.5. The single-user spectral efficiency in this case is

$$\eta = \frac{R_b}{W} = \frac{\log_2 M}{M} \quad [\text{bits/sec/Hz}]. \quad (1.14)$$

Figure 1.5 shows an example with  $\eta = 1/32$ , which yields  $M = 256$  and hence a message comprising  $\log_2 M = 8$  bits. The message duration in MC-MFSK is denoted by  $T$  and is the same as the signaling interval.

Figure 1.6 compares the transmission scheme of MC-MFSK with those of FH Multilevel FSK and FH MFSK. Since the single-user spectral efficiency  $\eta$  is constrained to be the same in all the cases, the eight bits are transmitted in the same total duration of  $8T_b$  secs over the same bandwidth of  $W$  Hz in all the cases. However, note that due to the constraints (1.12-1.14), different number of bits can be sent during each signaling interval in the three cases due to which the signaling intervals  $T$ ,  $\tilde{T}$  and  $\bar{T}$  can be of different lengths.

Even though the single-user spectral efficiency  $\eta$  is constrained to be the same in all the cases, it will be seen later in Chapter 2 that due to the differences in the signaling techniques, the total number of users that can be supported at a target message error

rate can be different in each case. Consequently, if we denote the total number of users supported in a system by  $K$ , then the total system spectral efficiency  $\eta_T = K\eta$  can be different in each case.

A block diagram of the MC-MFSK system is shown in Figure 1.7. Some of the potential advantages of using MC-MFSK over its FH counterpart are as follows: Since the MC-MFSK system is an OFDM-based technology [3,4], the IFFT/FFT operations eliminate the need for banks of oscillators and hence provide for ease of implementation [5] compared to FH Multilevel-FSK systems. The authors in [19] also mention the susceptibility of the FH Multilevel-FSK system to large delay spreads. The MC-MFSK system, on the other hand, helps combat the effects of large delay spreads by reducing the signaling rate on individual sub-channels. The MC-MFSK and FH systems do however share the desirable properties of frequency diversity and near-far resistance.

Although the MC-MFSK and DS-SS systems share the ability to resolve multipath, they differ in their resistance to the near-far effect. Unlike a matched-filter receiver based DS-SS system, the MC-MFSK is not susceptible to the near-far problem.

### **1.1.2 Noncoherent Multiuser Detection**

In order to improve the efficiency of multiple access systems that employ noncoherent detection, noncoherent multiuser detectors may be used. In this section, we discuss the related work in the literature in this particular area.

As discussed in Section 1, the ML detector for multiuser noncoherent communications with nonlinear modulation that estimates all users' messages jointly, has prohibitive complexity. ML multiuser detection, for both linear and nonlinear modulation, is NP-hard in the number of users, therefore, no efficient solution methodology is known [10].

For noncoherent systems, the complexity of optimal detection has directed attention

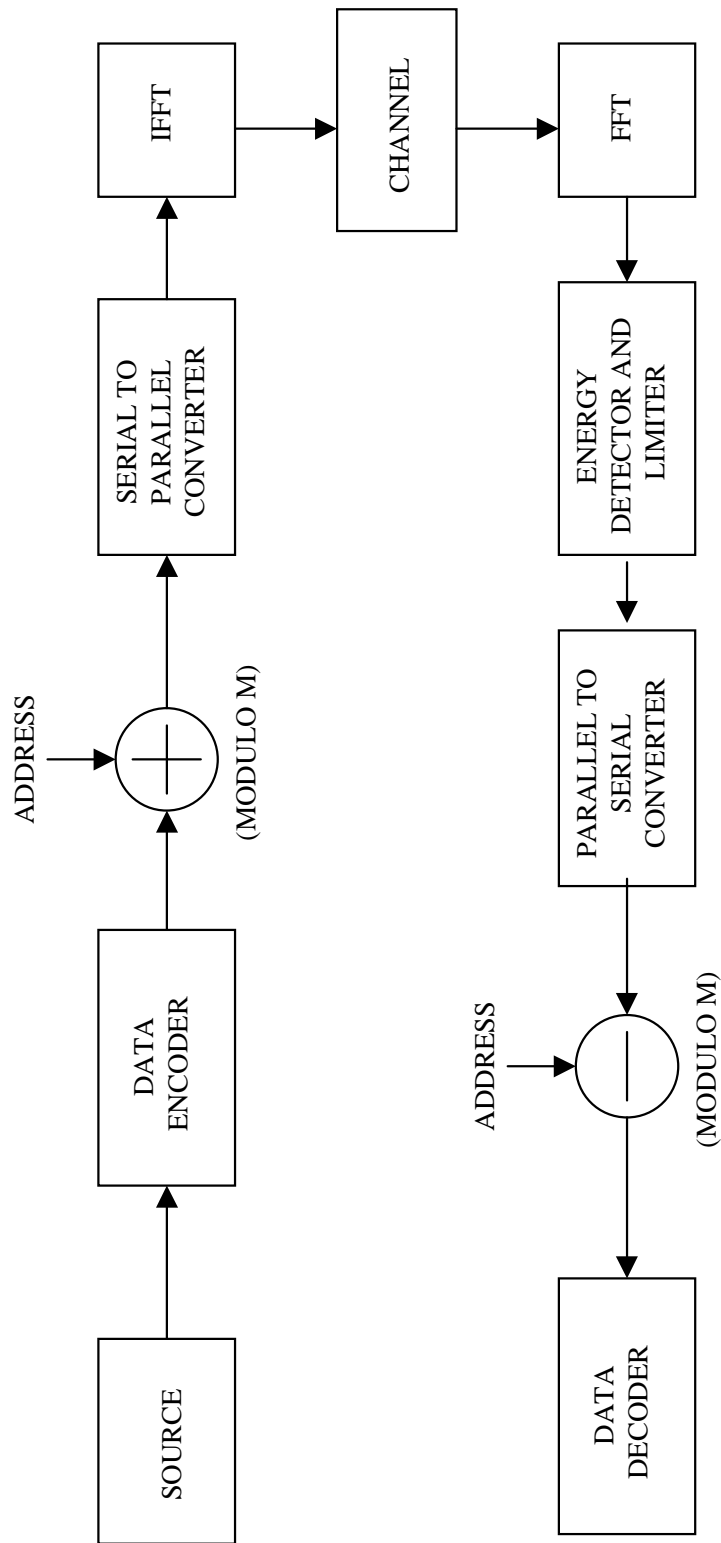


Figure 1.7: An MC-MFSK communication system

toward suboptimal interference suppression techniques [13, 25–28]. The work in [13] introduced a pseudo-linear representation (1.11) in which the signal space is spanned by  $MK$  signals corresponding to the  $M$  possible messages for each of the  $K$  users. This approach led naturally to two-step detectors in which decorrelative [13, 27] or MMSE [26] linear filtering for user separation is followed by noncoherent single-user detection as shown in Figure 1.8. Alternatively, [25, 28] employed decision-directed methods that use prior decisions to suppress the interference. The approach of [25] is to decorrelate against all possible interfering signals. Prior decisions reduce the space of possible interfering signals in that if a decision is made that user  $k$  transmitted signal  $m$ , then there is no need to decorrelate against the other  $M - 1$  possible transmissions of user  $k$ . In [28], the approach is to decorrelate against the known interfering signals identified by previous decisions. The resulting output is then passed to a bank of single-user matched filters followed by a maximum magnitude detector to determine the symbol.

In this thesis, we follow the strategy of [25, 28] and examine approaches that combine filtering with decision-directed methods. We propose low-complexity, suboptimal noncoherent detectors that take advantage of certain *a priori* information available regarding the multiuser signals [29, 30]. We incorporate this structure into the algorithms of various detector classes and provide numerical comparisons to demonstrate the near-optimum performance of the proposed detectors.

## 1.2 Thesis Overview

This thesis is divided into two parts. The first part discusses the MC-MFSK system and the second part investigates efficient noncoherent multiuser detection techniques.

In Chapter 2, we outline the basic system model of the MC-MFSK system. Since the MC-MFSK scheme is partly motivated by the FH Multilevel-FSK system, we review this system as well. We develop upper bounds for the probability of word error for

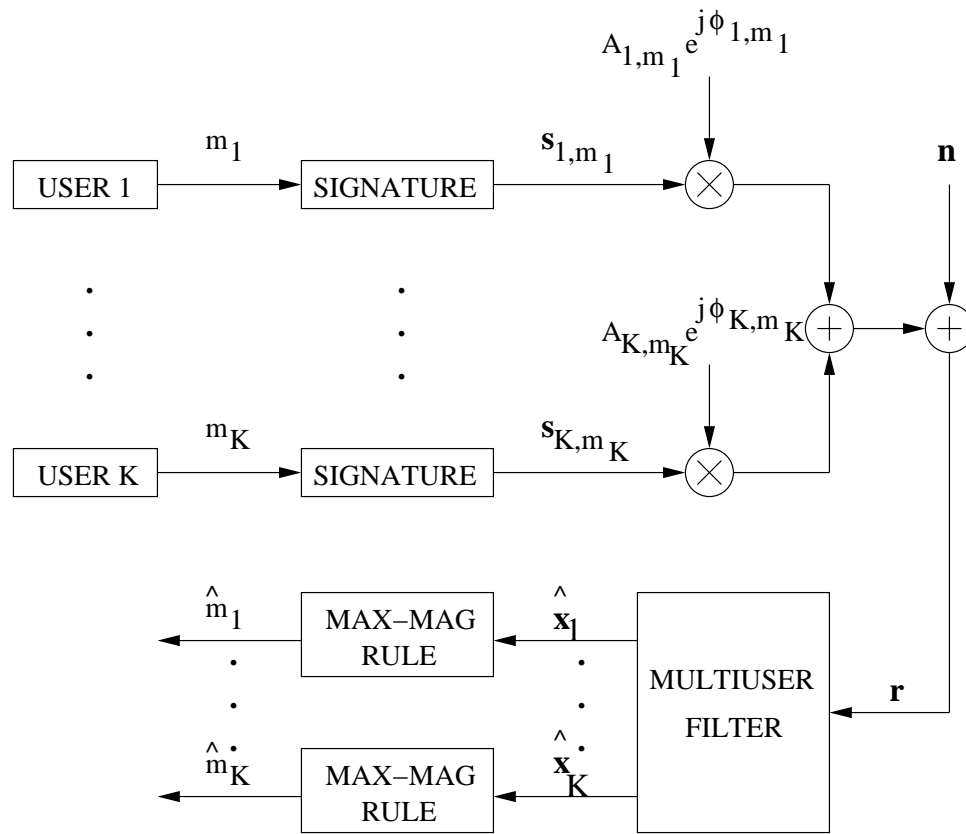


Figure 1.8: Noncoherent multiuser detector

the MC-MFSK scheme and then translate these into lower bounds on the capacity and spectral efficiency of the system. Next, we evaluate the performance of the MC-MFSK system in Rayleigh fading channels. Since the MC-MFSK system employs noncoherent detection followed by a combiner, the optimal combiner (in the ML sense) is also derived in a multiuser scenario for Rayleigh fading channels. As the optimal combiner does not have a closed-form expression, its approximations will be derived and evaluated. Since the approximations to the optimal detector use a detection threshold, its selection is also discussed. Lastly, the performance of the MC-MFSK system is compared to that of FH  $M$ -ary FSK and FH Multilevel-FSK systems.

In Chapter 3, we investigate efficient techniques for noncoherent multiuser detection. First, we establish notation for the additive-noise, synchronous CDMA system model and describe the ML detector. Next, we discuss prior work on decorrelator and MMSE detectors proposed in the literature. We then introduce the constrained detectors which embed maximum amplitude information for the received signal components as constraints for nonlinear programming relaxations of the ML multiuser detector. Following this, we introduce noncoherent detectors based on different types of soft interference cancellers. In order to further improve the performance of the noncoherent multiuser detectors, we exploit additional *a priori* information regarding the signal in the form of *selective filtering* techniques. To illustrate the feasibility of the selective filters in scenarios with limited information regarding the interferers, e.g., a CDMA down-link, a blind adaptive implementation of the selective MMSE detector is also presented. We also suggest a successive interference suppression scheme, which, when used in conjunction with selective filtering, yields improved performance in near-far scenarios.

### 1.3 New Results

This thesis proposes a new spread-spectrum based multicarrier multiple-access technique for OFDM systems which shares the desirable properties of both FH and DS spread-spectrum systems.

The decoding heuristic proposed for the MC-MFSK system, although partly motivated by the FH Multilevel-FSK system, is also new. It is shown that in high-SNR, single-user channels, the decoding heuristic is in fact the optimal combiner.

In contrast to other related works, this thesis develops upper bounds on the probability of word error and then translates them into lower bounds on user capacity and spectral efficiency. The lower bounds provide a minimum system performance guarantee and hence are of importance.

The bound on user capacity derived in the thesis has a simple closed-form expression. This enables us to estimate, with considerable accuracy, important system parameters such as the frequency diversity factor  $L$  to be employed by the active users in the MC-MFSK system. Proper estimation of this parameter is of importance in a practical system.

Most of the FH-MFSK based schemes proposed in the literature employ envelope detection in their receivers. To compare their performance with the MC-MFSK system in Rayleigh fading channels, this thesis proposes a technique for the selection of the detection threshold for the MC-MFSK system.

This thesis also investigates and proposes techniques to improve performance of non-coherent multiuser detectors. The performance improvement is gained by exploiting certain *a priori* information regarding the structure of the multiple-access signal.

This thesis proposes the application of nonlinear programming techniques to obtain approximations to the optimal noncoherent multiuser detectors.

Several soft interference cancellation (soft-IC) techniques for noncoherent multiuser detectors are also proposed in this thesis.

One of the major contributions of this thesis in the area of noncoherent multiuser detection is the use of selective filtering. This technique uses *a priori* information regarding a user's signal to reduce the space of possible interfering signals. Selective filtering is applied to the decorrelator, MMSE detector as well as the soft-ICs to illustrate its versatility and effectiveness.

## Chapter 2

# Multicarrier MFSK: A Spread Spectrum Multiple Access Scheme for OFDM-based Systems

### 2.1 Introduction

In this chapter, we develop the OFDM based MC-MFSK system model and evaluate its performance in various channel conditions. Performance comparisons are also made with other MFSK based systems.

OFDM based multicarrier systems have recently gained popularity due to their ability to offer high data rates on a wireless channel without succumbing to inter-symbol-interference problems caused due to channel impairments [2,31]. Multicarrier systems allow the transmission of multiple symbols in parallel over a channel thereby reducing the susceptibility of the transmissions to delay spreads. In order to serve multiple users efficiently, an OFDM based system requires a multiple-access technology. The MC-MFSK scheme proposed in this chapter seeks to serve this purpose [32,33]. An MC-MFSK based communication system is shown in Figure 1.7.

We use the framework developed in [34] to derive the *optimal* combining rule in the Maximum Likelihood (ML) sense. We show that in Rayleigh fading channels, the optimal combiner can be approximated by a *soft-limiter* in a multi-user scenario, and by a *linear-combiner* in a single-user scenario. The similarity between the decoding heuristic proposed for MC-MFSK and the optimal combiner is also highlighted. Optimal combiners are also derived for the special cases of a single user in Rayleigh fading and

AWGN channels. Since the soft-limiter and other approximations to the optimal combiner involve a detection threshold, techniques are proposed for selecting this threshold for the different cases.

The spectral efficiency of a system, defined as the total number of bits/sec/Hz that can be transmitted reliably, is an important measure of a system's performance. A lower bound on the spectral efficiency of the MC-MFSK system is obtained and compared to spectral efficiency obtained from simulations. The spectral efficiency of the MC-MFSK system is also compared to those of other MFSK based spread-spectrum systems such as FH Multilevel-FSK and FH  $M$ -ary FSK.

## 2.2 System Model

We first consider a single-user, synchronous MC-MFSK system and a signaling scheme where the user transmits one of  $M$  signals. At the MC-MFSK transmitter, the bit rate is denoted by  $R_b$ , and it is assumed that every  $T$  seconds,  $B$  message bits are loaded into a shift register and transferred as a  $B$ -bit word  $m \in \{0, \dots, M-1\}$  to the buffer, where  $M = 2^B$ . It is assumed that the available system bandwidth  $W$  is divided into  $M$  orthogonal sub-channels as shown in Figure 2.1. The  $m$ th message is mapped to the transmission of a tone on the  $m$ th sub-channel. In the absence of AWGN, Multiple Access Interference (MAI), or fading, the transmitter could simply send this single tone and the receiver would correctly decode  $m$  as the desired message. However, if the detection of the transmitted tone is prone to channel errors or MAI, then the transmitter would need to use redundancy in its transmission scheme. In MC-MFSK, the transmitter uses *frequency-diversity* to introduce redundancy by transmitting a *signature* vector  $\tilde{\mathbf{s}}_m$  of  $L$  parallel tones for every tone  $m$ . The signature vector  $\tilde{\mathbf{s}}_m$  is obtained by adding an address vector  $\tilde{\mathbf{a}} = [\tilde{a}[0] \cdots \tilde{a}[L-1]]^\top$  (with distinct elements) to the tone

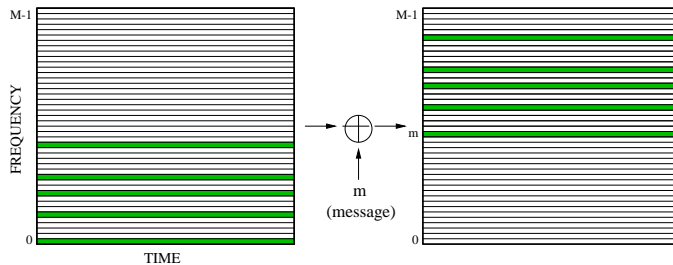


Figure 2.1: MC-MFSK transmitter

$m$  as follows:

$$\begin{aligned}
 \tilde{\mathbf{s}}_m &= (m \cdot \mathbf{1}) \oplus \tilde{\mathbf{a}} \\
 &= [m \cdots m]^\top \oplus [\tilde{a}[0] \cdots \tilde{a}[L-1]]^\top \\
 &= [\tilde{s}_m[0] \cdots \tilde{s}_m[L-1]]^\top
 \end{aligned} \tag{2.1}$$

where  $\mathbf{1}$  is a vector of ones of length  $L$ ,  $\oplus$  represents vector addition modulo  $M$  and each address element  $\tilde{a}[l] \in \{0, \dots, M-1\}$ .

Let  $\mathbf{a}$  be a binary vector of length  $M$  with a 1 at positions  $\tilde{a}[l]$ ,  $l = 0, \dots, L-1$ . Hence,  $\mathbf{a}$  represents the spectral occupancy of the vector  $\tilde{\mathbf{a}}$ . Similarly, let the signature vector  $\mathbf{s}_m$  represent the spectral occupancy of the vector  $\tilde{\mathbf{s}}_m$ . Let  $C_k$  and  $C_{-k}$  denote the operators which shift a vector *cyclically* by  $k$  and  $-k$ , respectively. Using these notations, we can write (2.1) alternatively as

$$\mathbf{s}_m = C_m \mathbf{a}. \tag{2.2}$$

Therefore, as shown in Figure 2.1, the message  $m$  is specified by the  $m$ -position cyclic rotation of the address vector  $\mathbf{a}$ . The receiver on the other hand, performs noncoherent detection on each of the sub-channels followed by a nonlinear operation  $G(\cdot)$ . The outputs of  $G(\cdot)$  are represented by the vector  $\mathbf{v}$ . Using  $\langle \cdot, \cdot \rangle$  to denote the dot-product of two vectors, an estimate of the desired message is obtained by using the following matched-filtering operation

$$\hat{m} = \arg \max_k \langle \mathbf{a}, C_{-k} \mathbf{v} \rangle. \tag{2.3}$$

The decoding rule (2.3) will be discussed in more detail in Section 2.4.

### 2.3 Review of FH Multilevel-FSK

As mentioned in Section 2.1, the MC-MFSK system is partly motivated by the FH Multilevel-FSK system proposed in [19]. From (1.13), we see that the single-user spectral efficiency is

$$\eta = \frac{R_b}{W} = \frac{\log_2 \tilde{M}}{\tilde{L}\tilde{M}} \quad [\text{bits/sec/hz}],$$

and hence,  $\tilde{L} = W \log_2 \tilde{M} / R_b \tilde{M}$ . This implies that for a given bandwidth  $W$ , a certain data rate  $R_b$ , and a fixed number of bits  $\log_2 \tilde{M}$ , the time-diversity factor  $\tilde{L}$  is also fixed. Therefore, in the FH Multilevel-FSK system, we cannot use a higher  $\tilde{L}$  to compensate for a poor channel. This limits the flexibility of the system. Another impairment associated with FH Multilevel-FSK is that of *delay-spread* [19]. The delay-spread of the multipath channel makes it difficult to precisely synchronize the arrival times at the base station. Consequently, the sub-channels may no longer be mutually orthogonal and *energy spillovers* may occur among adjacent sub-channels causing Inter Channel Interference (ICI). To avoid ICI, guard-bands may have to be introduced between channels which would require more bandwidth and hence reduce the spectral efficiency of the system.

The MC-MFSK system, on the other hand, has the following advantages over FH Multilevel-FSK. We can choose  $L$ , the frequency diversity parameter in this case, to be whatever the channel requires (within constraints on total transmitter power). This gives us an additional degree of freedom in designing our system and the opportunity to improve the performance dynamically as the channel conditions vary. The parallel approach can also potentially alleviate the problems of delay spread and synchronization as faced by the FH Multilevel-FSK system. Since our OFDM based multicarrier approach would reduce the data rates on the individual sub-channels, the delay spread would be less than the signaling interval and hence it may be easier to maintain synchronization [2]. This would help maintain the orthogonality between sub-channels and hence allow for higher spectral efficiency. Hardware implementation issues should

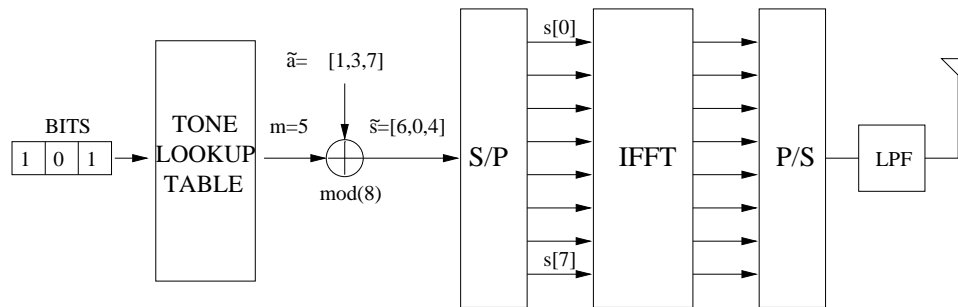


Figure 2.2: An OFDM based transmitter for MC-MFSK

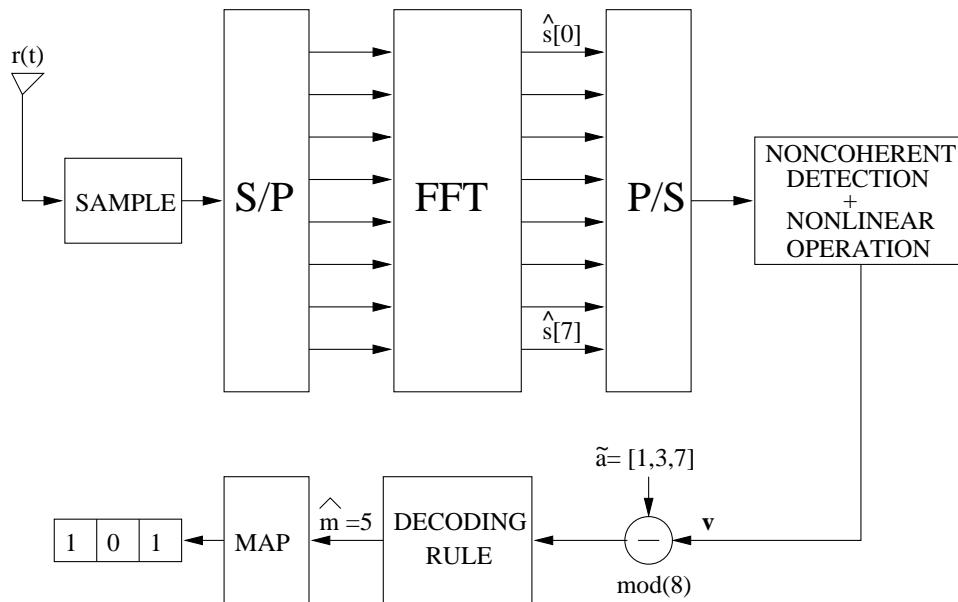


Figure 2.3: An OFDM based receiver for MC-MFSK

not pose a serious problem for our system since it can be implemented with readily available, off the shelf IFFT/FFT products [5] as shown in Figures 2.2 and 2.3.

## 2.4 MC-MFSK Decoder

At the receiver, let  $R_i$  be the output of the noncoherent detector tuned to sub-channel  $i$ . As will be seen in Section 2.5, in the presence of channel impairments such as AWGN and/or fading,  $R_i$  needs to be passed through a limiting function  $G(\cdot)$  which is

an approximation of the optimal limiter for the specified channel condition. We denote

$$\mathbf{v} = [G(R_0) \cdots G(R_{M-1})]^\top. \quad (2.4)$$

We first propose a heuristic-decoder for a single-user scenario, and then later, in Section 2.6.1, show its optimality in a high-SNR channel. Under the heuristic, the decoder first forms an  $L \times M$  matrix with the  $l$ th row consisting of the vector  $C_{-\tilde{a}[l]} \mathbf{v}$ . Then, the decoder adds up the entries in each column and declares the index of the column with the maximum entries as the desired message. In case of ties, a tie-breaker is used. Let  $[\mathbf{x}]_j$  denote the  $j$ th position in vector  $\mathbf{x}$ . The decoding rule can then be mathematically expressed as:

$$\hat{m} = \arg \max_j \left[ \sum_{l=0}^{L-1} C_{-\tilde{a}[l]} \mathbf{v} \right]_j. \quad (2.5)$$

Note that (2.5) may be re-written as a circular cross-correlation function, i.e.,

$$\begin{aligned} \left[ \sum_{l=0}^{L-1} C_{-\tilde{a}[l]} \mathbf{v} \right]_j &= \sum_{l=0}^{L-1} v[\tilde{a}[l] + j] \\ &= \sum_{n=0}^{M-1} a[n] v[n + j] \\ &= \langle \mathbf{a}, C_{-j} \mathbf{v} \rangle. \end{aligned} \quad (2.6)$$

The decoding rule can then be written as

$$\hat{m} = \arg \max_j \langle \mathbf{a}, C_{-j} \mathbf{v} \rangle. \quad (2.7)$$

As will be shown later in Section 2.6.1, in a high-SNR channel, the limiter  $G(R_i)$  reduces to an activity detector and yields a non-zero constant value  $G(1)$  on the sub-channels where there is at least one user present, and zero otherwise. For the single-user scenario, this implies that in a high-SNR channel

$$\mathbf{v} = G(1) \mathbf{s}_m = G(1) C_m \mathbf{a}. \quad (2.8)$$

Substituting (2.8) and the identity  $C_{-j} C_m \mathbf{a} = C_{m-j} \mathbf{a}$  in (2.7), we have

$$\hat{m} = \arg \max_j \langle \mathbf{a}, G(1) C_{m-j} \mathbf{a} \rangle = \arg \max_j \langle \mathbf{a}, C_{m-j} \mathbf{a} \rangle. \quad (2.9)$$

Since  $\mathbf{a}$  has a *Hamming* weight of  $L$ ,  $\mathbf{a}^T \mathbf{a} = L$ . Moreover, on applying the Cauchy-Schwarz inequality [35] to the RHS of (2.9),

$$\langle \mathbf{a}, C_{m-j} \mathbf{a} \rangle \leq L \quad (2.10)$$

with equality *iff*  $C_{m-j} \mathbf{a} = \mathbf{a}$ . If  $\mathbf{a}$  is such that  $C_i \mathbf{a} = \mathbf{a}$  only for  $i \pmod{M} = 0$ , then the maximum in (2.9) is unique and noiseless decoding will be reliable.

### 2.4.1 Probability of Word Error

We now consider a multi-user scenario with  $K$  users. User  $k$  is assumed to be the desired user and the variables associated with it are indexed by the letter  $k$ . For example, the desired message is denoted by  $m_k$ . In this section, we evaluate the impact of only interferers on the performance of the desired user. The performance metric chosen is the probability of word error of the desired user. Since we are mainly interested in quantifying the extent to which the system is interference-limited, a high-SNR channel is considered.

In high-SNR channels, since the constant  $G(1)$  is just a scaling factor applied to all the sub-channels where there is at least one user present, we can ignore it in the probability-of-error calculations. Therefore, in this section, we assume that the elements of  $\mathbf{v}$  are Bernoulli r.v.'s:  $v[i] = 1$  indicating the presence of at least one user on sub-channel  $i$ , and  $v[i] = 0$ , an absence.

We now introduce notation to enable us to represent  $\mathbf{v}$  as a function of the users' addresses. Let  $x \wedge y$  denote the AND operation between any two scalars  $x$  and  $y$ , and let  $\mathbf{x} \wedge \mathbf{y}$  denote element-by-element AND operation between any two vectors  $\mathbf{x}$  and  $\mathbf{y}$ . Also, let  $x \vee y$  denote the OR operation between scalars  $x$  and  $y$ , and let  $\mathbf{x} \vee \mathbf{y}$  denote element-by-element OR operation for vectors  $\mathbf{x}$  and  $\mathbf{y}$ . For vectors  $\mathbf{x}_1, \dots, \mathbf{x}_K$ , define

$\bigvee_k \mathbf{x}_k = \mathbf{x}_1 \vee \mathbf{x}_2 \vee \dots \vee \mathbf{x}_K$ . Using these notations, in a high-SNR channel, we have

$$\mathbf{v} = \bigvee_{l=1}^K C_{m_l} \mathbf{a}_l. \quad (2.11)$$

From (2.7) the message estimate for the desired user is

$$\hat{m}_k = \arg \max_j \langle \mathbf{a}_k, C_{-j} \mathbf{v} \rangle. \quad (2.12)$$

Since  $\langle \mathbf{a}_k, C_{-j} \mathbf{v} \rangle = \langle C_j \mathbf{a}_k, \mathbf{v} \rangle$ , this can also be viewed as a matched-filtering operation where, in order to determine the candidates for the transmitted message, the desired user's receiver *correlates*  $\mathbf{v}$  with all  $M$  possible rotations of the desired user's address  $\mathbf{a}_k$ , retaining only the shifts that yield the maximum correlation value. The output of the  $k$ th user's  $i$ th correlator can be written as

$$S_{k,i} = \langle \mathbf{a}_k, C_{-i} \mathbf{v} \rangle \quad (2.13)$$

and let

$$S_k^* = \max_i S_{k,i}. \quad (2.14)$$

Since the Hamming weight of  $\mathbf{a}_k$  is  $L$  and that of  $\mathbf{v}$  is at least  $L$  (from (2.11)),

$$\langle \mathbf{a}_k, C_{-i} \mathbf{v} \rangle \leq L. \quad (2.15)$$

Therefore,  $S_k^* = L$  for all  $k$ . We define

$$W_{k,i} = \begin{cases} 1 & \text{if } S_{k,i} = S_k^* = L \\ 0 & \text{otherwise.} \end{cases} \quad (2.16)$$

The desired message is then estimated as

$$\hat{m}_k = i \quad \text{if } W_{k,i} = 1 \quad (2.17)$$

and, in case of ties, a tie-breaker is used. We now evaluate the probability of word error based on (2.17). Denote the total number of ties by

$$Z_k = \sum_{\substack{i=0 \\ i \neq m_k}}^{M-1} W_{k,i}. \quad (2.18)$$

If  $P(Z_k = z)$  is the probability of  $z$  ties, then the probability of decoding the desired user correctly can be written as

$$P_c = P_{Z_k}(0) + \frac{1}{2}P_{Z_k}(1) + \dots + \frac{1}{M}P_{Z_k}(M-1) \quad (2.19)$$

$$= \sum_{l=0}^{M-1} \frac{1}{l+1} P_{Z_k}(l). \quad (2.20)$$

The error probability is defined as

$$P_w = 1 - P_c. \quad (2.21)$$

Since it is hard to obtain a closed-form expression for the right side of (2.20), we use the lower bound  $P_c > P_{Z_k}(0)$ . Therefore, from (2.21),  $P_w$  can be upper bounded by

$$P_w < 1 - P_{Z_k}(0). \quad (2.22)$$

Assuming that user  $k$  transmitted message  $m_k = 0$ , we have from (2.18) and (2.22):

$$P_{w|m_k=0} < 1 - P(\cap_{i \neq m_k} \{W_{k,i} = 0\} | m_k = 0) \quad (2.23)$$

$$= P(\cup_{i \neq m_k} \{W_{k,i} = 1\} | m_k = 0) \quad (2.24)$$

$$\leq \sum_{i \neq m_k} P(W_{k,i} = 1 | m_k = 0) \quad (2.25)$$

$$= \sum_{i=1}^{M-1} P(S_{k,i} = L | m_k = 0), \quad (2.26)$$

where, in going from (2.23) to (2.24), we used the identity that for any two events  $A$  and  $B$ ,  $P(\bar{A} \cap \bar{B}) = 1 - P(A \cup B)$ . In going from (2.24) to (2.25), the union bound was used. The last equality in (2.26) follows from (2.16). We now investigate the expression  $P(S_{k,i} = L | m_k = 0)$  in a little more detail.

Substituting (2.11) in (2.13) yields

$$\begin{aligned} S_{k,i} &= \left\langle \mathbf{a}_k, C_{-i} \bigvee_{l=1}^K C_{m_l} \mathbf{a}_l \right\rangle \\ &= \left\langle \mathbf{a}_k, \bigvee_{l=1}^K C_{m_l - i} \mathbf{a}_l \right\rangle \end{aligned}$$

$$= \left\langle \mathbf{a}_k, C_{m_k-i}\mathbf{a}_k \vee \bigvee_{l \neq k}^K C_{m_l-i}\mathbf{a}_l \right\rangle \quad (2.27)$$

$$= \left\langle \mathbf{a}_k, C_{m_k-i}\mathbf{a}_k \vee \bigvee_{l \neq k}^K C_{n_l}\mathbf{a}_l \right\rangle \quad (2.28)$$

where, in going from (2.27) to (2.28), we use the fact that since  $m_k$  is uniformly distributed over  $\{0, \dots, M-1\}$ , so is  $n_l = (m_l - i) \bmod M$ . Since  $\bigvee_{l \neq k}^K C_{n_l}\mathbf{a}_l$  is independent of index  $i$ , it can be written simply as a random vector

$$\mathbf{u} = \bigvee_{l \neq k}^K C_{n_l}\mathbf{a}_l. \quad (2.29)$$

Substituting (2.29) in (2.28) yields

$$S_{k,i} = \langle \mathbf{a}_k, C_{m_k-i}\mathbf{a}_k \vee \mathbf{u} \rangle. \quad (2.30)$$

For any two binary elements  $b$  and  $c$ , it can be shown using a truth table that  $b \vee c = b + c - b \wedge c$ . Applying it to (2.30), we have

$$S_{k,i} = \langle \mathbf{a}_k, C_{m_k-i}\mathbf{a}_k + \mathbf{u} - C_{m_k-i}\mathbf{a}_k \wedge \mathbf{u} \rangle \quad (2.31)$$

Expanding the right side of (2.31), substituting  $m_k = 0$ , and using  $\mathbf{a}_k^\top (C_{-i}\mathbf{a}_k \wedge \mathbf{u}) = \mathbf{u}^\top (\mathbf{a}_k \wedge C_{-i}\mathbf{a}_k)$ , we have

$$S_{k,i} = \langle \mathbf{a}_k, C_{-i}\mathbf{a}_k \rangle + \langle \mathbf{a}_k, \mathbf{u} \rangle - \langle \mathbf{a}_k, C_{-i}\mathbf{a}_k \wedge \mathbf{u} \rangle \quad (2.32)$$

$$= \mathbf{a}_k^\top C_{-i}\mathbf{a}_k + \mathbf{a}_k^\top \mathbf{u} - \mathbf{u}^\top (\mathbf{a}_k \wedge C_{-i}\mathbf{a}_k) \quad (2.33)$$

Since the distributions of the first and third terms on the right side of (2.33) are difficult to formulate, we consider the limiting case  $L/M \rightarrow 0$  to make the analysis tractable. The limiting case is characteristic of the MC-MFSK system and hence its assumption is a valid one. The way in which  $L/M \rightarrow 0$  is as follows: Typically, for the MC-MFSK system,  $M$  is very large both in absolute terms as well as compared to  $L$ . Also, as we show later, the optimal value of  $L$  that maximizes the number of users supported by the system is proportional to  $\ln(M/P_w)$ . Therefore, as  $M \rightarrow \infty$ ,  $L/M \rightarrow 0$ . Defining

$$\alpha_i = \mathbf{a}_k^\top C_{-i}\mathbf{a}_k, \quad (2.34)$$

from (A.9) in Appendix A.1, we have

$$\lim_{L/M \rightarrow 0} P(\alpha_i = 0) = 1 \quad i \neq 0. \quad (2.35)$$

Note that (2.35) also implies that

$$\lim_{L/M \rightarrow 0} P(\mathbf{a}_k \wedge C_{-i} \mathbf{a}_k = \mathbf{0}) = 1 \quad i \neq 0 \quad (2.36)$$

where  $\mathbf{0}$  is an  $M$ -dimensional zero vector. Incorporating (2.35) and (2.36) into (2.33) yields

$$\lim_{L/M \rightarrow 0} P(S_{k,i} = \mathbf{a}_k^\top \mathbf{u}) = 1 \quad i \neq 0. \quad (2.37)$$

Let us represent

$$\rho = \mathbf{a}_k^\top \mathbf{u}. \quad (2.38)$$

Note that  $P_w|_{m_k=0} = P_w$  by symmetry. Substituting (2.37) in (2.26), for  $L/M \rightarrow 0$  we have

$$P_w \leq \sum_{i=1}^{M-1} P(\rho = L) < MP(\rho = L) \quad (2.39)$$

We now evaluate  $P(\rho = L)$ . Since the entries of  $\tilde{\mathbf{a}}_k$  represent the location of the  $L$  1's in  $\mathbf{a}_k$ , we have

$$\rho = \sum_{l=0}^{L-1} u[\tilde{a}_k[l]] \quad (2.40)$$

which is a sum of *dependent* Bernoulli random variables. The expression for  $P(\rho = L)$  is derived in (A.29) in Appendix A.2. Since (A.29) does not have a closed form, it makes it difficult to proceed with the right side of (2.39). However, it is shown in (A.31) in Appendix A.2.1 that for small values of  $L/M$  (true for the MC-MFSK scheme),

$$P(\rho = L) \approx p_0^L \quad (2.41)$$

where  $p_0$  is the probability of at least one of the  $K - 1$  interferers occupying a particular sub-channel. From (A.15) in Appendix A.2, we have  $p_0 = 1 - (1 - L/M)^{K-1}$ .

For  $0 \leq x \leq 1$  and  $K > 1$ , we have the identity

$$1 - (1 - x)^{K-1} \leq (K - 1)x \quad (2.42)$$

The proof is simple: Let

$$f(x) = 1 - (1-x)^{K-1} - (K-1)x.$$

Thus,  $f(0) = 0$  and  $f'(x) \leq 0$  which yields the identity. Therefore,  $p_0 \leq (K-1)L/M$  and the right side of (2.39) can be written as

$$MP(\rho = L) = Mp_0^L \quad (2.43)$$

$$\leq M \left( \frac{(K-1)L}{M} \right)^L \quad (2.44)$$

$$< M \left( \frac{KL}{M} \right)^L \quad (2.45)$$

which yields a lower bound for  $K$  of the form

$$K > K_{lb}(L) \triangleq \frac{M}{L} \left( \frac{P_w}{M} \right)^{1/L}. \quad (2.46)$$

Further, we define

$$L^* = \arg \max_L K_{lb}(L) = \ln \frac{M}{P_w}. \quad (2.47)$$

In Figure 2.4, we plot  $K_{lb}(L)$  in (2.46) versus  $L$  for different values of  $M$  and compare with results obtained from simulations for  $P_w = 0.001$ . In the simulations,  $K_{max}$  represents the maximum number of users that could be admitted into the system at a given  $L$  and  $M$  under the constraint that  $P_w \leq 0.001$ . We can see that in spite of the large  $M$  assumption behind the derivation of (2.46), the formula behaves qualitatively similar to the results from the simulations even for small values of  $M$  and provides good estimates of  $L$  at which  $K_{max}$  peaks for a particular  $M$ .

We define the spectral efficiency  $\eta_T$  of a system as [23]

$$\eta_T = \frac{KR_b}{W} \quad [\text{bits/sec/Hz}]. \quad (2.48)$$

For the MC-MFSK system, substituting (1.14) in (2.48) yields

$$\eta_T = \frac{K \log_2 M}{M} \quad (2.49)$$

$$> \frac{K_{lb}(L) \log_2 M}{M} \quad (2.50)$$

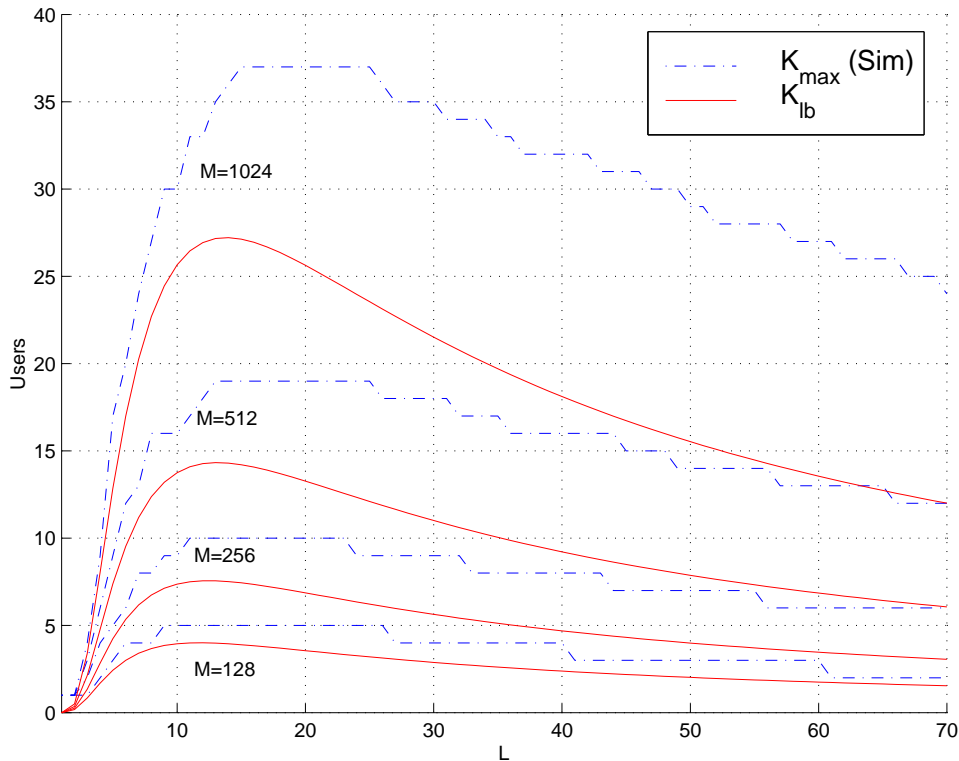


Figure 2.4: Comparison of system capacity obtained from simulations with the lower bound  $K_{lb}$

$$= \frac{M}{L} \left( \frac{P_w}{M} \right)^{1/L} \frac{\log_2 M}{M} \quad (2.51)$$

$$= \frac{\log_2 M}{L} \left( \frac{P_w}{M} \right)^{1/L}. \quad (2.52)$$

At the integer value of  $L = \lceil L^* \rceil$ ,

$$\eta_T(\lceil L^* \rceil) > \frac{\log_2 M}{\lceil L^* \rceil} \left( \frac{P_w}{M} \right)^{1/\lceil L^* \rceil} \quad (2.53)$$

$$= \frac{\log_2 M}{\lceil L^* \rceil} e^{-L^*/\lceil L^* \rceil} \quad (2.54)$$

$$\geq \frac{\log_2 M}{\lceil L^* \rceil} e^{-1} \quad (2.55)$$

$$\geq \frac{1}{e} \frac{\log_2 M}{L^* + 1} \triangleq \eta_T^*. \quad (2.56)$$

In going from (2.53) to (2.54), we used the fact that since  $L^* = \ln(M/P_w)$ ,  $P_w/M = e^{-L^*}$ . In going from (2.54) to (2.55), we used the identity  $-L^*/\lceil L^* \rceil \geq -1$ , and in going from (2.55) to (2.56), we used the identity  $1/\lceil L^* \rceil \geq 1/(L^* + 1)$ . Simplifying the

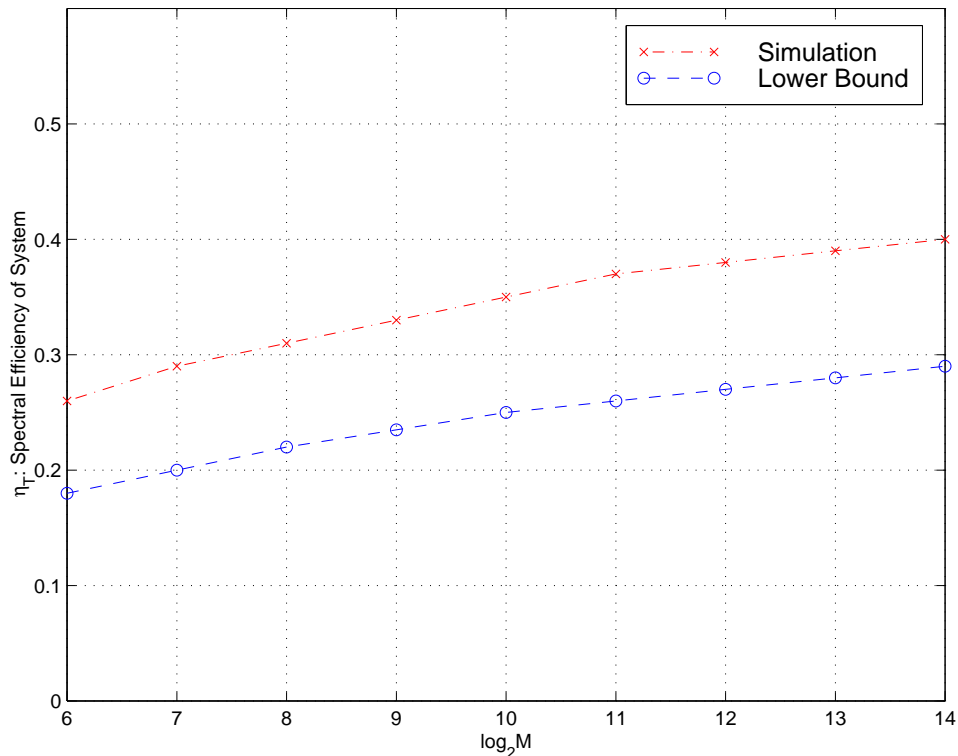


Figure 2.5: Comparison of simulated  $\eta_T$  with lower bound  $\eta_T^*$  at  $P_w = 10^{-3}$

expression for  $\eta_T^*$  in (2.56) yields

$$\eta_T^* = \frac{1}{e} \frac{\log_2 M}{\ln(M/P_w) + 1} \quad (2.57)$$

$$= \frac{1}{e} \frac{\log_2 M}{\ln(Me/P_w)} \quad (2.58)$$

$$= \frac{\log_2 e}{e} \frac{\log_2 M}{\log_2 e + \log_2 M - \log_2 P_w} \quad (2.59)$$

$$= \frac{0.53 \log_2 M}{\log_2 M + 11.41} \quad (2.60)$$

In going from (2.58) to (2.59), we used the identity  $\ln x = \log_2 x / \log_2 e$ . Equation (2.60) is the expression for  $\eta_T^*$  at  $P_w = 0.001$ . Figure 2.5 compares  $\eta_T^*$  in (2.60) with simulation results for different values of  $M$ .

## 2.5 Performance in Rayleigh Fading Channels

Wireless systems are susceptible to channel impairments such as log-normal fading, Doppler and multipath. In this section, we consider only the effect of multipath fading on an MC-MFSK system. It is assumed that the envelope of a user's multipath signal is Rayleigh distributed and independent between sub-channels. It is assumed that user  $k$  is the desired user and  $m_k = m$  the desired message. We define the signature vectors corresponding to the  $k$ th user's  $m$ th message as

$$\tilde{\mathbf{s}}_{k,m} = [\tilde{s}_{k,m}[0] \cdots \tilde{s}_{k,m}[L-1]]^\top \quad (2.61)$$

$$\mathbf{s}_{k,m} = [s_{k,m}[0] \cdots s_{k,m}[M-1]]^\top = C_m \mathbf{a}_k \quad (2.62)$$

where  $\tilde{s}_{k,m}[\cdot] \in \{0, \dots, M-1\}$  and  $s_{k,m}[\cdot] \in \{0, 1\}$ . We define an indicator variable  $c_{nm} = 1$  if sub-channel  $n$  is one of the  $L$  sub-channels used by user  $k$  in the transmission of message  $m$  and zero otherwise. That is

$$c_{nm} = \begin{cases} 1 & n \in \{\tilde{s}_{k,m}[0], \dots, \tilde{s}_{k,m}[L-1]\} \\ 0 & \text{otherwise.} \end{cases} \quad (2.63)$$

Since each of the  $K-1$  interferers in the system occupies a sub-channel with probability  $h_0 = L/M$  independent of the other users, the number of users  $J$  on sub-channel  $n$  has the binomial distribution

$$P_J(j) = B(K-1, j, h_0) \quad j = 0, \dots, K-1 \quad (2.64)$$

where,

$$B(K-1, j, h_0) = \begin{cases} \binom{K-1}{j} h_0^j (1-h_0)^{K-1-j} & j = 0, \dots, K-1 \\ 0 & \text{otherwise.} \end{cases} \quad (2.65)$$

For the  $i$ th user, the attenuation  $\lambda_i$  and phase  $\phi_i$  are assumed to be i.i.d random variables with  $\lambda_i$  being Rayleigh distributed with  $E[\lambda_i^2] = 1$  and  $\phi_i$  being uniformly distributed over  $[0, 2\pi]$ . It is also assumed that all the users have the same average received energy

$E_s$ . The aggregate faded received signal from the desired user and  $J$  interferers on sub-channel  $n$  is then

$$r_n(t) = \sqrt{\frac{2E_s}{T}} c_{nm} \lambda_k \cos(\omega_n t + \phi_k) + \sqrt{\frac{2E_s}{T}} \sum_{i=1}^J \lambda_i \cos(\omega_n t + \phi_i) + w(t) \quad (2.66)$$

where  $w(t)$  is an AWGN process with mean zero and variance  $N_0/2$ . The outputs of the in-phase and quadrature branches of the matched filters tuned to sub-channel  $n$  are

$$\begin{aligned} X_n &= \sqrt{\frac{2}{E_s T}} \int_0^T r_n(t) \cos(\omega_n t) dt \\ &= c_{nm} \lambda_k \cos(\phi_k) + \sum_{i=1}^J \lambda_i \cos(\phi_i) + \hat{w}_x \end{aligned} \quad (2.67)$$

$$\begin{aligned} Y_n &= \sqrt{\frac{2}{E_s T}} \int_0^T r_n(t) \sin(\omega_n t) dt \\ &= c_{nm} \lambda_k \sin(\phi_k) + \sum_{i=1}^J \lambda_i \sin(\phi_i) + \hat{w}_y \end{aligned} \quad (2.68)$$

where  $\hat{w}_x$  and  $\hat{w}_y$  are normalized AWGN r.v.'s with mean zero and variance  $d/2$  where  $d \triangleq N_0/E_s$ . Since  $\lambda_i \cos(\phi_i)$  and  $\lambda_i \sin(\phi_i)$  have zero means,  $X_n$  and  $Y_n$  have zero means as well. Moreover, since the terms on the right side of (2.67) and (2.68) are mutually independent Gaussian r.v.'s,  $X_n$  and  $Y_n$  are Gaussian distributed as well. Also, the variance of both  $X_n$  and  $Y_n$ , conditioned on  $J = j$ , is  $(c_{nm} + j + d)/2$ . The output of the  $n$ th detector is defined as

$$R_n = X_n^2 + Y_n^2. \quad (2.69)$$

Since both  $X_n$  and  $Y_n$  are zero-mean i.i.d Gaussian r.v.'s,  $R_n$  is exponentially distributed with mean  $\mu_j = c_{nm} + j + d$  and PDF

$$f_{R_n|J}(r|j) = \frac{1}{\mu_j} e^{-r/\mu_j} \quad r \geq 0. \quad (2.70)$$

The characteristic function of  $R_n$  is given by [1]

$$E[e^{j\omega R_n} | m_k = m] = \sum_{j=0}^{K-1} \frac{B(K-1, j, h_0)}{1 - j\omega(c_{nm} + j + d)} \quad (2.71)$$

which can be inverse Fourier transformed to give the PDFs

$$p(R_n|m) = \begin{cases} f_0(R_n) = \sum_{j=0}^{K-1} \frac{B(K-1, j, h_0) e^{-R_n/(j+d)}}{j+d} & c_{nm} = 0 \\ f_1(R_n) = \sum_{j=0}^{K-1} \frac{B(K-1, j, h_0) e^{-R_n/(1+j+d)}}{1+j+d} & c_{nm} = 1. \end{cases} \quad (2.72)$$

### 2.5.1 Optimum Combining

Several combining techniques for FH Multilevel-FSK have been proposed and studied in the literature [22, 34, 36–43]. The author in [34] discusses the *optimum* combining methods (in the ML sense) for the FH Multilevel-FSK system. We use this framework for the MC-MFSK system as well.

Since the detector outputs  $R_n, n \in \{0, \dots, M-1\}$  have been assumed to be statistically independent, the PDF under hypothesis  $H_m$ , i.e., the  $m$ th message was transmitted, is the product of the  $M$  densities:

$$p(R_0, \dots, R_{M-1}|m) = \prod_{n=0}^{M-1} p(R_n|m). \quad (2.73)$$

The ML test is then to choose  $H_m$  if

$$p(R_0, \dots, R_{M-1}|m) > p(R_0, \dots, R_{M-1}|l), \quad \text{for all } l \neq m. \quad (2.74)$$

Let us assume that of the  $L$  positions where  $\mathbf{s}_{k,m} = 1$ , there are  $L'$  positions where  $\mathbf{s}_{k,l}$  is a zero. These positions are indexed by elements of the vector  $\boldsymbol{\varepsilon}$ . This also implies that there is a different set of  $L'$  positions where  $\mathbf{s}_{k,m}$  is a zero but  $\mathbf{s}_{k,l}$  is a one. These positions are indexed by elements of the vector  $\boldsymbol{\delta}$ . The  $L - L'$  positions where both  $\mathbf{s}_{k,m}$  and  $\mathbf{s}_{k,l}$  are a one are indexed by elements of the vector  $\boldsymbol{\zeta}$ . Note that the PDFs corresponding to these  $L - L'$  positions are the same on both sides of (2.74). In the remaining  $M - 2L' - (L - L')$  positions where both  $\mathbf{s}_{k,m}$  and  $\mathbf{s}_{k,l}$  are zero, the PDFs on both sides of (2.74) are the same, and in this case we cancel them out. Therefore, (2.74) can be rewritten as

$$\prod_{j=1}^{L'} f_1(R_{\boldsymbol{\varepsilon}_j}) \prod_{i=1}^{L'} f_0(R_{\boldsymbol{\delta}_i}) \prod_{e=1}^{L-L'} f_1(R_{\boldsymbol{\zeta}_e}) \stackrel{H_m}{>} \prod_{j=1}^{L'} f_0(R_{\boldsymbol{\varepsilon}_j}) \prod_{i=1}^{L'} f_1(R_{\boldsymbol{\delta}_i}) \prod_{e=1}^{L-L'} f_1(R_{\boldsymbol{\zeta}_e}) \quad \text{for all } l \neq m \quad (2.75)$$

Dividing both sides of (2.75) by  $\prod_{e=1}^{L-L'} f_0(R_{\boldsymbol{\zeta}_e})$  and rearranging terms, we obtain

$$\prod_{j=1}^{L'} \frac{f_1(R_{\boldsymbol{\varepsilon}_j})}{f_0(R_{\boldsymbol{\varepsilon}_j})} \prod_{e=1}^{L-L'} \frac{f_1(R_{\boldsymbol{\zeta}_e})}{f_0(R_{\boldsymbol{\zeta}_e})} \stackrel{H_m}{>} \prod_{i=1}^{L'} \frac{f_1(R_{\boldsymbol{\delta}_i})}{f_0(R_{\boldsymbol{\delta}_i})} \prod_{e=1}^{L-L'} \frac{f_1(R_{\boldsymbol{\zeta}_e})}{f_0(R_{\boldsymbol{\zeta}_e})} \quad \text{for all } l \neq m \quad (2.76)$$

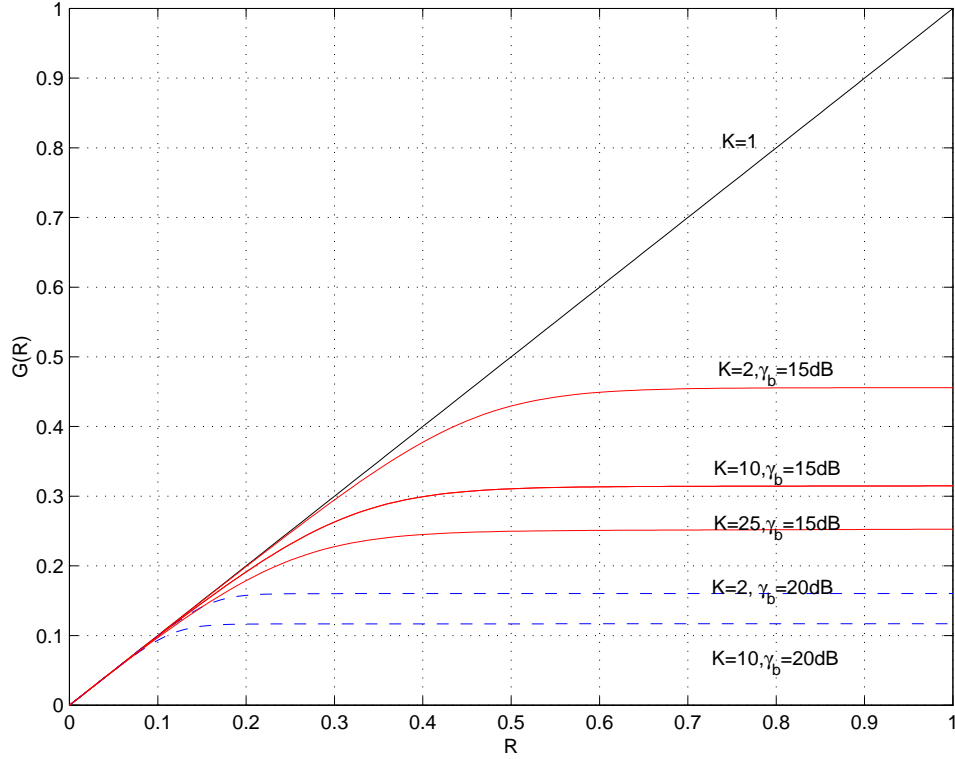


Figure 2.6: Optimum nonlinearity  $G(R)$  for different combinations of total users  $K$  and SNR/bit  $\gamma_b$

or,

$$\sum_{j=1}^{L'} \ln \left[ \frac{f_1(R_{\epsilon_j})}{f_0(R_{\epsilon_j})} \right] + \sum_{e=1}^{L-L'} \ln \left[ \frac{f_1(R_{\zeta_e})}{f_0(R_{\zeta_e})} \right] \stackrel{H_m}{>} \sum_{i=1}^{L'} \ln \left[ \frac{f_1(R_{\delta_i})}{f_0(R_{\delta_i})} \right] + \sum_{e=1}^{L-L'} \ln \left[ \frac{f_1(R_{\zeta_e})}{f_0(R_{\zeta_e})} \right]. \quad (2.77)$$

On the left side of (2.77), note that the  $L'$  elements of  $\epsilon$  and the  $L - L'$  elements of  $\zeta$  together represent the  $L$  positions indexed by  $\tilde{s}_{k,m} = [\tilde{s}_{k,m}[0] \cdots \tilde{s}_{k,m}[L-1]]^\top$ . The same applies for the right side of (2.77). Therefore, the left side and right side of (2.77) can be rewritten as single summations

$$\sum_{j \in \tilde{s}_{k,m}} \ln \left[ \frac{f_1(R_j)}{f_0(R_j)} \right] \stackrel{H_m}{>} \sum_{i \in \tilde{s}_{k,l}} \ln \left[ \frac{f_1(R_i)}{f_0(R_i)} \right] \quad \text{for all } l \neq m. \quad (2.78)$$

The summand on the right side of (2.78) can be represented by the nonlinear function

$$g(R_i) = \ln \left[ \frac{f_1(R_i)}{f_0(R_i)} \right] \quad (2.79)$$

which can be normalized to have an intercept of zero and slope of unity to yield

$$G(R_i) = \frac{g(R_i) - g(0)}{g'(0)}. \quad (2.80)$$

$G(R)$  is plotted in Figure 2.6 for different combinations of total users  $K$  and SNR/bit  $\gamma_b$ . Note that the optimum nonlinearity  $G(R)$  resembles a *linear-combiner* for a single user ( $K = 1$ ) and a *soft-limiter* (also known as *clipper*) for  $K > 1$ . Hence, from (2.78-2.80), the optimum combining method is to apply the function  $G(\cdot)$  to the detector outputs and then sum the  $L$  outputs to obtain the statistic

$$\begin{aligned}\Lambda_l &= \sum_{i \in \mathcal{S}_{k,l}} G(R_i) \\ &= \sum_{i=0}^{M-1} G(R_i) s_{k,l}[i].\end{aligned}\quad (2.81)$$

Recalling from (2.4) that  $\mathbf{v} = [G(R_0) \cdots G(R_{M-1})]^\top$ , (2.81) can be rewritten as

$$\Lambda_l = \mathbf{v}^\top \mathbf{s}_{k,l} = \langle \mathbf{v}, C_l \mathbf{a}_k \rangle = \langle \mathbf{a}_k, C_{-l} \mathbf{v} \rangle \quad (2.82)$$

where, the second equality in (2.82) follows from (2.62). Therefore, the decoding rule can be written as

$$\hat{m}_k = \arg \max_l \Lambda_l = \arg \max_l \langle \mathbf{a}_k, C_{-l} \mathbf{v} \rangle. \quad (2.83)$$

Note that the decoding rule in (2.83) is similar to the heuristic proposed in the single-user case in (2.7).

Next, we consider some special cases. First, we show mathematically that the optimal combiner for a single user in Rayleigh fading channels is a linear-combiner. Following that, we derive the optimal combiner for a single user in an AWGN channel.

### 2.5.2 Special Case of a Single User in a Rayleigh Fading Channel

For zero interferers (hence,  $K = 1$  total users) in (2.72) and (2.79), the optimum nonlinearity reduces to

$$g(R_i) = \ln \left[ \frac{d}{1+d} \frac{e^{-R_i/(1+d)}}{e^{-R_i/d}} \right] \quad (2.84)$$

$$= \ln \left[ \frac{d}{1+d} \right] + \frac{R_i}{d(1+d)}. \quad (2.85)$$

Since  $d$  is a constant independent of the transmitted message, it can be ignored in calculating the optimum combining rule:

$$\Lambda_l = \sum_{i \in \tilde{\mathcal{S}}_{k,l}} R_i. \quad (2.86)$$

Therefore, for the special case of a single user in a Rayleigh faded channel, the optimum combining rule is to linearly combine the squared outputs of the sub-channels. This observation is consistent with those regarding other MFSK systems in the literature [41, 44].

### 2.5.3 Special Case of a Single User in an AWGN Channel

In this case, on the sub-channels where the user is present,  $R_n$  has a *noncentral chi-squared* PDF [1] with noncentrality parameter  $s^2 = E^2[X_n] + E^2[Y_n] = 2$  and  $X_n$  and  $Y_n$  both have the common variance  $d/2$ . Therefore, the corresponding PDFs in (2.72) are given by

$$p(R_n|m) = \begin{cases} f_0(R_n) = \frac{1}{d}e^{-R_n/d} & c_{nm} = 0 \\ f_1(R_n) = \frac{1}{d}e^{-(2+R_n)/d}I_0\left(\frac{2\sqrt{2R_n}}{d}\right) & c_{nm} = 1. \end{cases} \quad (2.87)$$

Therefore, from (2.79) and (2.87), the optimum nonlinearity is given by

$$g(R_i) = \ln \left[ \frac{d}{1+d} \frac{e^{-(2+R_i)/d}}{e^{-R_i/d}} I_0(2\sqrt{2R_i}/d) \right] \quad (2.88)$$

$$= \ln \frac{d}{1+d} + \frac{-2}{d} + \ln I_0(2\sqrt{2R_i}/d) \quad (2.89)$$

$$\approx \ln \frac{d}{1+d} + \frac{-2}{d} + \frac{2\sqrt{2}}{d} \sqrt{R_i} \quad (2.90)$$

where, in going from (2.89) to (2.90), we used the approximation  $I_0(x) \approx e^x$  [44]. Ignoring the constants, this yields the well known result that the optimum nonlinearity for

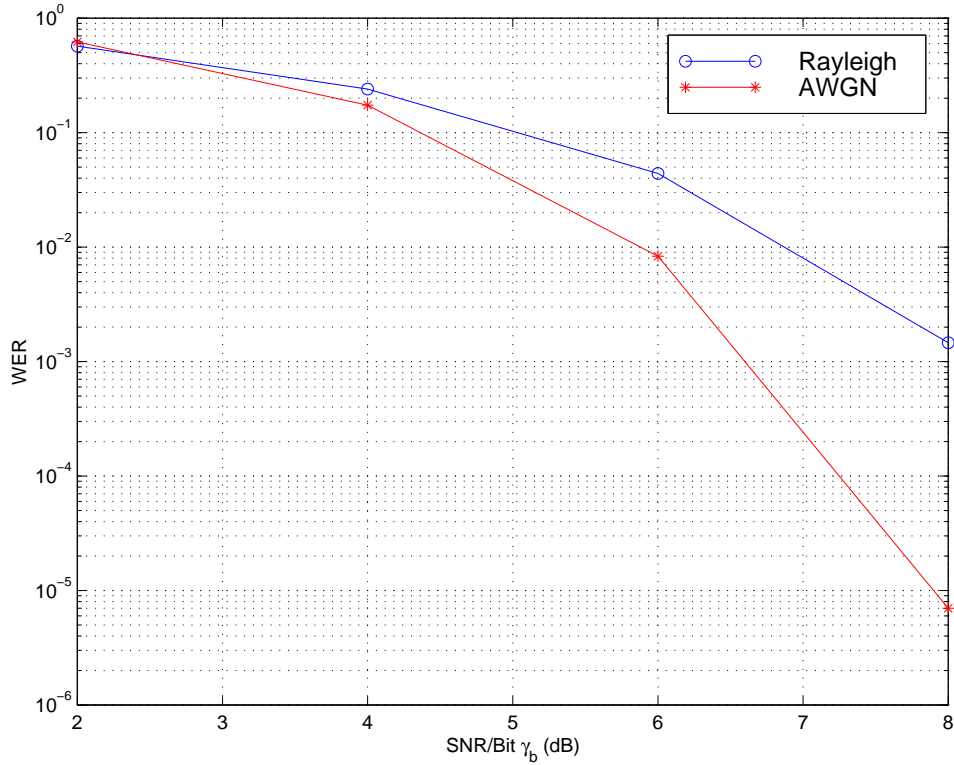


Figure 2.7: Simulated WER for a single user at low SNRs in different channel conditions at  $(L, M) = (20, 1328)$

a single user employing noncoherent detection in an AWGN channel is the *envelope-detector* [1]. The optimum combining rule in this case is

$$\Lambda_l = \sum_{i \in \mathfrak{s}_{k,l}} \sqrt{R_i}. \quad (2.91)$$

Figure 2.7 compares, through simulations, the performance of a single user at low SNRs, in Rayleigh fading and AWGN channel conditions. The linear combiner (2.86) was used for the Rayleigh fading case and the envelope detector (2.91) was used for the AWGN case.

## 2.6 Selection of Detection Threshold

In Section 2.5.1 it was shown that the optimal detector can be approximated by a soft-limiter (2.80). The soft-limiter uses a detection threshold to clip the signal. In this

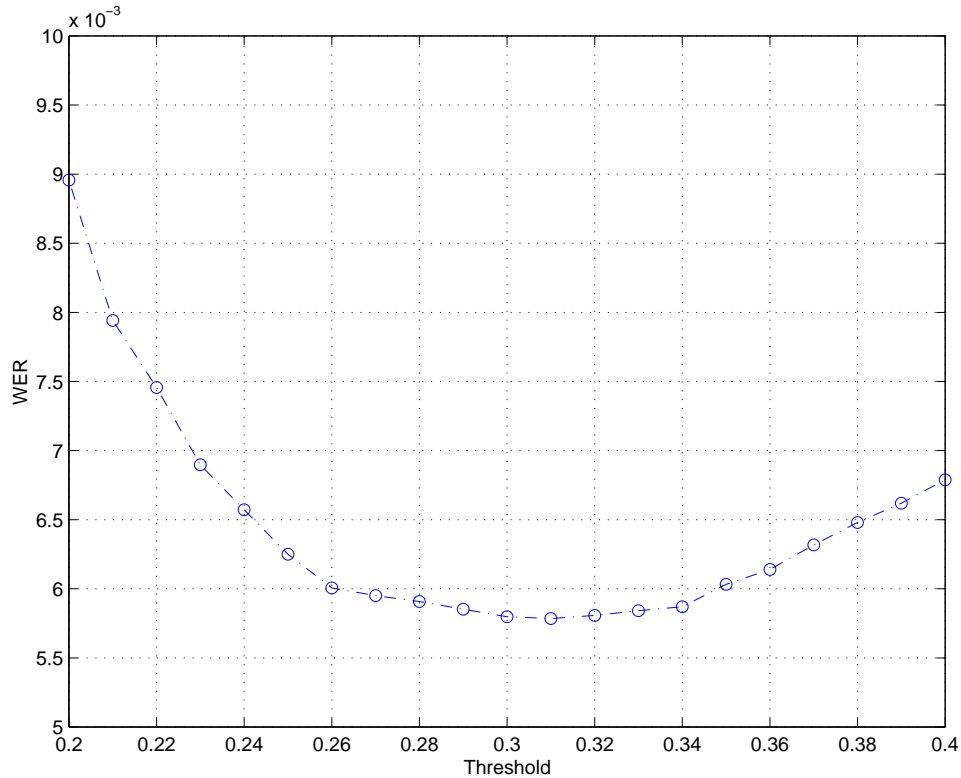


Figure 2.8: Simulated WER versus detection threshold for the soft-limiter for  $(K, L, M) = (25, 20, 1328)$  at  $\gamma_b = 15\text{dB}$

section, we discuss the selection of this threshold for the soft-limiter as well as other detectors.

### 2.6.1 Threshold Selection for Soft Limiter

From (2.71) since  $E[R_n|m] = c_{nm}$  in the absence of interferers and AWGN, we select  $G(1)$  as the detection threshold for the soft-limiter. As also observed in [34], the Word Error Rate (WER) is not very sensitive to the selection of this threshold. As an illustration of this, consider the plot of WER against the detection threshold at  $\gamma_b = 15\text{dB}$  shown in Figure 2.8. From the figure, it can be seen that the threshold that yields the minimum WER of  $5.78e - 3$  is 0.31 where as selecting  $G(1) = 0.25$  as the threshold yielded a WER of  $6.25e - 3$ , a difference of 8.06%. Using  $G(1)$  as the detection threshold, the soft-limiter detector can be defined as

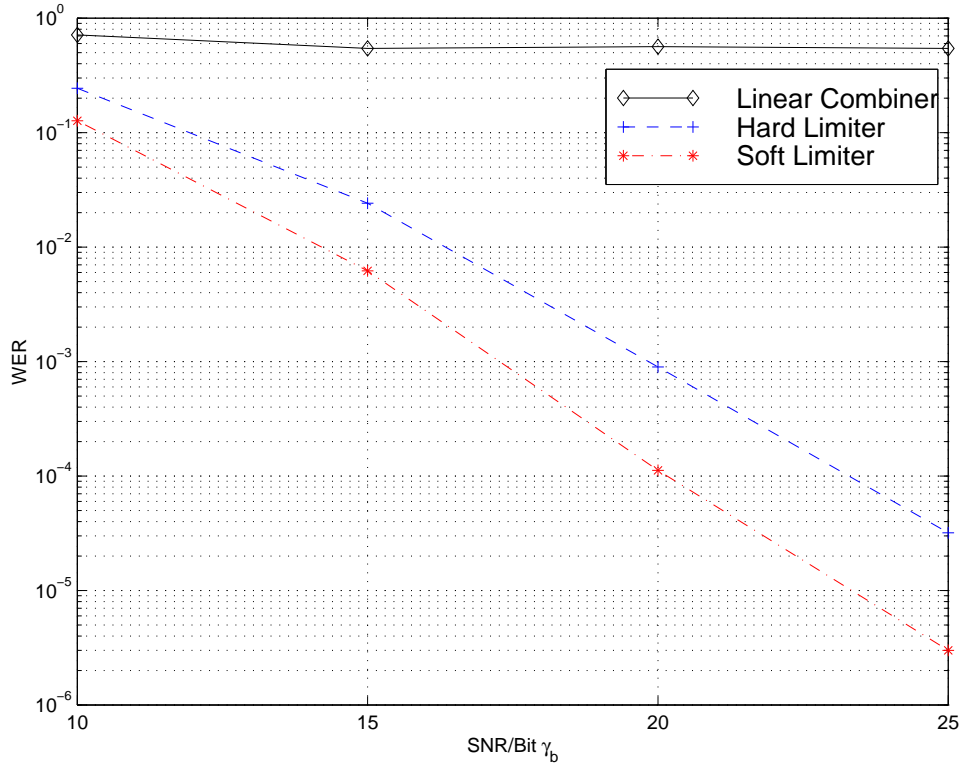


Figure 2.9: Simulated WER versus average SNR/bit in a Rayleigh fading channel for  $(K, L, M) = (25, 20, 1328)$

$$G_S(R) = \begin{cases} R, & 0 \leq R \leq G(1) \\ G(1), & G(1) < R < \infty. \end{cases} \quad (2.92)$$

We consider two other approximations to  $G(R)$ , namely the hard-limiter

$$G_H(R) = \begin{cases} 0, & 0 \leq R \leq G(1) \\ G(1), & G(1) < R < \infty \end{cases} \quad (2.93)$$

and the linear-combiner

$$G_L(R) = R, \quad 0 \leq R < \infty. \quad (2.94)$$

The hard and soft limiters will jointly be referred to as the *limiters*. Figure 2.9 compares the WER versus  $\gamma_b$  performance of the various detectors in a moderately loaded system in a Rayleigh fading channel. Figure 2.10 plots the same for only the limiters in a heavily loaded system. It is shown that in the high-SNR regime, the systems become

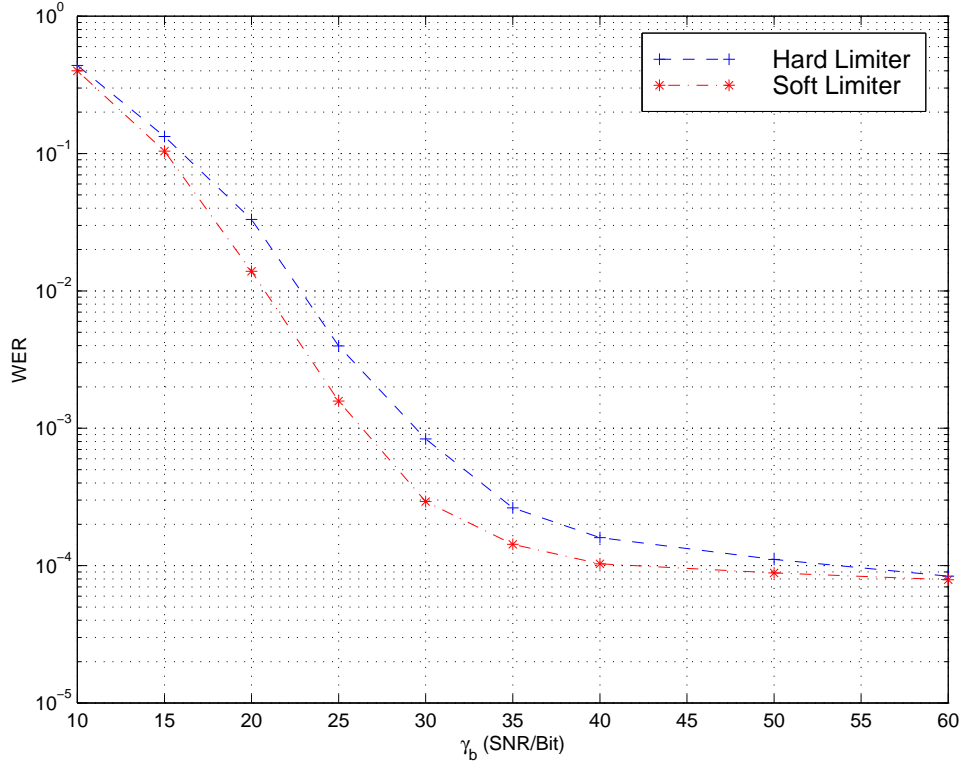


Figure 2.10: Simulated WER versus average  $\gamma_b$  in a Rayleigh fading channel for a heavily loaded system for  $(K, L, M) = (40, 20, 1328)$

interference limited, as a result of which, the limiters asymptotically approach the same WER. This is due to the fact that for high values of  $\gamma_b$ , the detection threshold  $G(1)$  approaches zero as shown in Figure 2.11. Moreover from (2.69), at high-SNRs, the normalized noise variance  $d \approx 0$  yielding  $R \approx 0$  on sub-channels where no user is present. This reduces the limiters to simple activity detectors, yielding a non-zero value of  $G(1)$  on the sub-channels where at least one user is present, and zero otherwise. Therefore, in a high-SNR channel, the channel reduces to an OR channel, yielding

$$G(R_i) = G(1) \bigvee_j s_{j,m_j}[i]. \quad (2.95)$$

Further, using the definition of  $\mathbf{v} = [G(R_0) \cdots G(R_{M-1})]^\top$  from (2.4) yields

$$\mathbf{v} = G(1) \bigvee_j \mathbf{s}_{j,m_j} = G(1) \bigvee_j C_{m_j} \mathbf{a}_j. \quad (2.96)$$

In a single-user scenario,

$$\mathbf{v} = G(1) C_m \mathbf{a} \quad (2.97)$$

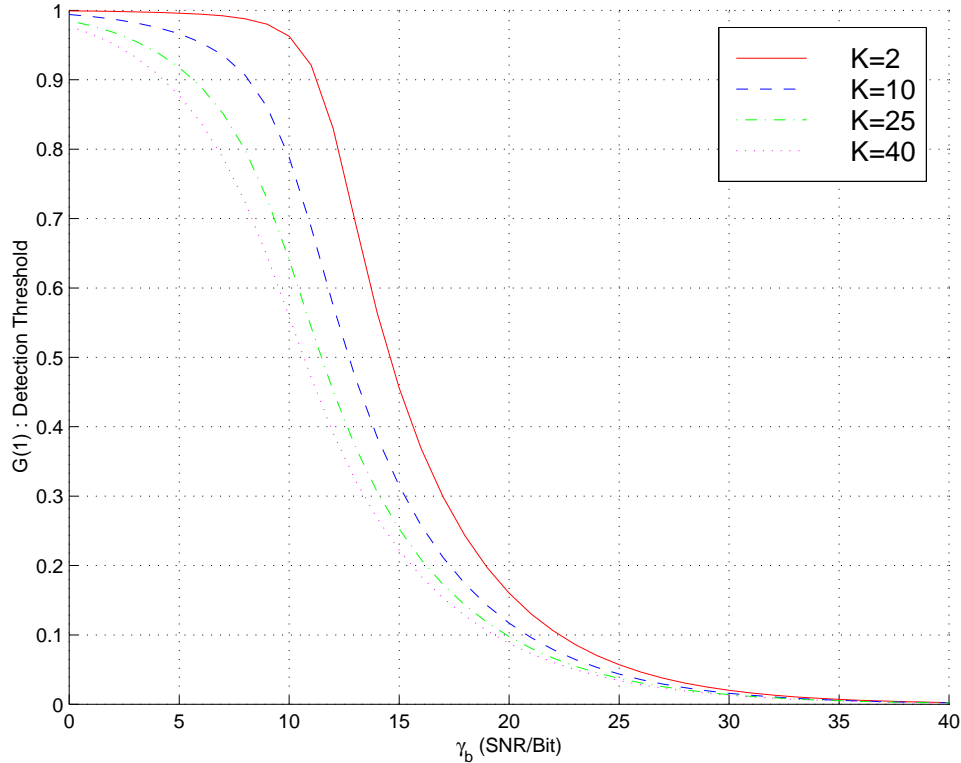


Figure 2.11: Detection threshold  $G(1)$  as a function of  $\gamma_b$  for different number of total users  $K$

which is exactly the same as (2.8). Hence, (2.83) and (2.97) together show that the decoding heuristic proposed in Section 2.4 is optimal in the ML sense for a single user in high-SNR channels.

## 2.6.2 Threshold Selection for an Envelope Detector

Later, in Section 2.7, the MC-MFSK system will be compared to other FH-MFSK systems [19, 23]. Since all the FH-MFSK systems discussed in this chapter use envelope detection, for a fair comparison, the performance of the MC-MFSK system should also be evaluated with an envelope detector. In this section, we develop a method for determining the detection threshold for an envelope-detector in a Rayleigh fading channel.

If we denote the number of users on a particular sub-channel by the random variable

$N$ , then, from (2.64)

$$P_N(n) = B(K, n, h_0) \quad n = 0, \dots, K. \quad (2.98)$$

The output of the envelope detector tuned to sub-channel  $m$  is defined as

$$U_m = \sqrt{R_m} = \sqrt{X_m^2 + Y_m^2} \quad (2.99)$$

where  $X_m$  and  $Y_m$  are defined in (2.67-2.68). Therefore, conditioned on the number of users  $N$ ,  $U_m$  is Rayleigh distributed with CDF [1]

$$F_{U_m|N}(u|n) = 1 - e^{-u^2/(n+d)} \quad u \geq 0. \quad (2.100)$$

The complementary CDF is denoted by  $\bar{F}_{U_m|N}(u|n)$ .

After performing energy measurement on all the  $M$  sub-channels, the receiver performs a hypothesis test on each of them. For each sub-channel,  $H_0 = \{N = 0\}$  is the hypothesis that only noise is present, whereas  $H_1 = \{N > 0\}$  is the hypothesis that at least one user is present. Let  $P[H_0]$  and  $P[H_1]$  be the *a priori* probabilities of  $H_0$  and  $H_1$ , respectively. A *false-alarm* is said to occur when the receiver declares  $H_1$  given  $H_0$  was true, and a *deletion* is said to occur when the receiver declares  $H_0$  given  $H_1$  was true. The false-alarm and deletion probabilities are denoted by  $P_{FA}$  and  $P_{MISS}$ , respectively. Given a detection threshold  $\hat{u}$ ,

$$P_{MISS} \triangleq F_{U_m|H_1}(\hat{u}|H_1) \quad (2.101)$$

$$P_{FA} \triangleq \bar{F}_{U_m|H_0}(\hat{u}|H_0). \quad (2.102)$$

From (2.100), the PDFs of  $u$  under the two hypotheses are:

$$H_0 \quad : \quad f_{U_m|H_0}(u|H_0) = \frac{2u}{d} e^{-u^2/d} \quad u \geq 0 \quad (2.103)$$

$$H_1 \quad : \quad f_{U_m|H_1,N}(u|H_1, n) = \frac{2u}{n+d} e^{-u^2/(n+d)} \quad u \geq 0, n \geq 1. \quad (2.104)$$

An example of the two PDFs is plotted in Figure 2.12.

The error probability on a sub-channel can be written as [45]

$$P_e = P_{MISS}P[H_1] + P_{FA}P[H_0] \quad (2.105)$$

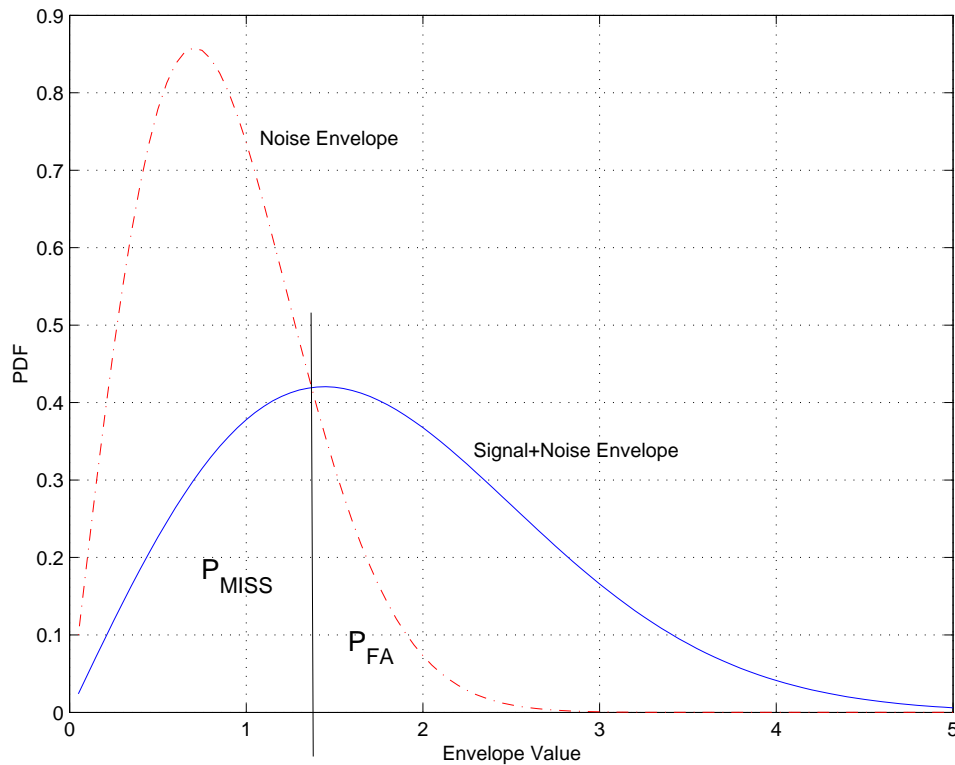


Figure 2.12: PDFs corresponding to hypotheses  $H_0$  and  $H_1$

$$= F_{U_m|H_1}(\hat{u}|H_1)P[H_1] + \bar{F}_{U_m|H_0}(\hat{u}|H_0)P[H_0] \quad (2.106)$$

$$= \sum_{n=1}^K F_{U_m|H_1,N}(\hat{u}|H_1, n)P(N=n|H_1)P[H_1] + \bar{F}_{U_m}(\hat{u}|H_0)P[H_0]$$

$$= \sum_{n=1}^K F_{U_m|N}(\hat{u}|n)P(N=n) + \bar{F}_{U_m}(\hat{u}|H_0)P[H_0]. \quad (2.107)$$

We now evaluate the optimum detection threshold  $\hat{u} = \beta$ , which minimizes (2.107) above. Since there is no closed-form expression for the first term on the right side of (2.107), we develop an upper bound instead to obtain a simple decision threshold that yields good performance. From (2.100) we have

$$F_{U_m|N}(\hat{u}|n) = 1 - e^{-\hat{u}^2/(n+d)}. \quad (2.108)$$

Observe that for a fixed  $\hat{u}$ ,  $F_{U_m|N}(\hat{u}|n)$  decreases with increasing  $n$ , or that

$$F_{U_m|N}(\hat{u}|n) \leq F_{U_m|N}(\hat{u}|1). \quad (2.109)$$

Therefore, for a fixed  $\hat{u}$ , an increase in  $n$  leads to a decrease in  $P_{MISS}$  while  $P_{FA}$  remains

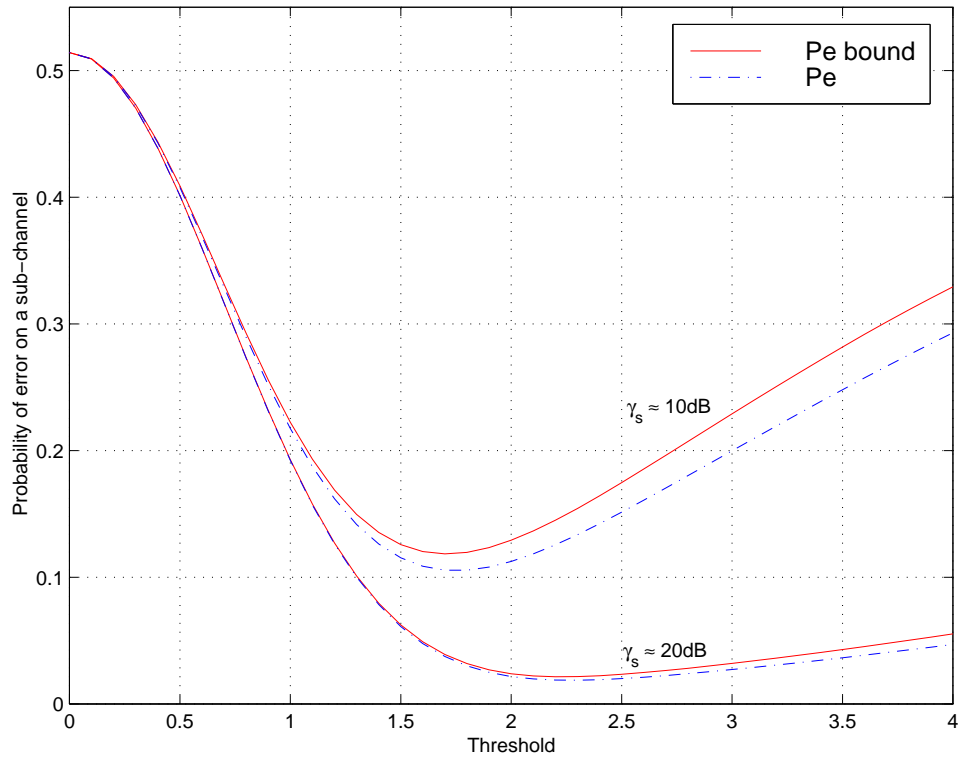


Figure 2.13: Comparison of  $P_e$  and  $\bar{P}_e$  for  $(K, L, M)=(35, 25, 1328)$

unaffected. Also,

$$\sum_{n=1}^K P(N = n) = 1 - P(N = 0) \triangleq P[H_1]. \quad (2.110)$$

Substituting (2.109) and (2.110) into (2.107) yields

$$P_e \leq F_{U_m|N}(\hat{u}|1)P[H_1] + \bar{F}_{U_m}(\hat{u}|H_0)P[H_0] \quad (2.111)$$

$$= \left(1 - e^{-u^2/(1+d)}\right) P[H_1] + \left(e^{-u^2/d}\right) P[H_0] \quad (2.112)$$

$$\triangleq \bar{P}_e. \quad (2.113)$$

Let

$$\gamma_s = \frac{1}{d} = \frac{E_s}{N_0} \quad (2.114)$$

be the average SNR per user per sub-channel. As can be seen in Figure 2.13, for high  $\gamma_s$ , the upper-bound  $\bar{P}_e$  is very close to  $P_e$ , and hence, we can minimize  $\bar{P}_e$  instead to obtain the normalized threshold

$$\beta = \sqrt{d(1+d) \ln \left[ \left(1 + \frac{1}{d}\right) \frac{P_0}{P_1} \right]} \quad (2.115)$$

where,

$$P_0 \triangleq P[H_0] \quad (2.116)$$

$$P_1 \triangleq P[H_1] = 1 - P[H_0]. \quad (2.117)$$

We denote the bit-energy by  $E_b$ . Since  $\log_2 M$  bits are transmitted as  $L$  parallel tones, each with energy  $E_s$ , we have

$$E_b \log_2 M = E_s L. \quad (2.118)$$

Therefore, substituting (2.114) in (2.118) yields

$$\gamma_s = \frac{\log_2 M E_b}{L N_0} \quad (2.119)$$

$$= \frac{\log_2 M}{L} \gamma_b. \quad (2.120)$$

Substituting  $d = 1/\gamma_s$  in (2.115), for  $\gamma_s \gg 1$

$$\beta \approx \sqrt{\frac{1}{\gamma_s} \ln \left( \frac{\gamma_s P_0}{P_1} \right)}. \quad (2.121)$$

Let  $\alpha = P_0/P_1$ . From (2.102), at  $\hat{u} = \beta$ , we have

$$P_{FA} = e^{-\beta^2/d} \quad (2.122)$$

$$= e^{-\ln(\gamma_s \alpha)} \quad (2.123)$$

and comparing (2.105) and (2.111), we have

$$P_{MISS} \leq 1 - e^{-\beta^2/(1+d)} \quad (2.124)$$

$$= 1 - e^{-\frac{1}{\gamma_s} \ln(\gamma_s \alpha)}. \quad (2.125)$$

Since

$$\lim_{\gamma_s \rightarrow \infty} \frac{\ln(\gamma_s \alpha)}{\gamma_s} = 0, \quad (2.126)$$

as  $\gamma_s \rightarrow \infty$ , both  $P_{MISS}$  and  $P_{FA}$  approach 0 as expected.

The WER versus  $\gamma_b$  performance of the envelope-detector was found to be quite similar to that of the hard-limiter.

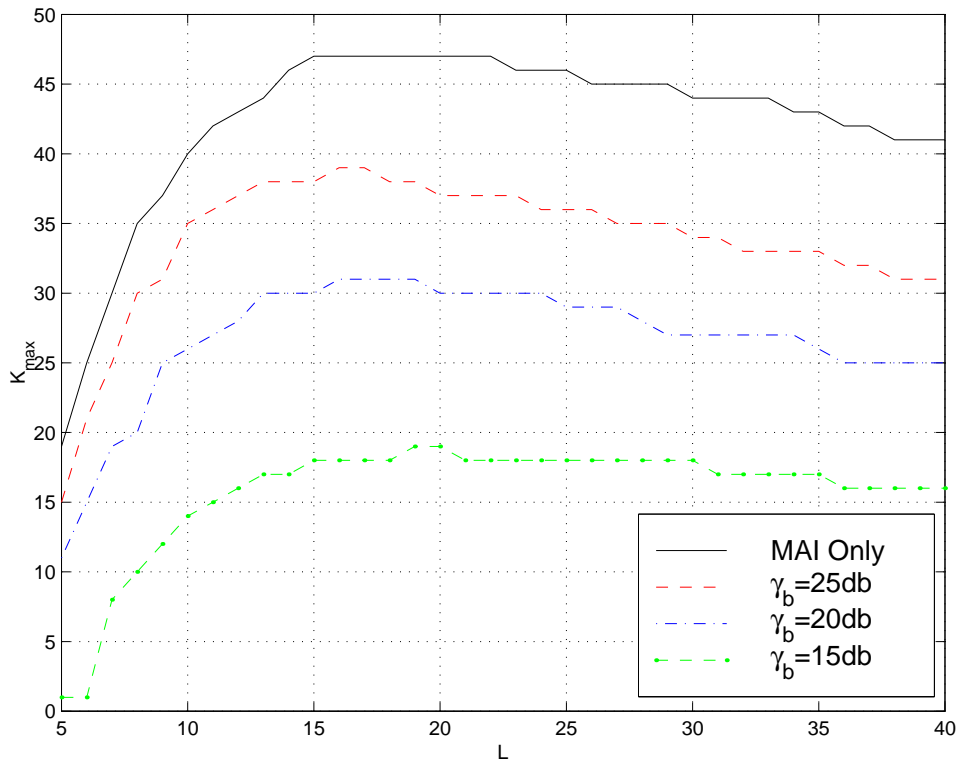


Figure 2.14: Simulated MC-MFSK system capacity versus diversity factor  $L$  in a Rayleigh fading channel with a soft-limiter for  $M = 1328$

## 2.7 Capacity of MC-MFSK and Comparison with FH-MFSK Systems

Figure 2.14 illustrates the user capacity of an MC-MFSK system using a soft-limiter in a Rayleigh fading channel based on simulation results. In the experiments, the sub-channels were subjected to *flat* and uncorrelated fading. As expected, the capacity first increases with diversity factor  $L$  and then decreases due to excessive mutual interference between the users. Also, since the diversity required increases with deteriorating channel conditions, the capacity-maximizing value of  $L$  increases as  $\gamma_b$  decreases in the figure.

Next, we compare through simulations, the performance of the MC-MFSK system

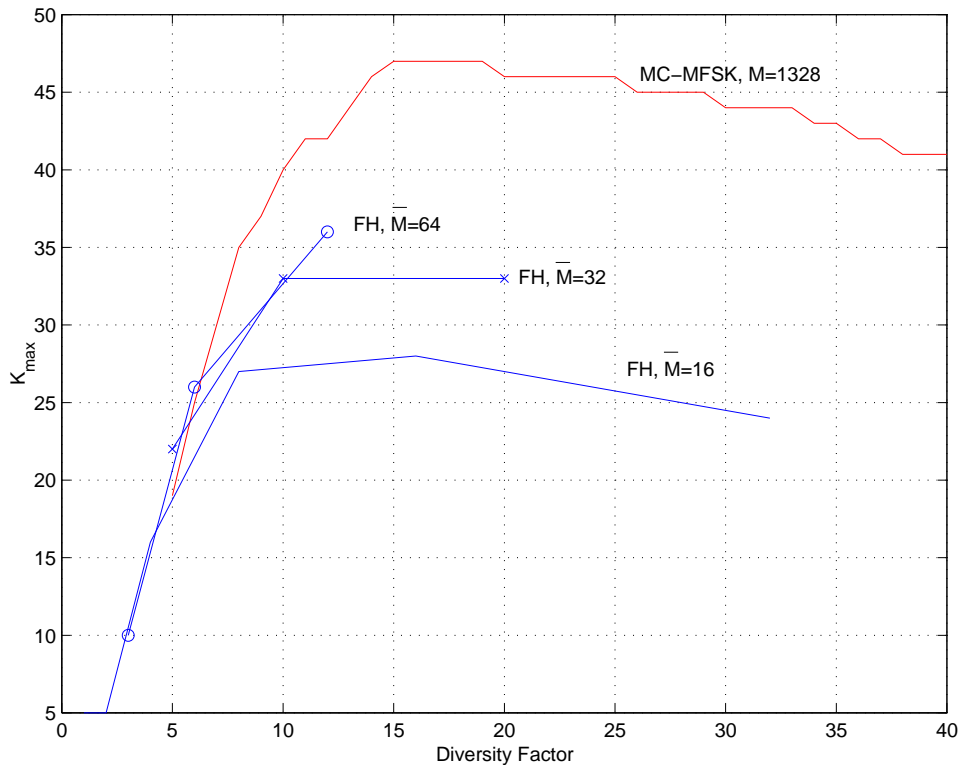


Figure 2.15: Simulated  $K_{max}$  versus diversity factor ( $L$  for MC-MFSK and  $\bar{L}$  for FH-MFSK) using envelope detectors for  $W/R_b = 128$  and  $\gamma_b = \infty$  dB

with that of FH-MFSK systems in Rayleigh fading channels. In each system, the sub-channels were simulated to experience *flat* and uncorrelated fading. Typically, for a fixed system bandwidth  $W$  and bit-rate  $R_b$ , the signaling intervals in the FH-MFSK system are shorter than those in the MC-MFSK system, as shown in Figure 1.6. Consequently, the sub-channels in the FH-MFSK system are typically wider than those in the MC-MFSK system and may experience frequency-selective fading instead of flat-fading. However, in the case of FH-MFSK systems, we made the optimistic assumption that the receivers are designed to successfully combat any frequency-selective fading effects and are only susceptible to the flat-fading phenomena. As in [23], we fixed  $W/R_b = 128$ . Since the inverse of this ratio is the spectral efficiency of a single user (1.12), for the FH-MFSK system,

$$\eta = \frac{R_b}{W} = \frac{\log_2 \bar{M}}{\bar{L} \bar{M} N} = \frac{1}{128}, \quad (2.127)$$

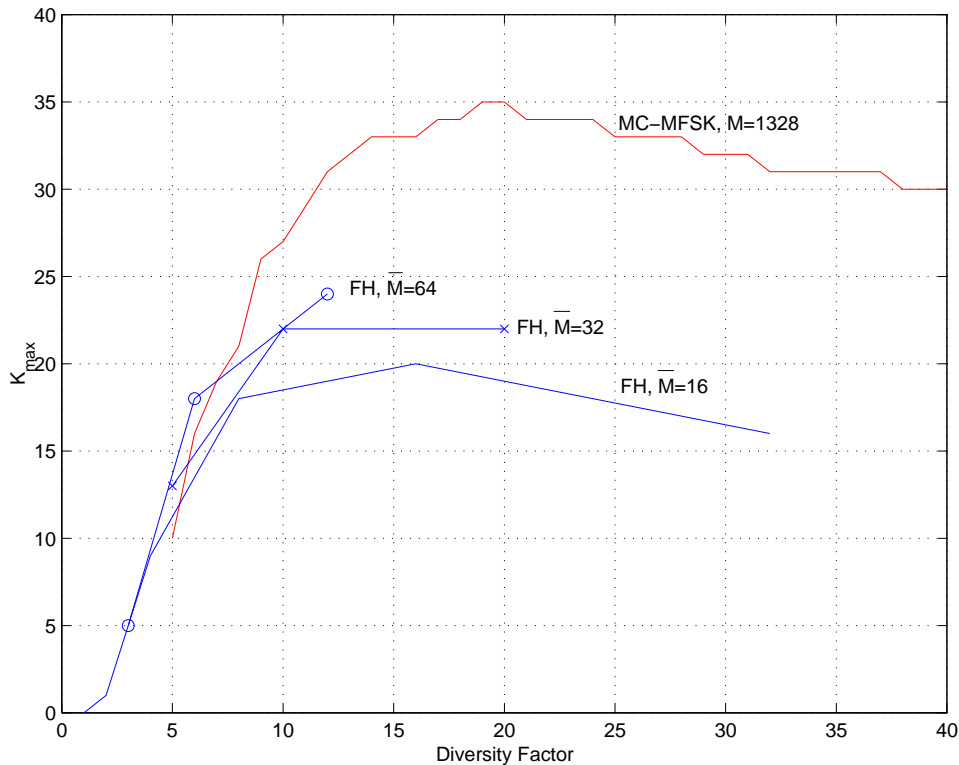


Figure 2.16: Simulated  $K_{max}$  versus diversity factor ( $L$  for MC-MFSK and  $\bar{L}$  for FH-MFSK) in Rayleigh fading channels using envelope detectors for  $W/R_b = 128$  and average  $\gamma_b = 25\text{dB}$

where, as shown in Figure 1.6,  $N$  is the number of channels,  $\bar{M}$  is the number of sub-channels per channel, and  $\bar{L}$  is the number of *serial* transmissions.

For the MC-MFSK system, from (1.14) we have

$$\eta = \frac{R_b}{W} = \frac{\log_2 M}{M} = \frac{1}{128}, \quad (2.128)$$

which yields  $M = 1328$ .

Figure 2.15 plots  $K_{max}$  versus the diversity factor ( $L$  for MC-MFSK and  $\bar{L}$  for FH-MFSK systems) in a very high SNR channel. It can be seen that the MC-MFSK system outperforms the FH-MFSK system in all cases. In all cases, we used (2.115) for selecting the threshold (with  $h_0 = 1/\bar{M}\bar{N}$  for the FH-MFSK systems) and (2.120) for determining  $\gamma_s$ . In the simulations, for each value of the diversity factor, we kept adding users to the system as long as the WER  $P_w \leq 10^{-3}$ . Also, as is evident from the figure,

$\gamma_b$	$K^*$		Spectral Efficiency $\eta_T$	
	FH-MFSK	MC-MFSK	FH-MFSK	MC-MFSK
15 dB	6	13	0.047	0.101
20 dB	17	26	0.132	0.203
25 dB	24	35	0.187	0.273
35 dB	34	45	0.265	0.351
$\infty$ dB	36	47	0.281	0.367

Table 2.1: Simulated capacity and spectral efficiency comparisons of MC-MFSK and FH-MFSK systems in Rayleigh fading for  $W/R_b = 128$

for a particular  $\bar{M}$  in FH-MFSK, not all pairs  $(\bar{L}, N)$  are allowed due to the constraint in (2.127). As in [23], it can be seen that for the FH-MFSK system, for higher values of  $\bar{M}$ , the maximum number of users can be supported at  $N = 1$ . Recall that  $N = 1$  corresponds to the FH Multilevel-FSK case proposed in [19]. For example, consider the case of  $\bar{M} = 64$  which results in  $\bar{L}N = 12$  from (2.127). It can be seen from the figure, that for this case,  $K_{max}$  peaks at  $\bar{L} = 12$  and  $N = 1$ . Hence, the figure also confirms that the FH Multilevel-FSK system outperforms the conventional FH-MFSK system. Figure 2.16 compares the performance of MC-MFSK and FH-MFSK systems in a Rayleigh fading channel at an average SNR of 25dB, and as before, it can be seen that the MC-MFSK system outperforms the FH-MFSK system in all cases. In both Figures 2.15 and 2.16, for the FH-MFSK system, the cases corresponding to  $\bar{M} = 128$  and  $\bar{M} = 256$  have been omitted as the maximum number of users in each case is less than the maximum for  $\bar{M} = 64$  and also they map to very few points due to the constraint in (2.127).

In Table 2.1, we compare  $K^*$ , the maximum number of users that can be supported at  $P_w \leq 0.001$  and spectral efficiency  $\eta_T$  (2.48) of the MC-MFSK system to that of the FH-MFSK system at different values of SNR. It can be seen that the gain of MC-MFSK over the FH-MFSK system is quite significant.

Other variations of  $M$ -ary FSK have been published in the literature as well. References

[46–48] consider an  $M$ -ary FSK system, where, different permutations of a subset of the  $M$  sub-channels within a particular channel are transmitted in parallel. However, all the design and analysis considers only a single-user scenario, and it is not clear how a desired user will be decoded in a multiuser setting. Therefore, due to lack of multiuser results, a direct comparison of such systems with the MC-MFSK system cannot be carried out. Reference [49] also considers an  $M$ -ary FSK system where tones are transmitted in parallel within a particular channel. This system is not very spectrally efficient as even for  $P_w = 0.01$ , with  $W = 3$  MHz and  $R_b = 10$  kbps, only 15 users can be supported in an AWGN channel yielding a spectral efficiency of only 0.05 (compared to 0.36 at  $P_w = 0.001$  for the MC-MFSK system).

## 2.8 Near-Far Resistance of the MC-MFSK System

In wireless systems, users near the base station may overpower users that are farther away and hence considerably degrade their communication links. This phenomenon is known as the *near-far* problem and is common in CDMA systems [11]. One of the techniques used in practice to combat the near-far problem is power control. Power control increases the complexity of the system and may be difficult to achieve in environments such as the unlicensed bands where the interferers with unknown and uncontrollable powers may cause rapid variations in the channel conditions. Hence, resistance to the near-far problem is a desirable attribute in a system.

Figure 2.17 compares through simulations, the performance of the different combiners in a Rayleigh fading channel in a scenario where the desired user's power is different from those of the interferers. The system parameters chosen were  $L = 20$  and  $M = 1328$ . The desired user had an SNR of 10dB, whereas the SNRs of 9 equal-powered interferers were varied from 4 to 20dB as shown in the figure. When the interferers are received with low powers compared to the desired user, the AWGN is the main

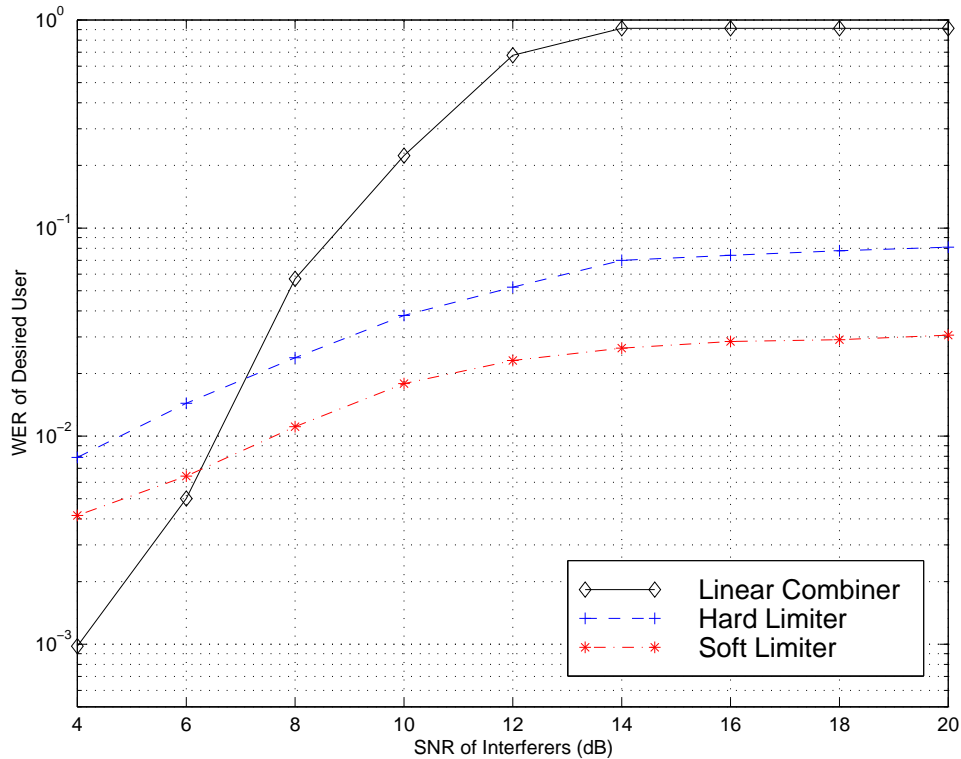


Figure 2.17: Performance comparison of the different combiners in a Rayleigh fading channel with 9 equal-powered interferers. Desired user's SNR  $\gamma_b = 10\text{dB}$

source of error, and hence, the linear-combiner being the optimal combiner in this scenario (2.86), outperforms the hard and soft limiters. However, as the powers of the interferers increase and the interferers become the dominant source of error, the limiters (2.81) outperform the linear combiner as expected. Moreover, the figure illustrates that in the near-far regime (interferers' power  $> 16\text{dB}$ ), the performance of the desired user with hard and soft limiters remains unaffected by an increase in the powers of the interferers.

## 2.9 Chapter Summary

In this chapter, we proposed a new spread-spectrum multiple-access scheme called MC-MFSK for OFDM-based systems. The system performance was evaluated in terms of an upper bound on the word error probability  $P_w$  for a single user in a high-SNR,

multiuser scenario. The upper bound on  $P_w$  was translated into a lower bound on the spectral efficiency which provides a minimum system performance guarantee. The optimum combiner (in the ML sense) was developed for different channel models and their approximations were also discussed. Finally, the MC-MFSK scheme was compared to the FH-MFSK systems and shown to yield improved performance.

## Chapter 3

# Noncoherent Multiuser Communications: Multistage Detection and Selective Filtering

### 3.1 Introduction

In this chapter, we consider noncoherent multiuser detection techniques for a system employing nonlinear modulation of non-orthogonal signals.

We follow the general spirit of [25, 28] and examine approaches that combine filtering with decision-directed methods. We propose low-complexity, sub-optimal noncoherent detectors that take advantage of certain *a priori* information available regarding the structure of the multiuser signals. We incorporate this structure into the algorithms of three detector classes [29, 30]: *constrained* detectors, soft interference cancellers, and *selective filtering* detectors discussed below.

The constrained detectors embed maximum amplitude information for the received signal components as constraints for nonlinear programming relaxations of the ML multiuser detector.

In the class of interference cancellers, we explore three variations that arise due to the noncoherent nature of the detection scheme: the serial, clipped, and parallel soft-IC (Interference Canceller). The soft-IC detectors employ the same fundamental multi-stage detection approach as their linear modulation and coherent detection counterparts, e.g., [50]. Each of these cancellers embeds the multiuser signal structure in its

detection algorithm in a different way. For the most part, our results show the soft-ICs yield better performance than the non-selective decorrelating and MMSE filters, especially in near-far scenarios.

We further improve the performance of the noncoherent multiuser detectors by exploiting additional information in the form of *selective filtering*. The selective filters use the *a priori* information that the desired user selects for transmission only one of the  $M$  messages available in its constellation. Unlike the non-selective filters of [13, 26, 27], selective filtering for the desired user attempts to suppress only the possible signals of the interfering users. Selective versions of the decorrelator, MMSE filter, and serial soft-IC are implemented. To illustrate the feasibility of the selective filters in scenarios with limited information regarding the interferers, e.g., a CDMA down-link, a blind adaptive implementation of the selective MMSE detector is also presented.

We evaluate the performance of the proposed constrained detectors, the soft-ICs, and the selective detectors and compare them with the non-selective detectors proposed in [13, 26]. Since the exact symbol error rate expressions are cumbersome or intractable for the detectors considered herein, we resort to simulations for performance evaluations.

### 3.2 System Model and Optimal Detection

We consider a synchronous CDMA system with  $K$  active users, processing gain  $N$ , and a signaling scheme where each user transmits one of  $M$  signals. A discrete-time model can be obtained by projecting the received signal onto an  $N$ -dimensional orthonormal basis. Using the pseudo-linear representation introduced in [13], we view the signal space as being an expanded signal space spanned by the  $MK$  signals:  $M$  messages for each of the  $K$  users. We concentrate on cases where the possible waveforms for all messages of all users are linearly independent. The channel is assumed to be AWGN,

and the receiver observes a superposition of the  $K$  signals.

For user  $k$ , the  $N \times 1$  vector  $\mathbf{s}_{k,m}$  denotes the signature corresponding to message  $m$  while the  $N \times M$  matrix  $\mathbf{S}_k \triangleq [\mathbf{s}_{k,1} \cdots \mathbf{s}_{k,M}]$  denotes the signature matrix. It is assumed that the signatures in  $\mathbf{S}_k$  are complex-valued, have unit norm, and are time limited. The amplitude and phase of message  $m$  of user  $k$  are denoted by  $A_{k,m}$  and  $\phi_{k,m}$ , with corresponding diagonal matrices  $\mathbf{A}_k \triangleq \text{diag}[A_{k,1}, \dots, A_{k,M}]$  and  $\mathbf{\Phi}_k \triangleq \text{diag}[e^{j\phi_{k,1}}, \dots, e^{j\phi_{k,M}}]$ . The phases are assumed to be independent and uniformly distributed over  $[0, 2\pi]$ . Let  $m_k$  be the transmitted message of user  $k$ . We define the vector  $\mathbf{b}_k = [b_{k,1} \cdots b_{k,M}]^\top$  where

$$b_{k,m} = \begin{cases} 1 & m = m_k \\ 0 & \text{otherwise.} \end{cases} \quad (3.1)$$

We note that  $\mathbf{b}_k$  belongs to the set  $F = \{\mathbf{e}_1, \dots, \mathbf{e}_M\}$  where  $\mathbf{e}_k \in \{0, 1\}^M$  has  $k$ th entry  $e_{k,k}$  equal to one and zero for all other entries. It is assumed that the  $M$  messages of a user are equiprobable. The received vector at the output of the bank of chip-matched filters can be written as

$$\mathbf{r} = \sum_{k=1}^K \mathbf{S}_k \mathbf{A}_k \mathbf{\Phi}_k \mathbf{b}_k + \mathbf{n} \quad (3.2)$$

where  $\mathbf{n}$  is an appropriately-sized AWGN vector with mean zero and covariance matrix  $\sigma^2 \mathbf{I}$ . Further,  $\mathbf{r}$  can be expressed in terms of the  $MK$ -length vector  $\mathbf{b} = [\mathbf{b}_1^\top \cdots \mathbf{b}_K^\top]^\top$ , the  $N \times MK$  matrix  $\mathbf{S} \triangleq [\mathbf{S}_1 \cdots \mathbf{S}_K]$ , the  $MK \times MK$  matrices  $\mathbf{A} \triangleq \text{diag}[\mathbf{A}_1, \dots, \mathbf{A}_K]$  and  $\mathbf{\Phi} \triangleq \text{diag}[\mathbf{\Phi}_1, \dots, \mathbf{\Phi}_K]$  as

$$\mathbf{r} = \mathbf{S} \mathbf{A} \mathbf{\Phi} \mathbf{b} + \mathbf{n}. \quad (3.3)$$

The aim of the multiuser detector is to recover the message vector  $\mathbf{b} \in F^K$ . For a given  $\mathbf{b}$ , let the vector  $\phi = [e^{j\phi_{1,m_1}} \cdots e^{j\phi_{K,m_K}}]^\top$  represent the phases corresponding to the  $K$  nonzero entries of  $\mathbf{b}$ . With known  $\mathbf{A}$  and  $\mathbf{\Phi}$ , the ML estimate of  $\mathbf{b}$  given  $\mathbf{r}$  is the solution to the *optimum* multiuser detector [11]. The estimate may be written as

$$\hat{\mathbf{b}} = \arg \max_{\mathbf{b} \in F^K} f(\mathbf{r} | \mathbf{b}, \phi, \mathbf{A}). \quad (3.4)$$

In the AWGN channel, the optimization (3.4) becomes the familiar distance minimization problem

$$\hat{\mathbf{b}} = \arg \min_{\mathbf{b} \in F^K} \|\mathbf{r} - \mathbf{S}\mathbf{A}\Phi\mathbf{b}\|^2. \quad (3.5)$$

Note that (3.4) and (3.5) describe a *coherent* detector since knowledge of  $\Phi$  is assumed.

Next, consider the case where the amplitudes,  $\mathbf{A}$ , are known at the receiver as in (3.4), but both  $\Phi$  and  $\mathbf{b}$  are unknown. Since each element of  $\phi$  must belong to the unit circle  $C_1$ , the joint ML estimate of  $\mathbf{b}$  and  $\phi$  is

$$(\hat{\mathbf{b}}, \hat{\phi}) = \arg \max_{\mathbf{b} \in F^K} \max_{\phi \in C_1^K} f(\mathbf{r}|\mathbf{b}, \phi, \mathbf{A}). \quad (3.6)$$

The implementation of this detector requires an exhaustive search over possible vectors  $\mathbf{b}$ . Further, since each of the elements of  $\phi$  lie on a unit circle, the inner maximization in (3.6) is over a non-convex set and hence there is no guarantee of finding the global minimum in (3.5). However, relaxing the constraints and allowing each of the elements of  $\phi$  to lie on the unit disk  $\overline{C}_1$  yields a convex set for the inner optimization. The resulting detector is

$$(\hat{\mathbf{b}}, \hat{\phi}) = \arg \max_{\mathbf{b} \in F^K} \max_{\phi \in \overline{C}_1^K} f(\mathbf{r}|\mathbf{b}, \phi, \mathbf{A}). \quad (3.7)$$

This detector will be referred to as the *joint* detector. The joint detector effectively assumes that  $\mathbf{A}$  characterizes the maximum amplitudes of the signals. Both the detector (3.6) and the joint detector (3.7) are generalized likelihood ratio test (GLRT) detectors that differ in their assumptions regarding the received signal amplitudes. In particular, when all elements of  $\mathbf{A}$  become large, the maximum amplitude constraint of the joint detector becomes trivial and the joint detector approaches the GLRT detector in [28] which treats the signal amplitudes as unknown.

### 3.3 Non-Selective Detection

Recently, several detection methods with reasonable complexity have been formulated that *approximate* the solution of the NP-hard ML multiuser detection problem [12,

14]. Further results using nonlinear programming techniques to approximate the ML multiuser detector for linear modulation can be found in [15, 51, 52]. In this section, similar to the linear modulation counterparts considered in [12, 14, 15], we *relax* the constraint set of the ML multiuser detection problem. We represent the structure of the signal in the form of a constraint set and explore various detectors with the same objective function yet different constraint sets.

### 3.3.1 Prior Work

To place the constrained multiuser detectors in proper context, we start by examining the decorrelative and the MMSE two-stage detectors proposed in [13, 26, 27]. These detectors combine two stages: linear filtering and single-user detection. We will denote  $\mathbf{x} = \Phi\mathbf{b}$ . Further, let  $\mathbf{z} = \widehat{\mathbf{A}\mathbf{x}}$  be the estimate of the desired vector  $\mathbf{A}\mathbf{x}$ . Then, the output of the matched filters can be written as

$$\mathbf{y} = \mathbf{S}^H \mathbf{r} = \mathbf{R}\mathbf{A}\mathbf{x} + \mathbf{S}^H \mathbf{n} \quad (3.8)$$

where  $\mathbf{R} = \mathbf{S}^H \mathbf{S}$  is the cross-correlation matrix. The first stage of the decorrelative detector [13] applies the decorrelating filter  $\mathbf{R}^{-1}$  to  $\mathbf{y}$  to obtain

$$\mathbf{z} = \mathbf{R}^{-1} \mathbf{y} = \mathbf{A}\mathbf{x} + \mathbf{R}^{-1} \mathbf{S}^H \mathbf{n}. \quad (3.9)$$

If the signals are linearly dependent, we can replace  $\mathbf{R}^{-1}$  by the Moore-Penrose generalized inverse [53]; however, for simplicity, we will assume that the signals are linearly independent.

In the first stage of the MMSE detector we apply the matrix transformation  $\mathbf{C}^H$  to the output  $\mathbf{r}$  to obtain the estimate  $\mathbf{z} = \widehat{\mathbf{A}\mathbf{x}} = \mathbf{C}^H \mathbf{r}$  that minimizes the mean-squared error  $E \left[ \|\mathbf{C}^H \mathbf{r} - \mathbf{A}\mathbf{x}\|^2 \right]$ . The solution is given in [26] as

$$\mathbf{C} = \mathbf{H}^{-1} \mathbf{S} \mathbf{E} \quad (3.10)$$

where  $\mathbf{H} = E[\mathbf{r}\mathbf{r}^H] = \mathbf{S}\mathbf{E}\mathbf{S}^H + \sigma^2\mathbf{I}_N$ ,  $\mathbf{E} = E[\mathbf{A}\mathbf{x}\mathbf{x}^H\mathbf{A}] = (1/M)\mathbf{A}^2$ , and  $\mathbf{I}_n$  is the identity matrix of dimension  $n$ . Equivalently, if the MMSE filter is applied to the matched filter output  $\mathbf{y}$  in (3.8) instead of  $\mathbf{r}$ , then  $\mathbf{z} = \tilde{\mathbf{C}}^H\mathbf{y}$ , where

$$\tilde{\mathbf{C}} = (\mathbf{R} + \sigma^2\mathbf{E}^{-1})^{-1}. \quad (3.11)$$

Note that in case of linear modulation,  $\mathbf{E} = \mathbf{A}^2$  and the familiar expression  $\mathbf{z} = (\mathbf{R} + \sigma^2\mathbf{A}^{-2})^{-1}\mathbf{y}$  is obtained [11, 54].

For both decorrelative and MMSE filtering, the filter output  $\mathbf{z}$  is an  $MK$ -length vector that is the concatenation  $\mathbf{z} = [\mathbf{z}_1^\top \cdots \mathbf{z}_K^\top]^\top$  of  $M$ -length component vectors  $\mathbf{z}_k$ . To describe decision rules for particular users, we adopt the general convention that  $\mathbf{z}_k = [x_{M(k-1)+1} \cdots x_{Mk}]^\top$  denotes the  $k$ th vector component of an  $MK$ -length vector  $\mathbf{z}$ . To address the specific elements of  $\mathbf{z}_k$ , we write  $\mathbf{z}_k = [z_{k,1} \cdots z_{k,M}]^\top$ .

In the second stage of these detectors, we follow [26, 27] who suggest using the  $k$ th component vector  $\mathbf{z}_k$  as a decoupled decision statistic to obtain an estimate  $\hat{m}_k$  of the  $k$ th user's message. The simplest such method is the maximum magnitude (MM) rule, denoted  $\mu(\mathbf{z}_k)$ , and defined by

$$\hat{m}_k = \mu(\mathbf{z}_k) \triangleq \arg \max_{m \in \{1, \dots, M\}} |z_{k,m}|^2. \quad (3.12)$$

In the event of ties, the MM rule arbitrarily chooses one of the maximizing entries. For orthogonal signaling over a single user AWGN channel, the MM rule is optimum; however, since the decorrelative and MMSE filters introduce correlation in the additive noise and/or interference components of  $\mathbf{z}_k$ , the MM rule is merely a heuristic. Single-user decoding rules for user  $k$  that exploit the correlation structure are developed in [13, 26].

### 3.3.2 Constrained Noncoherent Multiuser Detection

Our starting point for the relaxations of the constraints is the ML detector (3.6) in which the amplitudes  $\mathbf{A}$  are known but the symbols  $\mathbf{b}$  and phases  $\phi$ , or equivalently  $\Phi$ , are unknown. In this case, we estimate them jointly as  $\mathbf{x} = \Phi\mathbf{b}$ . We define the set

$$G = \left\{ e^{j\phi}\mathbf{e} \mid \mathbf{e} \in F, 0 \leq \phi \leq 2\pi \right\} \quad (3.13)$$

and observe that  $\mathbf{x} \in G^K$ . Rewriting (3.6), the jointly optimal estimate is

$$\hat{\mathbf{x}} = \arg \min_{\mathbf{x} \in G^K} \|\mathbf{r} - \mathbf{S}\mathbf{A}\mathbf{x}\|^2. \quad (3.14)$$

We observe that the minimization (3.14) is difficult because  $G^K$  is a non-convex constraint set. Due to the high complexity associated with the ML detector, reduced complexity approximations can be obtained by solving a relaxation of the original problem [55]. If we relax the constraint set such that the new constraint set is convex, then the optimizer of the quadratic objective function in (3.14) can be found efficiently via a variety of nonlinear programming methods. This observation is the key towards formulation of the approximate solutions presented in the remainder of this section.

We start with the case where the vector  $\mathbf{x}$  containing *all* the users' messages is constrained. Although the constraint  $\mathbf{x}^H\mathbf{x} = K$  is non-convex, a relaxation of the form  $\mathbf{x}^H\mathbf{x} \leq K$  results in a convex set. The estimate  $\hat{\mathbf{x}}$  is the solution to the optimization problem

$$\begin{aligned} & \text{minimize} && \|\mathbf{r} - \mathbf{S}\mathbf{A}\mathbf{x}\|^2 \\ & \text{subject to} && \|\mathbf{x}\|^2 \leq K. \end{aligned} \quad (3.15)$$

The convex set  $\|\mathbf{x}\|^2 \leq K$  can be thought of as the interior of an  $MK$ -dimensional hypersphere of radius  $\sqrt{K}$ . The solution to the above problem, derived in Appendix A.3 is the *generalized MMSE* detector [12, 14]

$$\hat{\mathbf{x}} = \mathbf{A}^{-1}(\mathbf{R} + \lambda^* \mathbf{A}^{-2})^{-1} \mathbf{y} \quad (3.16)$$

where  $\lambda^*$  is the optimum Lagrange multiplier corresponding to the global constraint (3.15). Note that (3.16) reduces to the MMSE solution [54] for  $\lambda^* = \sigma^2$ . We apply the MM rule to the filter output  $\hat{\mathbf{x}}$  to obtain the symbol decision  $\hat{m}_k = \mu(\hat{\mathbf{x}}_k)$ . The resulting detector, consisting of the filter (3.16) followed by the MM rule, will be referred to as the *global* constrained detector.

Now we consider local constraints for each individual user  $k$ . Recalling that  $\mathbf{x} = \Phi\mathbf{b}$ , the  $k$ th vector component of  $\mathbf{x}$  is  $\mathbf{x}_k = \Phi_k\mathbf{b}_k$ . Since  $\mathbf{x}_k \in G$ ,  $\mathbf{x}_k^H\mathbf{x}_k = 1$  for all  $k$ . If we relax the local constraint  $\mathbf{x}_k^H\mathbf{x}_k = 1$  to be the convex set  $\mathbf{x}_k^H\mathbf{x}_k \leq 1$ , which represents the interior of an  $M$ -dimensional hypersphere of unit radius, then the estimate  $\hat{\mathbf{x}}$  is the solution to

$$\begin{aligned} & \text{minimize} && \|\mathbf{r} - \mathbf{S}\mathbf{A}\mathbf{x}\|^2 \\ & \text{subject to} && \|\mathbf{x}_k\|^2 \leq 1 \quad k = 1, \dots, K. \end{aligned} \quad (3.17)$$

The solution to (3.17) is (see Appendix A.4)

$$\hat{\mathbf{x}} = \mathbf{A}^{-1}(\mathbf{R} + \Lambda^*\mathbf{A}^{-2})^{-1}\mathbf{y} \quad (3.18)$$

where  $\Lambda^*$  is a diagonal matrix containing the Lagrange multipliers. We then apply the MM rule described in (3.12) to the  $k$ th component vector  $\hat{\mathbf{x}}_k$  to obtain  $\hat{m}_k = \mu(\hat{\mathbf{x}}_k)$ . This detector will be referred to as the *local* constrained detector. Note that the local constrained detector is not the same as the joint detector (3.7). Although both detectors are obtained by enforcing a maximum amplitude constraint on each user  $k$ , the joint detector searches only over vectors  $\mathbf{x}$  for which each component vector  $\mathbf{x}_k$  is of the form  $ae^{j\phi_k}\mathbf{b}_k$  where  $\mathbf{b}_k \in F$  and  $0 \leq a \leq 1$ .

Note that there may be other sub-optimal schemes with different constraints that yield better performance with lower complexity compared to the detectors proposed here. Also, it is not clear whether using a more adequately constrained search space is better than the expanded search space we have considered with virtually all magnitudes and phases that satisfy a maximum energy bound (local and global constraints). These

issues require further research.

Performance comparisons of the various detectors discussed in this section will now be presented based on simulation results. It will be assumed that the  $M$  messages of user  $k$  are received with equal power, or that  $A_{k,m} = A_k$ . The SNR of user  $k$  is defined as  $A_k^2/2\sigma^2$ . In near-far scenarios, all interferers are assumed to be at the same SNR.

In the figures,  $P_s$  represents the probability of symbol error. Figure 3.1 plots  $P_s$  versus the SNR for  $K = 2$  users,  $M = 4$  messages per user, and a processing gain of  $N = 20$  for the detectors studied in this section. The parameters  $K$  and  $M$  were chosen to be small due to the implementation complexity of the *joint* detector in (3.7). However, we note that although the number of users is small,  $KM$  itself is a sizeable fraction of the processing gain  $N$  (experiments with larger processing gains are considered later for the detectors proposed in this chapter). Note also that the *global* (3.16) and *local* (3.18) constrained detectors perform very close to the MMSE detector (3.10). A similar observation has been made in [12] as well, and this may be attributed to the resemblance of the analytical solutions of constrained optimization problems to the generalized MMSE solution. Figure 3.2 shows  $P_s$  of the desired user versus the SNR of the interferers in a near-far scenario. Since the *local* constrained detector performs only slightly better than the *global* detector, it has been omitted from this figure. In the figure, when the SNRs of the interferers are high, the asymptotic error rate of the desired user with the joint detector is equivalent to the single-user case. This can be attributed to the fact that when the powers of the interferers are relatively high, the primary source of errors committed in the demodulation of the desired user is the AWGN.

### 3.3.3 Soft Interference Cancellation

Multistage detectors, also referred to as *multistage interference cancellers*, fall in the class of decision-directed multiuser detectors and are viable alternatives to popular

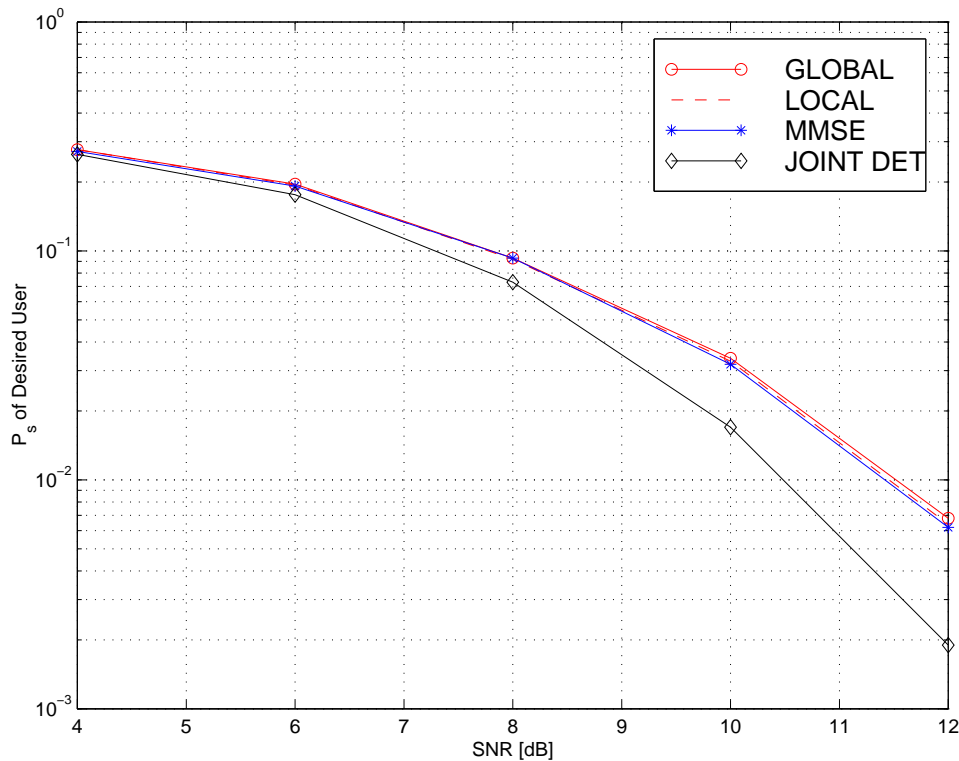


Figure 3.1: Comparison of various noncoherent detectors with  $(K, M, N)=(2, 4, 20)$

linear detectors such as the decorrelator and MMSE detectors, due to their excellent BER performance and reasonably low complexity [11]. Several multistage coherent detectors for linear modulation have been proposed in the literature, including versions using serial and parallel implementations and versions using hard and soft bit estimates [12, 50, 56–60]. The contributions of this section are: first, the detectors proposed here are noncoherent realizations of the decision directed, nonlinear detectors proposed in [50, 59]; second, new techniques are proposed to incorporate the signal structure into the decision algorithms. In particular, we propose three detectors: the serial soft-IC, the clipped soft-IC, and the parallel soft-IC.

In this section, a stage refers to a single pass through the detectors of all users. All implementations here use the decorrelator outputs in the first stage, followed by multiple stages of processing of these outputs. The goal, once again, is to obtain  $\hat{\mathbf{x}}$ , the estimate of all transmitted messages. To obtain the estimate  $\hat{\mathbf{x}}_k$  for the  $k$ th user's message, soft

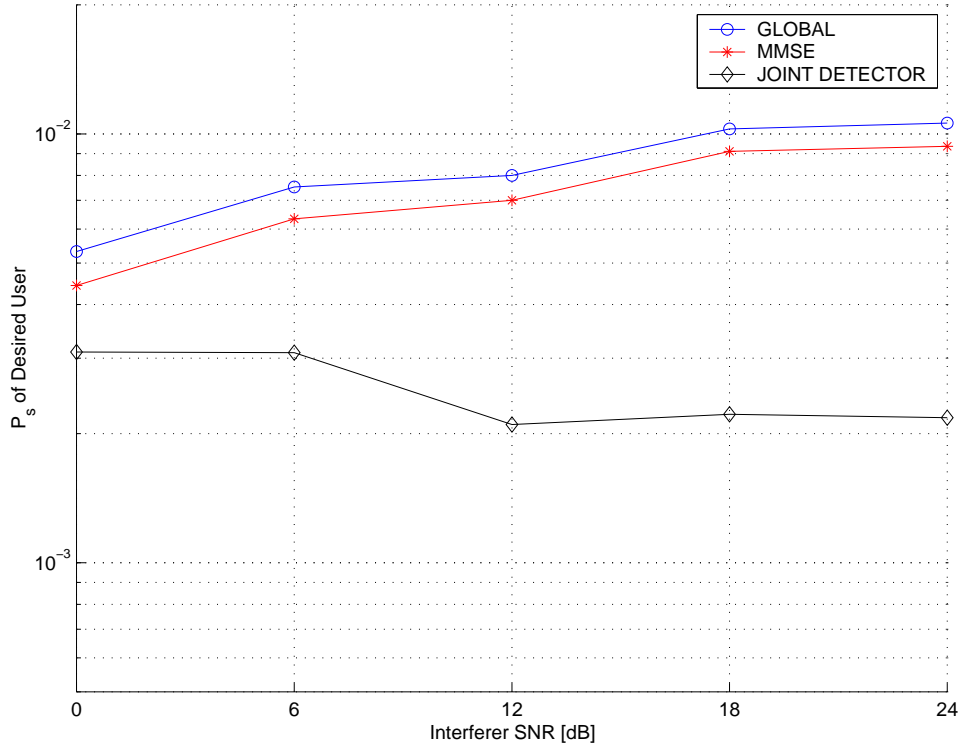


Figure 3.2: Performance in the near-far scenario with  $(K, M, N) = (2, 4, 20)$ . Desired user's SNR = 12dB

estimates are used to reconstruct the interference that is then subtracted from that user's matched filter output. The differences between these detectors arise in their implementation, e.g., serial or parallel, as well as in the types of decisions that are communicated between the users' detectors.

In the serial soft-IC detector, as shown in Figure 3.3, the first step is to determine sequentially the  $M$  estimates  $\tilde{x}_{k,1}, \dots, \tilde{x}_{k,M}$  of the  $M$  possible messages of user  $k$ . In the second step, only the entry  $\tilde{x}_{k,m}$  with the largest magnitude is retained while the other  $M - 1$  entries are forced to 0. This estimated-and-mapped vector for user  $k$  is denoted by  $\hat{\mathbf{x}}_k$ . The mapping ensures that  $\hat{\mathbf{x}}_k$  has a structure similar to that of  $\mathbf{x}_k$ . Following from (3.8), the estimate for message  $m$  of user  $k$  is (see Appendix A.5)

$$\tilde{x}_{k,m} = \frac{y_{k,m}}{A_{k,m}} - \frac{1}{A_{k,m}} \sum_{i=1}^{k-1} \sum_{j=1}^M \mathbf{s}_{k,m}^H \mathbf{s}_{i,j} A_{i,j} \hat{x}_{i,j} - \frac{1}{A_{k,m}} \sum_{j=1}^{m-1} \mathbf{s}_{k,m}^H \mathbf{s}_{k,j} A_{k,j} \tilde{x}_{k,j}$$

$$- \frac{1}{A_{k,m}} \sum_{j=m+1}^M \mathbf{s}_{k,m}^H \mathbf{s}_{k,j} A_{k,j} x_{k,j} - \frac{1}{A_{k,m}} \sum_{i=k+1}^K \sum_{j=1}^M \mathbf{s}_{k,m}^H \mathbf{s}_{i,j} A_{i,j} x_{i,j} \quad (3.19)$$

where the components on the right side of (3.19) are (from left to right): the matched filter output, the estimates of the previous  $k - 1$  users' messages, the previously detected estimates of messages of user  $k$ , the not-yet-detected messages of user  $k$ , and the not-yet-detected messages of the other users. After the  $M$  entries of user  $k$  are determined, the estimated vector  $\tilde{\mathbf{x}}_k$  is then mapped to  $\hat{\mathbf{x}}_k$  using the maximum magnitude rule

$$\hat{\mathbf{x}}_k = \mathbf{e}_{\mu(\tilde{\mathbf{x}}_k)} \tilde{\mathbf{x}}_{k,\mu(\tilde{\mathbf{x}}_k)}. \quad (3.20)$$

This vector estimate  $\hat{\mathbf{x}}_k$  is then used by user  $k + 1$  in (3.19) above for estimating its vector, and so on. The whole procedure can be repeated for multiple stages to refine the estimates.

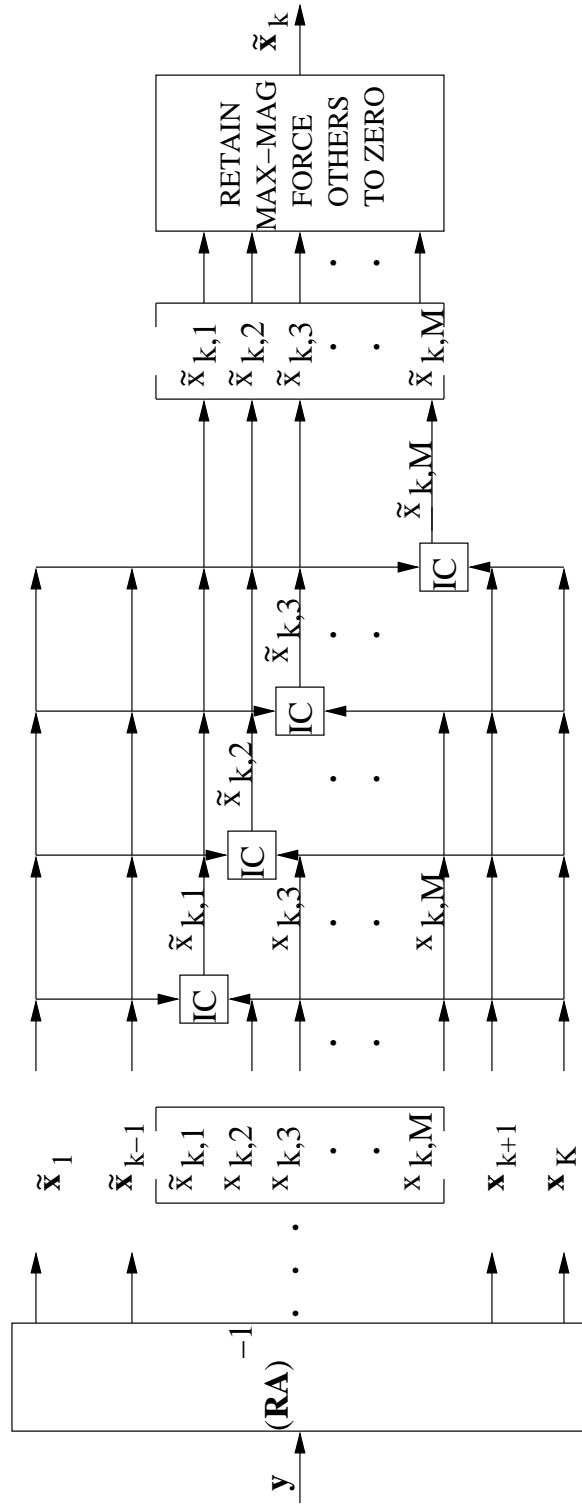


Figure 3.3: Serial soft interference canceller (Soft-IC)

The implementation of the clipped soft-IC detector employs the same first step (3.19) as also shown in Figure 3.3. In the second step, however, we incorporate the relaxed constraint  $|x_{k,i}| \leq 1$  by clipping in accordance with the following rule:

$$\hat{x}_{k,i} = \begin{cases} \tilde{x}_{k,i} & |\tilde{x}_{k,i}| \leq 1 \\ \tilde{x}_{k,i}/|\tilde{x}_{k,i}| & \text{otherwise.} \end{cases} \quad (3.21)$$

Thus, the difference between the serial soft-IC and the clipped soft-IC lies in the type of decision fed between the users.

Lastly, the parallel soft-IC differs from the serial soft-IC only in the first step. Instead of serial estimation of each element  $\tilde{x}_{k,m}$ , the parallel soft-IC estimates all elements of  $\tilde{\mathbf{x}}_k = [\tilde{x}_{k,1} \cdots \tilde{x}_{k,M}]^T$  in parallel as shown in Figure 3.4. From (3.2), we can write the received signal  $\mathbf{r}$  in terms of the components  $\mathbf{x}_k = \Phi_k \mathbf{b}_k$  as

$$\mathbf{r} = \sum_{j=1}^K \mathbf{S}_j \mathbf{A}_j \mathbf{x}_j + \mathbf{n}. \quad (3.22)$$

The matched filter vector output for user  $k$  is

$$\mathbf{y}_k = \mathbf{S}_k^H \mathbf{r} = \mathbf{R}_{kk} \mathbf{A}_k \mathbf{x}_k + \sum_{j \neq k} \mathbf{R}_{kj} \mathbf{A}_j \mathbf{x}_j + \mathbf{S}_k^H \mathbf{n}, \quad (3.23)$$

where  $\mathbf{R}_{kj} = \mathbf{S}_k^H \mathbf{S}_j$ . Therefore,  $\mathbf{x}_k$  can be estimated as

$$\tilde{\mathbf{x}}_k = (\mathbf{R}_{kk} \mathbf{A}_k)^{-1} \left( \mathbf{y}_k - \sum_{j=1}^{k-1} \mathbf{R}_{kj} \mathbf{A}_j \hat{\mathbf{x}}_j - \sum_{j=k+1}^K \mathbf{R}_{kj} \mathbf{A}_j \mathbf{x}_j \right). \quad (3.24)$$

The components on the right side of (3.24) are (from left to right): the matched filter output, the  $k-1$  processed users with their estimated-and-mapped vectors  $\hat{\mathbf{x}}_j$ , and the users that are yet to be processed. In the second step, the parallel soft-IC obtains the users' message decisions using the same maximum magnitude mapping rule (3.20) as the serial soft-IC detector.

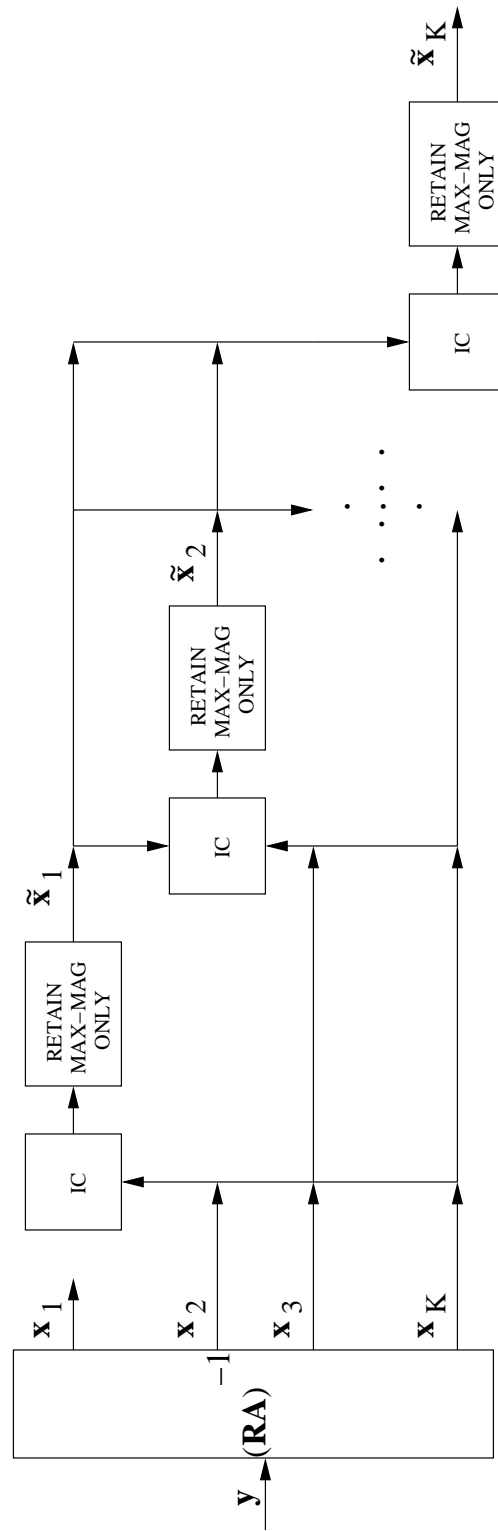


Figure 3.4: Parallel soft interference canceller

Since the serial soft-IC estimates message elements  $x_{k,m}$  one at a time, its granularity is finer than that of the parallel soft-IC which estimates the entire vector  $\mathbf{x}_k$  in one step. Hence, it is to be expected that the serial soft-IC will perform slightly better. Also, note that the serial and parallel soft-ICs can be implemented without the knowledge of the individual amplitudes  $A_{k,m}$ . Instead of estimating just  $x_{k,m}$  in (3.19), the element  $A_{k,m}x_{k,m}$  can be jointly estimated, followed by (3.20). Since the maximum-magnitude rule uses only the *relative* magnitudes, the individual amplitudes do not have to be known explicitly. It is easy to observe from (3.19) and (3.21) that this is not the case for the *clipped* soft-IC for which amplitude values must be known.

Figure 3.5 compares the performance of the various soft-ICs proposed in this chapter (3.19-3.24) to the non-selective decorrelative and MMSE detectors in a near-far scenario. In all the soft-ICs, a decorrelative first stage was followed by two more stages of matched-filter-output processing. Interestingly, the non-selective MMSE detector (3.10), (3.11) does not converge to the decorrelator in the high interferer-power region, in contrast with the performance obtained by multiuser detectors that employ linear modulation. This is a direct consequence of the fact that, in the near-far situation, the powers of the interferers are high compared to the powers associated with all possible messages of the desired user. Also, the non-selective detectors take the undesired  $M - 1$  messages of the desired user (with relatively low powers) as well as all interferers' signals (with high powers) into account in decoding the desired user's message. Thus, unlike the decorrelator, the non-selective MMSE filter does not zero-force the contributions of the  $M - 1$  undesired messages of the desired user, resulting in a performance improvement in near-far scenarios. Note that this issue does not arise for selective filters, and the selective MMSE and decorrelative detectors do converge in the near-far situations.

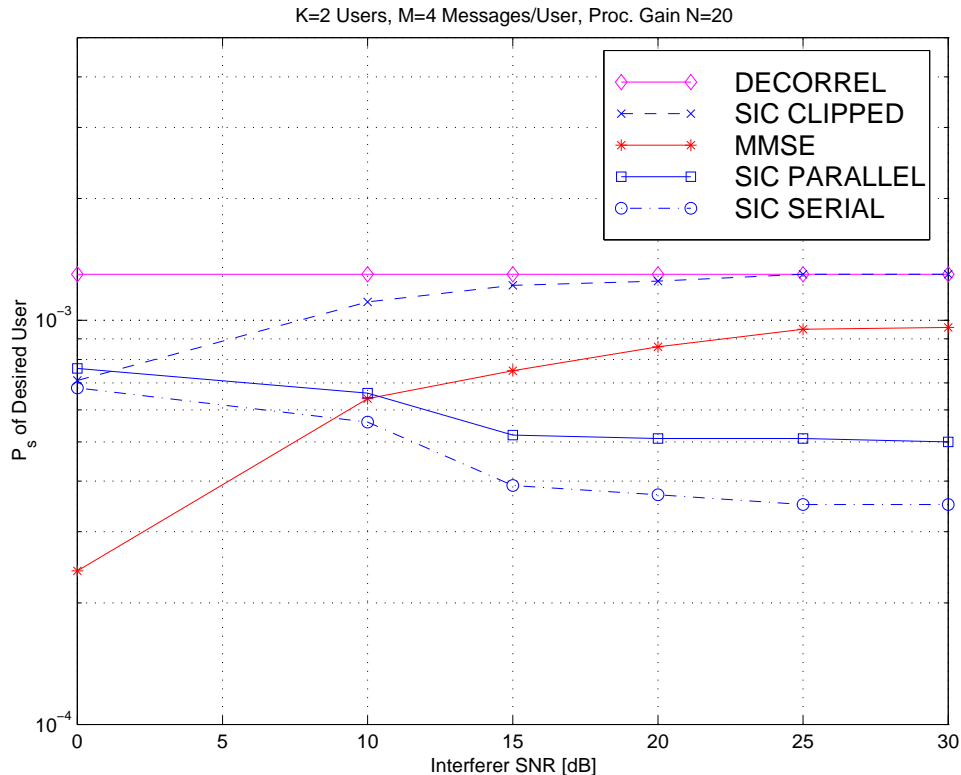


Figure 3.5: Comparison of soft-ICs in near-far scenario with  $(K, M, N) = (2, 4, 20)$ . Desired user's SNR = 14dB

### 3.4 Selective Filtering

To detect whether user  $k$  transmitted message  $m$  the non-selective detectors of Section 3.3 consider all possible signals of interferers  $j \neq k$ , as well as the other  $M - 1$  possible signals of user  $k$  as sources of interference. However, it is known *a priori* that user  $k$  transmits precisely one of its  $M$  messages. Therefore, for  $m \in \{1, \dots, M\}$ , one and only one of the  $x_{k,m}$  is nonzero for each user  $k \in \{1, \dots, K\}$ . Selective filtering makes use of this observation. Note that if the desired user's signatures (associated with the  $M$  messages) are mutually orthogonal, then the selective and non-selective detectors for this user yield identical performance. In this section, we will examine selective implementations of the decorrelator detector, the MMSE detector and a blind implementation thereof, and the soft interference canceller. To further enhance the performance of the selective detectors, a successive interference suppression (SIS) scheme

is also proposed.

In the following,  $d(i)$  will denote the  $i$ th element of a vector  $\mathbf{d}$ , while  $D(i, j)$  and  $D(i, :)$  will denote the  $(i, j)$ th element and  $i$ th row of a matrix  $\mathbf{D}$ , respectively. For notational convenience, all vectors and matrices associated with selective filtering will be denoted by a bar above the entry. Without loss of generality, we assume  $k = 1$  to be the desired user, thus, we focus on the selective detection of  $x_{1,m}$ . Specifically,  $\bar{\mathbf{y}}_m$  is constructed from  $y_{1,m}$  and the  $M(K - 1)$  entries of  $\mathbf{y}$  belonging to the interferers, the selective signature set  $\bar{\mathbf{S}}_m$  is constructed from  $\mathbf{s}_{1,m}$  and the  $M(K - 1)$  entries of  $\mathbf{S}$  belonging to the interferers, and the matrix  $\bar{\mathbf{A}}_m$  is constructed in a manner similar to  $\bar{\mathbf{S}}_m$ .

### 3.4.1 Selective Decorrelation

To formulate the selective decorrelator, we define  $H_m$  as the hypothesis that the first user transmitted signal  $\mathbf{s}_{1,m}$ . Our problem is to determine which hypothesis among  $\{H_1, \dots, H_M\}$  is correct. From (3.22), the received signal under hypothesis  $H_m$  is

$$H_m : \quad \mathbf{r} = \mathbf{s}_{1,m}A_{1,m}x_{1,m} + \sum_{k=2}^K \mathbf{S}_k \mathbf{A}_k \mathbf{x}_k + \mathbf{n} \quad (3.25)$$

and the decorrelating transformation to suppress all users  $k \neq 1$  is given by  $(\bar{\mathbf{S}}_m^H \bar{\mathbf{S}}_m)^{-1} \bar{\mathbf{S}}_m^H$  [11]. Thus we first construct

$$\bar{\mathbf{y}}_m = \bar{\mathbf{S}}_m^H \mathbf{r} = \bar{\mathbf{S}}_m^H \mathbf{S} \mathbf{A} \mathbf{x} + \bar{\mathbf{S}}_m^H \mathbf{n} \quad (3.26)$$

followed by the *selective* transformation

$$\bar{\mathbf{z}}_m = \bar{\mathbf{R}}_m^{-1} \bar{\mathbf{y}}_m = \bar{\mathbf{R}}_m^{-1} \bar{\mathbf{S}}_m^H \mathbf{S} \mathbf{A} \mathbf{x} + \bar{\eta}_m \quad (3.27)$$

where  $\bar{\mathbf{R}}_m = \bar{\mathbf{S}}_m^H \bar{\mathbf{S}}_m$ , and  $\bar{\eta}_m = \bar{\mathbf{R}}_m^{-1} \bar{\mathbf{S}}_m^H \mathbf{n}$  is zero-mean Gaussian with covariance matrix  $\sigma^2 \bar{\mathbf{R}}_m^{-1}$ . Since only the first entry of  $\bar{\mathbf{z}}_m$  contains the information regarding the first user's information, we construct a new vector  $\mathbf{v}$  consisting of only the first entries of

the  $M$  selective filter outputs,  $\bar{\mathbf{z}}_1, \dots, \bar{\mathbf{z}}_M$ , as follows

$$\mathbf{v} = \begin{bmatrix} \bar{\mathbf{z}}_1(1) \\ \vdots \\ \bar{\mathbf{z}}_M(1) \end{bmatrix} = \begin{bmatrix} \bar{\mathbf{R}}_1^{-1}(1, :) \bar{\mathbf{S}}_1^H \mathbf{S} \mathbf{A} \mathbf{x} + \bar{\eta}_1(1) \\ \vdots \\ \bar{\mathbf{R}}_M^{-1}(1, :) \bar{\mathbf{S}}_M^H \mathbf{S} \mathbf{A} \mathbf{x} + \bar{\eta}_M(1) \end{bmatrix} = \mathbf{U} \mathbf{S} \mathbf{A} \mathbf{x} + \bar{\boldsymbol{\eta}} \quad (3.28)$$

where the matrix  $\mathbf{U}$  consists of  $\bar{\mathbf{R}}_m^{-1}(1, :) \bar{\mathbf{S}}_m^H$  as its  $m$ th row, and  $\bar{\boldsymbol{\eta}}$  consists of the first element of  $\bar{\boldsymbol{\eta}}_m$  as its  $m$ th element. Note that  $\mathbf{v}$  is also the estimate  $\widehat{\mathbf{A}}_1 \mathbf{x}_1$ , therefore, we apply the MM rule to  $\mathbf{v}$  to obtain  $\hat{m}_1$ . An observation that will be useful later on is that

$$\bar{\mathbf{R}}_m^{-1}(1, :) \bar{\mathbf{S}}_m^H \mathbf{s}_{k,l} = 0, \quad k \neq 1, m = 1, \dots, M, l = 1, \dots, M. \quad (3.29)$$

That is, the interference from the messages of the other  $K - 1$  interferers is suppressed in the vector  $\mathbf{U} \mathbf{S} \mathbf{A} \mathbf{x}$ . However, the cross-correlations between users do appear in the transformed noise vector  $\bar{\boldsymbol{\eta}}$ .

The selective decorrelator uses the MM rule which is based on a heuristic. Hence, it is of interest to see how well it compares to the *optimum* decision rule. The optimum selective decorrelator is derived in Appendix A.6. A union bound on the message error probability is derived in Appendix A.7. Figure 3.6 compares the performance of the MM-rule based selective decorrelator with the optimum decision rule and the union bound.

### 3.4.2 Selective MMSE Detection

The MMSE detector is popular due to its amenability to adaptive implementation. Blind adaptive implementations of detectors are useful since they only require the signature and timing of the desired user. They are especially attractive for the CDMA downlink, where due to the dynamic environment, it may be difficult for a mobile user to obtain accurate information regarding signatures and timings of other active users in the system [61–63]. In this section, we will first discuss the selective version of the MMSE filter (3.10) and then we will formulate a blind adaptive implementation.

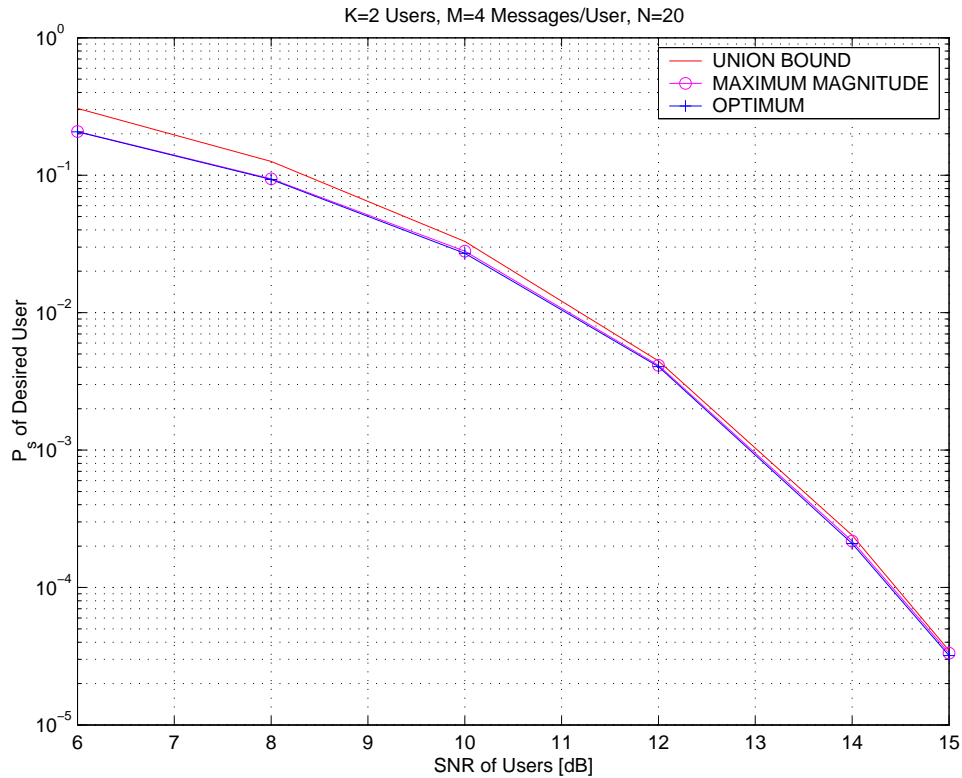


Figure 3.6: Performance comparison of the MM-rule based selective decorrelator, the optimum decision rule, and the union bound

The selective MMSE filter for the first user is obtained using an approach similar to the one used to obtain the selective decorrelator, specifically, we apply an MMSE transformation to the received signal (3.25), under each hypothesis  $m \in \{1, \dots, M\}$ . From (3.10), the selective MMSE filter corresponding to the  $m$ th signature is

$$\bar{\mathbf{C}}_m = \bar{\mathbf{H}}_m^{-1} \bar{\mathbf{S}}_m \bar{\mathbf{E}}_m \quad (3.30)$$

where  $\bar{\mathbf{E}}_m = (1/M) \bar{\mathbf{A}}_m^2$  and  $\bar{\mathbf{H}}_m = \bar{\mathbf{S}}_m \bar{\mathbf{E}}_m \bar{\mathbf{S}}_m^H + \sigma^2 \mathbf{I}_N$ . The filter vector  $\bar{\mathbf{c}}_{1,m}$  corresponding to the  $m$ th signature of the first user is the first column of  $\bar{\mathbf{C}}_m$ , i.e.,  $\bar{\mathbf{c}}_{1,m} = \bar{\mathbf{C}}_m(:, 1)$ .

We will now discuss a blind adaptive implementation of (3.30) above. A blind adaptive implementation of the noncoherent non-selective MMSE detector was proposed in [26]. We extend that algorithm to implement a blind adaptive version of the selective MMSE detector. Since the first user is the user of interest, the filter coefficients of only this user are adaptively varied. Representing the  $m$ th diagonal entry of  $\mathbf{E}$  by  $E_m$ ,

the filter vector  $\mathbf{c}_{1,m}$  corresponding to the  $m$ th signature of the first user can be obtained as

$$\mathbf{c}_{1,m} = (\bar{\mathbf{S}}_m \bar{\mathbf{E}}_m \bar{\mathbf{S}}_m^H + \sigma^2 \mathbf{I}_N)^{-1} \mathbf{s}_{1,m} E_m. \quad (3.31)$$

Note that  $\mathbf{c}_{1,m}$  corresponds to the first column of  $\bar{\mathbf{C}}_m$ . If we denote

$$\bar{\mathbf{r}}_m = \bar{\mathbf{S}}_m \bar{\mathbf{A}}_m \bar{\mathbf{x}}_m + \mathbf{n} \quad (3.32)$$

then

$$\mathbf{c}_{1,m} = (E[\bar{\mathbf{r}}_m \bar{\mathbf{r}}_m^H])^{-1} \mathbf{s}_{1,m} E_m. \quad (3.33)$$

Note that in the non-selective version in [26], the filter (3.33) involves the term  $\mathbf{r} \mathbf{r}^H$  which is readily available. In contrast, only a subset of that information  $\bar{\mathbf{r}}_m$  is needed here and it cannot be obtained explicitly due to a lack of knowledge of the signature set  $\bar{\mathbf{S}}_m$ . This problem can be circumvented by writing  $\bar{\mathbf{r}}_m$  as

$$\bar{\mathbf{r}}_m = \mathbf{r} - \sum_{i \neq m} \mathbf{s}_{1,i} A_{1,i} x_{1,i} \quad (3.34)$$

$$= \mathbf{r} - \tilde{\mathbf{S}}_m \tilde{\mathbf{A}}_m \tilde{\mathbf{x}}_m \quad (3.35)$$

where  $\tilde{\mathbf{S}}_m$  is the signature matrix of the first user without the  $m$ th signature. Hence, its dimension is  $N \times (M - 1)$ . The terms  $\tilde{\mathbf{A}}_m$ ,  $\tilde{\mathbf{E}}_m$  and  $\tilde{\mathbf{x}}_m$  may be interpreted in a similar manner. It can be shown that

$$E[\bar{\mathbf{r}}_m \bar{\mathbf{r}}_m^H] = E[\mathbf{r} \mathbf{r}^H] - \tilde{\mathbf{S}}_m \tilde{\mathbf{E}}_m \tilde{\mathbf{S}}_m^H. \quad (3.36)$$

Since the receiver knows the signatures of the desired user, it can construct  $\tilde{\mathbf{S}}_m \tilde{\mathbf{E}}_m \tilde{\mathbf{S}}_m^H$  and extract  $\bar{\mathbf{r}}_m$  from the received signal  $\mathbf{r}$ . Extending the stochastic gradient algorithm in [26], the adaptation for the  $m$ th filter vector may then be expressed as

$$\mathbf{c}_{1,m}[n+1] = \mathbf{c}_{1,m}[n] - \mu [(\mathbf{r}[n] \mathbf{r}^H[n] - \tilde{\mathbf{S}}_m \tilde{\mathbf{E}}_m \tilde{\mathbf{S}}_m^H) \mathbf{c}_{1,m}[n] - E_m \mathbf{s}_{1,m}]. \quad (3.37)$$

We use the Normalized Squared Error (NSE) criterion [26] to study the convergence properties of the filter coefficients. The NSE at the  $n$ th iteration is defined as

$$\text{NSE}[n] = \frac{1}{M} \sum_{m=1}^M \frac{\|\bar{\mathbf{c}}_{1,m} - \mathbf{c}_{1,m}[n]\|^2}{\|\bar{\mathbf{c}}_{1,m}\|^2}. \quad (3.38)$$

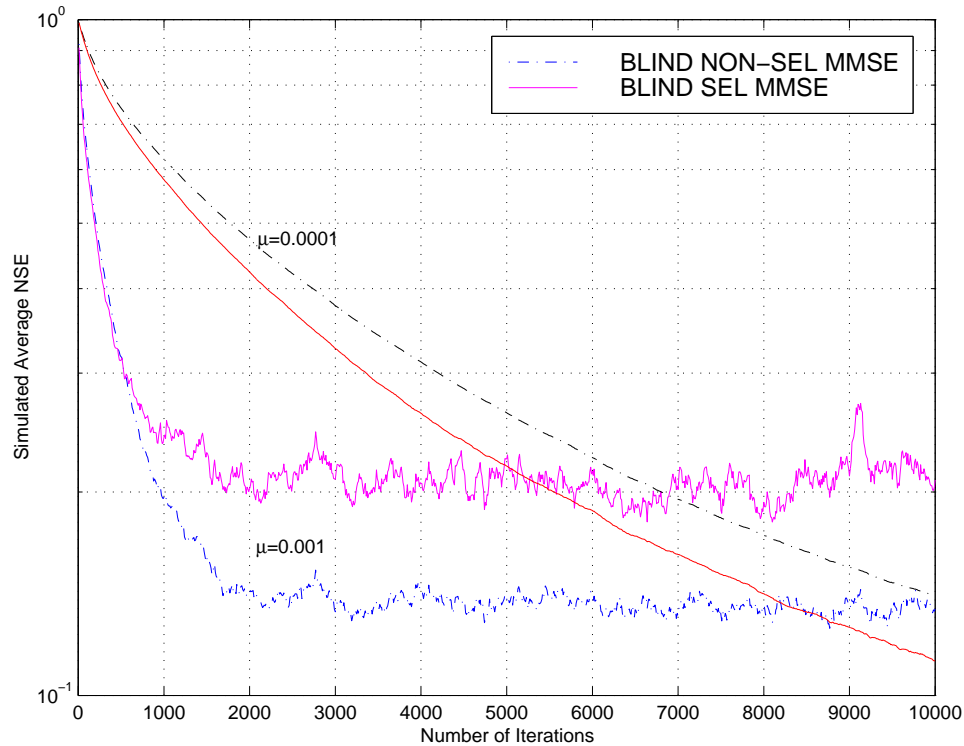


Figure 3.7: Comparison of the convergence rates of the blind adaptive selective and non-selective MMSE filters with  $(K, M, N)=(5, 4, 20)$  and variable step-size  $\mu$

Note that since the structures of the non-selective and selective MMSE detectors are similar, the convergence analysis of the former [26] can be easily extended to the latter to obtain the upper bound on the step size  $\mu$  to ensure convergence.

Figure 3.7 shows the NSE (3.38) of the blind adaptive selective (3.37) and non-selective MMSE detectors [26] averaged over 10 runs, for different step sizes  $\mu$ . The limiting MSE (mean squared error) of the detector is proportional to the value of NSE to which the filter coefficients converge. The step size impacts both the rate of convergence as well as the limiting MSE, and the tradeoff between the two is apparent from the figure. It can be seen that a larger  $\mu$  brings about faster convergence but at the cost of a higher limiting MSE. The selective detector converges to a lower value of NSE compared to its non-selective counterpart at  $\mu = 0.0001$  and vice-versa at  $\mu = 0.001$ . The performance of the blind selective MMSE detector is illustrated in Figure 3.8 and compared with that of the blind non-selective MMSE (Figure 7(b) of [26]) as well as the non-blind

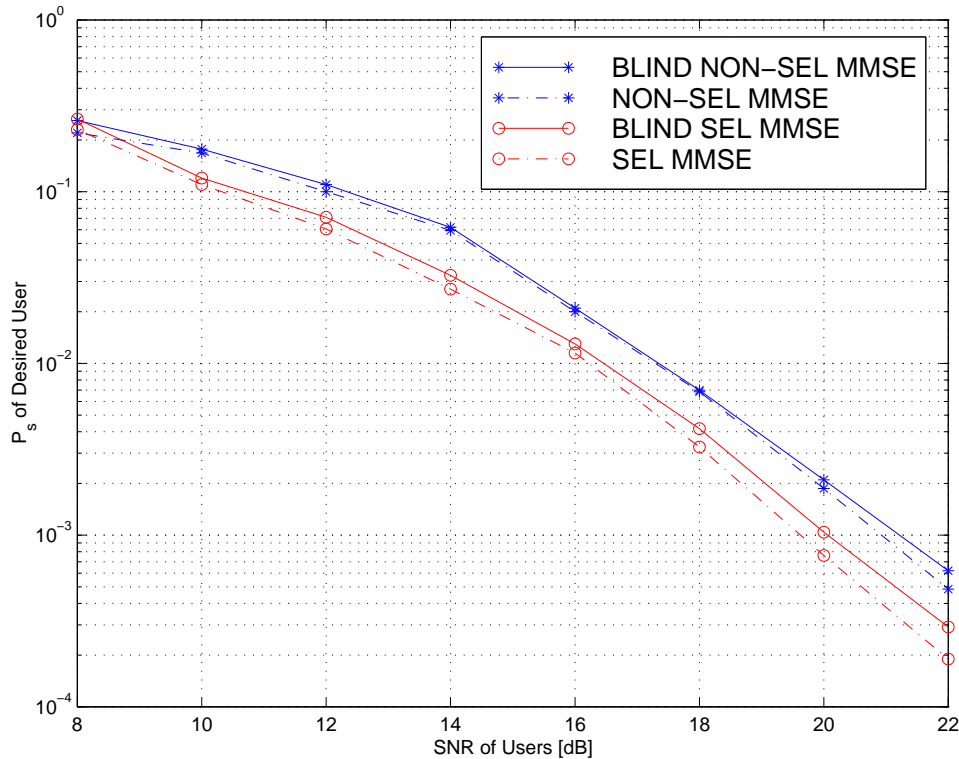


Figure 3.8: Comparison of the performance of the blind adaptive selective and non-selective MMSE filters with  $(K, M, N) = (5, 4, 20)$

selective and non-selective MMSE detectors (Figure 3(a) of [26]). For lower values of SNR,  $\mu = 0.001$  was used, whereas for the higher values of SNR,  $\mu = 0.0001$  had to be used to ensure proper convergence. The ability of the blind filter coefficients to track their non-blind deterministic counterparts is reflected in the similarity between the error probability curves for the blind and the non-blind implementations.

### 3.4.3 Selective Soft-IC

Next, we consider the selective implementation of the serial soft-IC scheme described in Section 3.3.3. We use a *selective*

$$\tilde{x}_{k,m} = \frac{1}{A_{k,m}} \left( y_{k,m} - \sum_{i=1}^{k-1} \sum_{j=1}^M \mathbf{s}_{k,m}^H \mathbf{s}_{i,j} A_{i,j} \hat{x}_{i,j} - \sum_{i=k+1}^K \sum_{j=1}^M \mathbf{s}_{k,m}^H \mathbf{s}_{i,j} A_{i,j} x_{i,j} \right) \quad (3.39)$$

then (3.20) is applied to obtain  $\hat{x}_{k,m}$ . Note that in going from (3.19) to (3.39) above, selective filtering has suppressed the terms containing the other  $M - 1$  messages of user  $k$ . Once all  $M$  soft-outputs of user  $k$  are obtained in this manner, the MM rule is applied to obtain the message decision  $\hat{m}_k$ .

Figure 3.9 compares the performance of the selective and non-selective filters for a lightly loaded system with  $K = 2$  users,  $M = 4$  signals per user, and  $N = 20$  dimensions. Figure 3.10 compares the performance of the selective and non-selective implementations of the decorrelator and MMSE for a fully loaded system with  $K = 5$ ,  $M = 4$ , and  $N = 20$ . Note that the non-selective decorrelator and MMSE curves compare well with those of Figure 3(a) in [26]. Next, we increase both the processing gain  $N$  as well as  $M$ , the number of messages per user. Figures 3.11 and 3.12 show the relative performance of the detectors for a moderately loaded and a fully loaded system, respectively. It can be seen that the selective detectors consistently outperform the non-selective detectors at all values of SNR. Among the selective detectors, the serial soft-IC is better able to cancel interferers at higher powers, hence the cross-over in Figure 3.12.

### 3.4.4 Selective Filtering with Successive Interference Suppression

Although it is expected that the selective filters will yield performance improvements over their non-selective counterparts, further improvements are possible through the use of successive decisions. We call the resulting technique *selective filtering with successive interference suppression* (SIS). For a user whose message has already been decoded, we need only to suppress the signal corresponding to the decoded message. This is analogous to the successive interference cancellation (SIC) scheme in [64] where a decoded user's signal is reconstructed and explicitly subtracted from the received signal  $\mathbf{r}$ . The algorithm for SIS is as follows:

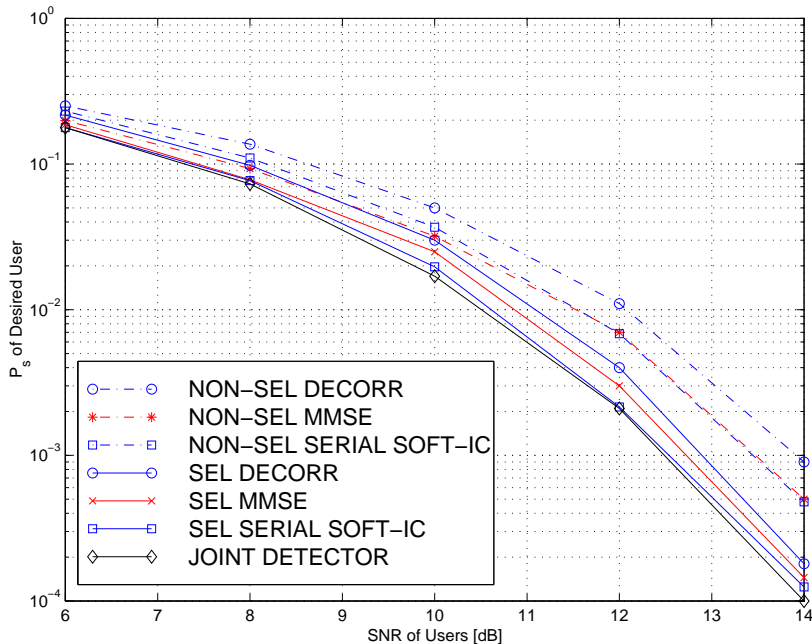


Figure 3.9: Comparison of selective and non-selective detectors in a lightly loaded system with  $(K, M, N) = (2, 4, 20)$

1. Select the maximum-magnitude matched filter output corresponding to the  $M$  messages of user  $k$ .
2. Sort the users in order of decreasing maximum-magnitudes.
3. For each user  $k \in \{1, \dots, K\}$ :
  - Perform selective filtering for the  $k$ th user in the sorted list.
  - Assume the message  $\hat{m}_k$  of the  $k$ th user is correct and retain only signature  $\mathbf{s}_{k, \hat{m}_k}$  in the selective filter matrix used to detect the message for user  $k + 1$ .

In the above algorithm, we can potentially employ any of the selective detectors proposed in Section 3.4. We will present performance results for the selective decorrelator with SIS in the next section. Note that the selective decorrelator with SIS and the non-coherent decision feedback detector proposed in [25] share the similarity that for the users whose messages have been decoded, both schemes decorrelate only against the

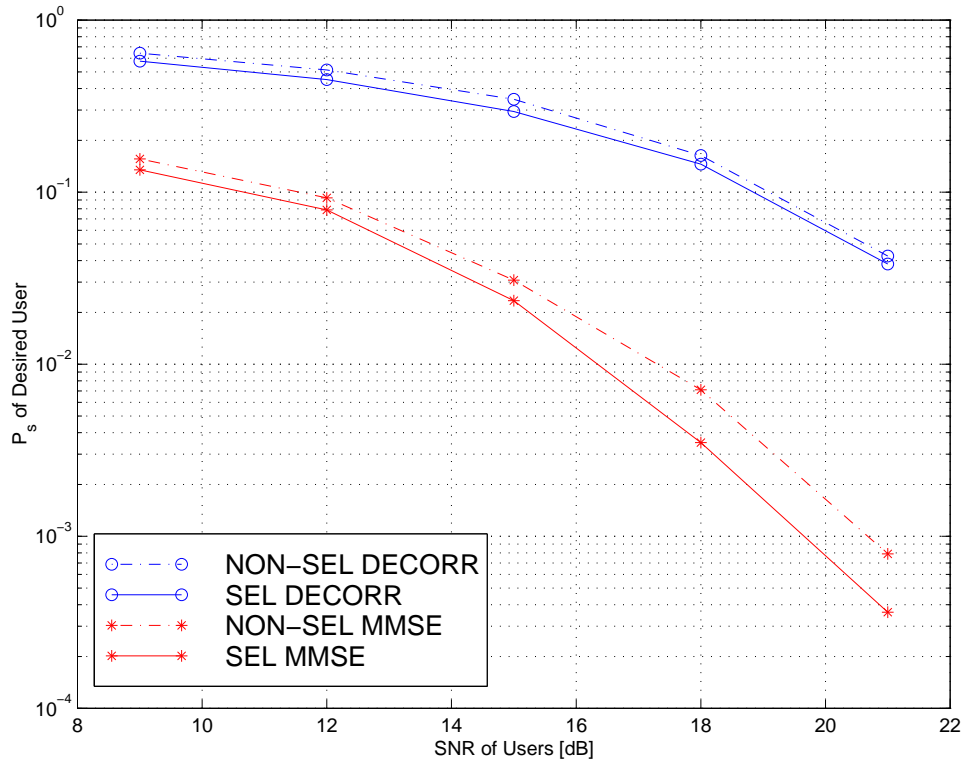


Figure 3.10: Comparison of selective and non-selective detectors in a fully loaded system with  $(K, M, N) = (5, 4, 20)$

signatures corresponding to the decoded messages. However, they differ in that [25] performs non-selective decorrelation against the  $M-1$  signatures of the desired user and it uses a second-stage single-user GLRT detector instead of the MM rule for symbol decisions.

Figure 3.13 illustrates the performance gained by using the SIS scheme with the selective decorrelator. Since the non-selective decorrelator is near-far resistant [13], the probability of symbol error for the desired user remains unchanged with interference power. The selective decorrelator also exhibits a similar behavior since it projects the received signal onto a space orthogonal to the interferers' subspace which remains unaffected by a change in the interferers' SNR. With SIS however, the situation is different. When the interferers' SNRs are lower than the desired user's SNR, the desired user is decoded first and it does not benefit from the SIS scheme. Hence, in the low SNR regions, its performance is similar to that of the selective decorrelator without

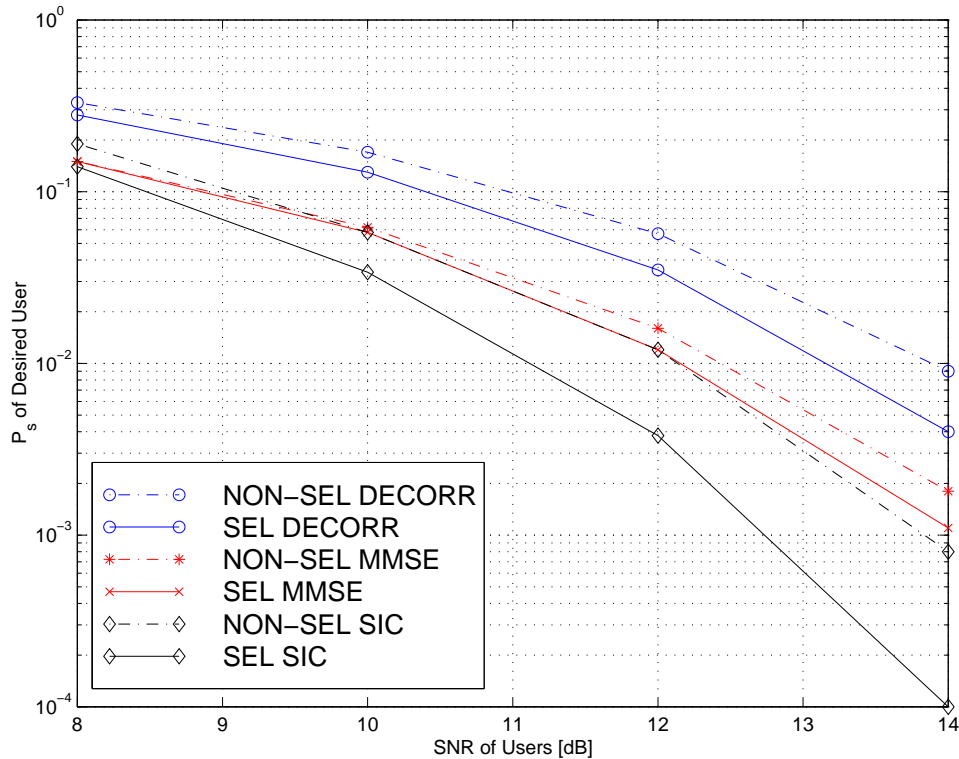


Figure 3.11: Comparison of selective and non-selective detectors with higher processing gain  $N = 64$  in a moderately loaded system with  $(K, M, N) = (4, 8, 64)$

SIS. In the high SNR regime, the desired user is decoded last with very high probability and hence it benefits the most from the SIS scheme (due to a reduction in the space of possible interfering signals) yielding an improvement in symbol error rate of around two orders of magnitude over the selective decorrelator without SIS. The SIS curve flattens out in the high SNR region because the dimensionality of the interference subspace remains unaffected by a change in the interferers' SNRs.

### 3.5 Chapter Summary

We showed that judicious use of *a priori* knowledge of the users' selective transmission mechanism can yield improved performance over the noncoherent multiuser detectors proposed in the literature. To this end, we proposed and investigated three categories

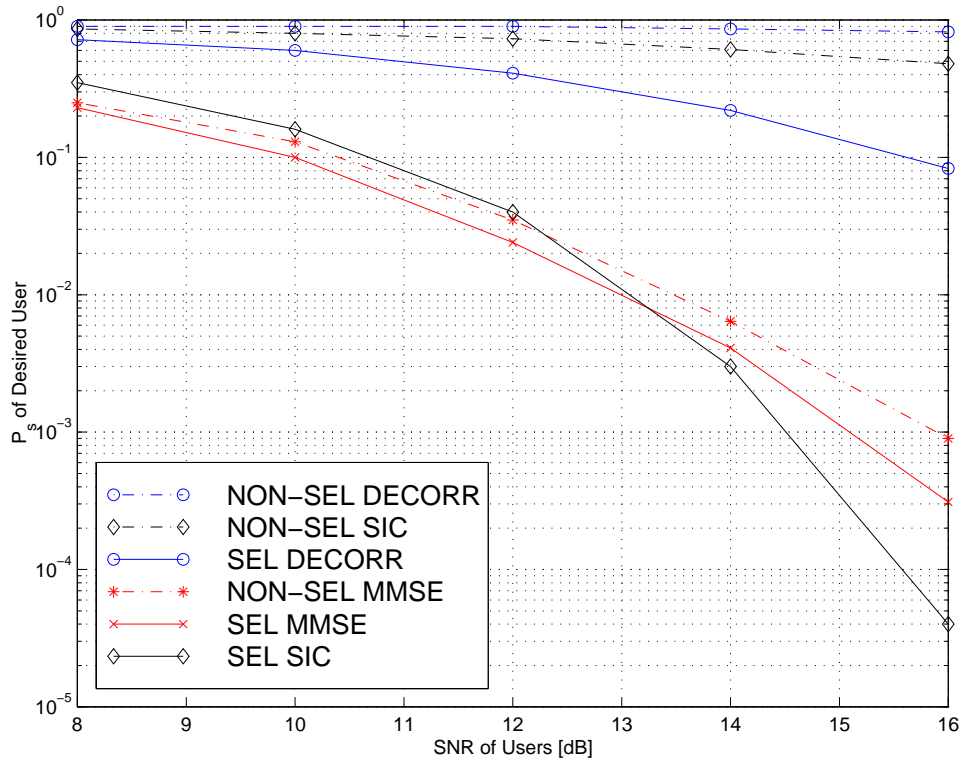


Figure 3.12: Comparison of selective and non-selective detectors with higher processing gain  $N = 64$  in a fully loaded system with  $(K, M, N)=(4, 16, 64)$

of detectors: First, the *joint* detector was derived to provide a benchmark for evaluating the performance of different detectors. Second, the serial, clipped, and parallel implementations of noncoherent soft-ICs were proposed and it was shown that the serial soft-IC outperforms the MMSE and decorrelative detectors in all scenarios. Third, we proposed and implemented a class of detectors that employed selective filtering. A blind adaptive implementation of the selective MMSE detector and selective detectors based on decision-directed successive user suppression were also presented. Numerical comparisons were provided to demonstrate the near-optimum performance of all the proposed detectors.

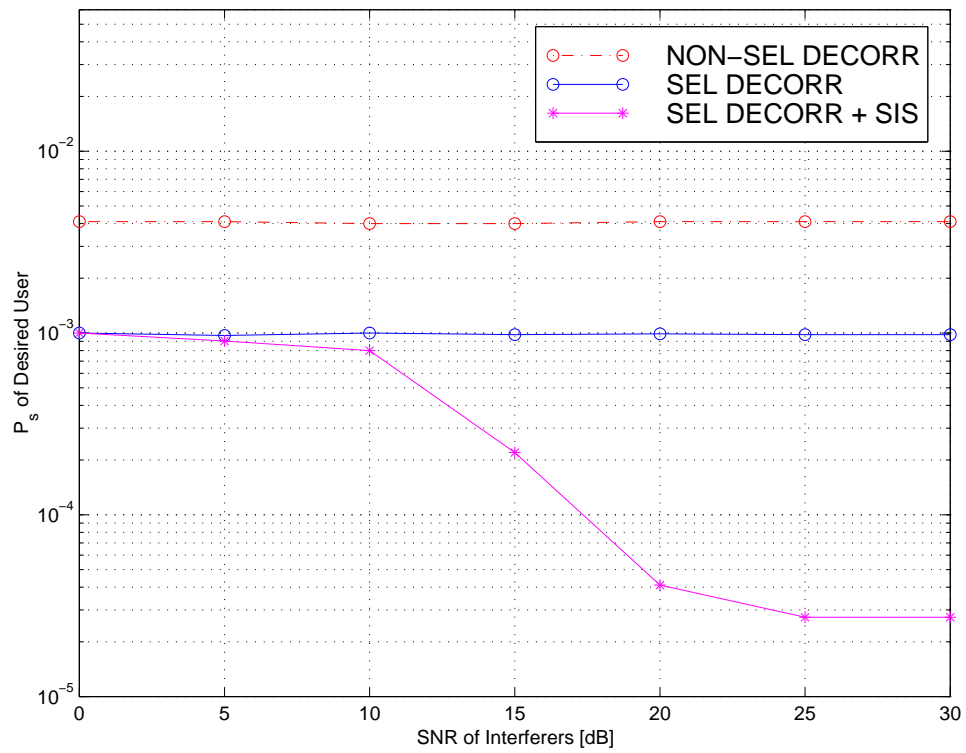


Figure 3.13: Performance of selective decorrelator with SIS with  $(K, M, N)=(3, 4, 20)$  and desired user's SNR= 15dB

## Chapter 4

### Conclusions

#### 4.1 Thesis Summary

This research is divided into two parts. The first part proposed a noncoherent, spread-spectrum multiple-access scheme for OFDM based systems. The second part proposed efficient multistage detection and selective filtering techniques for noncoherent multiuser detectors. We consider these two parts separately.

##### 4.1.1 The MC-MFSK Multiple-Access Scheme for OFDM-based Systems

In the first part of this thesis, we proposed a new spread-spectrum multiple-access scheme called MC-MFSK for OFDM based systems. A decoding heuristic was proposed for this system and it was shown that in high-SNR, single-user channels, the decoding heuristic was in fact the optimum combiner. An upper bound on the probability of decoding error  $P_w$  was derived for a multi-user scenario in high-SNR channels. Although a small sub-channel occupancy probability (i.e., a small  $L/M$ ) assumption was used to obtain a closed-form expression for the upper bound, the expression was shown to yield qualitatively similar results to those obtained from simulations for relatively large values of  $L/M$  as well. A lower bound on the spectral efficiency of the MC-MFSK system was also derived and shown to compare well qualitatively with

simulation results.

The performance of the MC-MFSK system was evaluated in Rayleigh fading channels and the optimal combining rule was derived. Approximations to the optimal combiner which are easier to implement were also discussed and compared. Since some of the approximations to the optimal detector involved a detection threshold, its selection was also discussed for the different cases.

Since the MC-MFSK system is partly motivated by the FH Multilevel-FSK system, the performance of the former was compared to the latter in AWGN and Rayleigh fading channels. The MC-MFSK system was also compared to the conventional FH  $M$ -ary FSK system. It was shown that for a fixed bandwidth  $W$  and bit-rate  $R_b$ , the MC-MFSK system outperformed both the FH Multilevel as well as the  $M$ -ary FSK systems. It was also shown that MC-MFSK systems based on either hard or soft limiters are near-far resistant.

It was illustrated that the MC-MFSK modem can be implemented with readily available, commercial FFT products. This ease of implementation coupled with the simple yet robust detection scheme makes the MC-MFSK system a suitable spread-spectrum multiple-access technology for OFDM based systems, especially those operating in unlicensed spectrum where power control may be infeasible.

#### **4.1.2 Noncoherent Multiuser Detection**

The second part of this thesis investigated efficient noncoherent multiuser detection techniques. It was shown that judicious use of *a priori* knowledge of the users' selective transmission mechanism can yield improved performance over the noncoherent multiuser detectors proposed in the literature. To this end, we proposed and investigated three categories of detectors.

First, a nonlinear programming approach to noncoherent multiuser detection was explored, where the structure of the multiuser signal was reflected in the various constraint sets analyzed. Using this technique, the *joint* detector was derived to provide a benchmark for evaluating the performance of different detectors. The *global* and *local* detectors were also derived as relaxations of the ML detector but with different constraint sets. These two detectors were shown to resemble the solution to the *generalized* MMSE detector, as previously observed for linear modulation and coherent detection.

Second, motivated by the ability of the soft-IC-based coherent detectors to perform well in near-far scenarios, the serial, clipped, and parallel implementations of noncoherent soft-ICs were suggested and investigated. The three detectors mainly differ in the manner in which they incorporate the *a priori* information regarding the structure of the signal. It was observed that the serial soft-IC not only outperforms the MMSE and the decorrelative detectors in near-far scenarios, but that it does so in equal-received-powers situations as well.

Third, we proposed a class of detectors that employ selective filtering. Unlike their non-selective counterparts, these detectors make use of the *a priori* information that of the  $M$  signals available to a user, only *one* is transmitted. The decorrelative, MMSE and soft-IC selective detectors were shown to outperform their non-selective counterparts in all cases. To illustrate the feasibility of the selective detectors in scenarios where limited information regarding the interferers is available, e.g., a CDMA down-link, a blind adaptive implementation of the selective MMSE detector was presented. Finally, an approach to improve the performance of the selective detectors based on decision-directed successive user suppression was presented in this thesis.

Our results indicate that incorporating the information regarding the signal structure offers performance improvements. In particular, detectors employing selective filtering have excellent performance and emerge as viable solutions in a variety of system conditions.

## Appendix A

### A.1 Derivation of $P(\alpha_i = 0)$

Let the random variables  $X_1, \dots, X_L$  represent the location of the  $L$  ones in the address vector  $\mathbf{a}_k$ . Then,

$$\begin{aligned} P(\alpha_i = 0) &= P(\mathbf{a}_k^\top C_{-i} \mathbf{a}_k = 0) \\ &= P\left(\sum_{j=1}^L a_k[X_j] a_k[X_j + i] = 0\right) \end{aligned} \quad (\text{A.1})$$

$$= P(\cap_{j=1}^L \{a_k[X_j] a_k[X_j + i] = 0\}) \quad (\text{A.2})$$

$$= 1 - P(\cup_{j=1}^L \{a_k[X_j] a_k[X_j + i] = 1\}) \quad (\text{A.3})$$

$$\geq 1 - \sum_{j=1}^L P(a_k[X_j] a_k[X_j + i] = 1) \quad (\text{A.4})$$

But,

$$\begin{aligned} P(a_k[X_j] a_k[X_j + i] = 1) &= \sum_{x=0}^{M-1} P(a_k[x] a_k[x + i] = 1 | X_j = x) P(X_j = x) \\ &= \sum_x P(a_k[x] = 1, a_k[x + i] = 1 | X_j = x) P(X_j = x) \\ &= \sum_x P(a_k[x + i] = 1 | X_j = x) P(X_j = x) \\ &= \sum_x \frac{L-1}{M-1} P(X_j = x) \\ &= \frac{L-1}{M-1}. \end{aligned} \quad (\text{A.5})$$

Therefore, substituting (A.5) in (A.4) yields

$$P(\alpha_i = 0) \geq 1 - \frac{L(L-1)}{M-1}. \quad (\text{A.6})$$

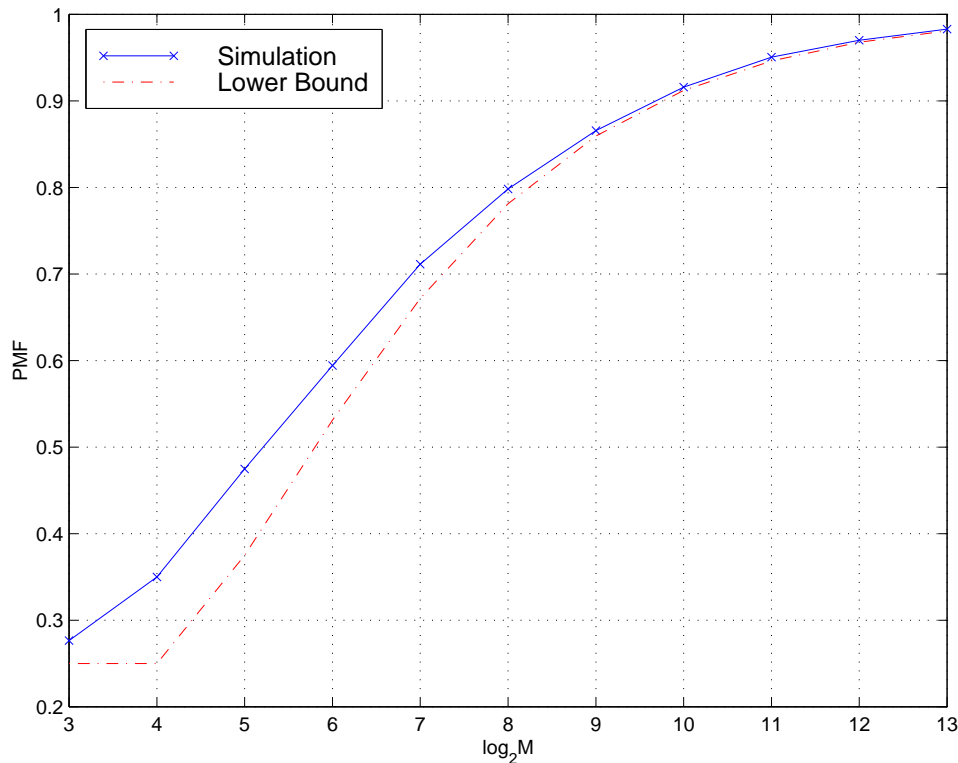


Figure A.1: Comparison of simulated value of  $P(\alpha_i = 0)$  with lower bound in (A.6)

Under the assumption that  $L$  is proportional to  $\ln(M/P_w)$ , or that  $L = c \ln(M/P_w)$  where  $c$  is a constant, it can be easily shown that

$$\lim_{L/M \rightarrow 0} \frac{L(L-1)}{M-1} = 0. \quad (\text{A.7})$$

Since  $P(\alpha_i = 0) \leq 1$ , we have

$$1 \leq \lim_{L/M \rightarrow 0} P(\alpha_i = 0) \leq 1, \quad (\text{A.8})$$

or,

$$\lim_{L/M \rightarrow 0} P(\alpha_i = 0) = 1. \quad (\text{A.9})$$

This is also evident from Figure A.1 where  $P(\alpha_i = 0)$  is determined from simulations and compared with the lower bound developed in (A.6). In the simulation, although different addresses were chosen for each run, the same value of  $i = 1$  was used to compute  $\alpha_i$  for all the runs. As can be expected, the results were found to be independent of the particular shift  $i$  used.

## A.2 Distribution of $\rho$

Recall that the vector  $\tilde{\mathbf{a}}_k$  represents the indices of the  $L$  locations occupied by user  $k$ . Let  $N_i$  represent the number of interferers on sub-channel  $\tilde{a}_k[i]$   $i = 0, \dots, L-1$ ,  $A_i$  the event that  $N_i > 0$ ,  $\bar{A}_i$  the event that  $N_i = 0$  and  $h_0 = L/M$  the probability that an interferer occupies a sub-channel. We will now evaluate  $P(\rho = L)$ . We have

$$P(\rho = L) = P(A_0 \cap \dots \cap A_{L-1}). \quad (\text{A.10})$$

Also,

$$P(A_j) = P(N_j \geq 1) = 1 - P(N_j = 0) = 1 - (1 - h_0)^{K-1}. \quad (\text{A.11})$$

Let  $h_1$  be the conditional probability of an interferer occupying a sub-channel  $j$  given that it is not present on another sub-channel  $i \neq j$ . Therefore,

$$h_1 = \frac{L}{M-1} = \frac{L}{M} \frac{M}{M-1} = h_0 \left(1 + \frac{1}{M-1}\right) \quad (\text{A.12})$$

$$P(A_j | \bar{A}_i) = P(N_j > 0 | N_i = 0) = 1 - P(N_j = 0 | N_i = 0) = 1 - (1 - h_1)^{K-1} \quad (\text{A.13})$$

In general, we define

$$h_i \triangleq \frac{L}{M-i} \quad i = 0, \dots, L-1. \quad (\text{A.14})$$

We will define another variable  $p_i$ ,  $i = 0, \dots, L-1$ , where

$$p_0 = P(A_0) = 1 - \left(1 - \frac{L}{M}\right)^{K-1} = 1 - (1 - h_0)^{K-1} \quad (\text{A.15})$$

$\vdots$

$$p_i = P(A_i | \bar{A}_0 \cap \dots \cap \bar{A}_{i-1}) = 1 - \left(1 - \frac{L}{M-i}\right)^{K-1} = 1 - (1 - h_i)^{K-1} \quad (\text{A.16})$$

Note that due to symmetry,

$$p_0 = P(A_i) \quad i = 0, \dots, L-1 \quad (\text{A.17})$$

$$p_1 = P(A_j | \bar{A}_i) = P(A_i | \bar{A}_j) \quad i \neq j. \quad (\text{A.18})$$

Further, define

$$\bar{p}_i = (1 - p_i) \quad (\text{A.19})$$

The expression for  $P(A_0 \cap \dots \cap A_{L-1})$  will now be derived using the following Lemma:

**Lemma 1** For any two events  $\mathcal{A}$  and  $\mathcal{B}$ ,

$$P(\mathcal{A} \cap \mathcal{B}) = P(\mathcal{A}) - P(\mathcal{A} | \bar{\mathcal{B}})P(\bar{\mathcal{B}})$$

We will now give a few examples to give some insight into the next Lemma. Using Lemma 1 and Equations (A.17-A.18),

$$\begin{aligned} P(A_0 \cap A_1) &= P(A_0) - P(A_0 | \bar{A}_1)P(\bar{A}_1) \\ &= p_0 - p_1 \bar{p}_0. \end{aligned} \tag{A.20}$$

If we denote

$$P(A_0 \cap A_1) = f(K, L, M), \tag{A.21}$$

then, it can be shown that

$$P(A_0 \cap A_1 | \bar{A}_2) = f(K, L, M - 1) = p_1 - p_2 \bar{p}_1. \tag{A.22}$$

Therefore,

$$\begin{aligned} P(A_0 \cap A_1 \cap A_2) &= P(A_0 \cap A_1) - P(A_0 \cap A_1 | \bar{A}_2)P(\bar{A}_2) \\ &= [p_0 - p_1 \bar{p}_0] - [(p_1 - p_2 \bar{p}_1) \bar{p}_0] \\ &= p_0 - 2p_1 \bar{p}_0 + p_2 \bar{p}_1 \bar{p}_0, \end{aligned} \tag{A.23}$$

and

$$\begin{aligned} P(A_0 \cap A_1 \cap A_2 \cap A_3) &= P(A_0 \cap A_1 \cap A_2) - P(A_0 \cap A_1 \cap A_2 | \bar{A}_3)P(\bar{A}_3) \\ &= p_0 - 3p_1 \bar{p}_0 + 3p_2 \bar{p}_1 \bar{p}_0 - p_3 \bar{p}_2 \bar{p}_1 \bar{p}_0. \end{aligned} \tag{A.24}$$

From (A.23) and (A.24), note that the coefficients of the terms are from a binomial expansion. This leads us to our next Lemma:

**Lemma 2**  $P(A_0 \cap \dots \cap A_n) = \sum_{i=0}^n \binom{n}{i} (-1)^i p_i \prod_{j=0}^{i-1} \bar{p}_j$

**Proof:** The proof will be by induction. Assume that the following is true:

$$P(A_0 \cap \dots \cap A_{n-1}) = \sum_{i=0}^{n-1} \binom{n-1}{i} (-1)^i p_i \prod_{j=0}^{i-1} \bar{p}_j$$

Then, from Lemma 1 we have

$$P(A_0 \cap \dots \cap A_{n-1} \cap A_n) = P(A_0 \cap \dots \cap A_{n-1}) - P(A_0 \cap \dots \cap A_{n-1} | \bar{A}_n) P(\bar{A}_n) \quad (\text{A.25})$$

Since  $P(\bar{A}_n) = \bar{p}_0$  from (A.17),

$$\begin{aligned} P(A_0 \cap \dots \cap A_n) &= \left[ \sum_{i=0}^{n-1} \binom{n-1}{i} (-1)^i p_i \prod_{j=0}^{i-1} \bar{p}_j \right] - \bar{p}_0 \left[ \sum_{i=0}^{n-1} \binom{n-1}{i} (-1)^i p_{i+1} \prod_{j=1}^i \bar{p}_j \right] \\ &= \left[ \sum_{i=0}^{n-1} \binom{n-1}{i} (-1)^i p_i \prod_{j=0}^{i-1} \bar{p}_j \right] - \left[ \sum_{i=0}^{n-1} \binom{n-1}{i} (-1)^i p_{i+1} \prod_{j=0}^i \bar{p}_j \right] \end{aligned}$$

Substituting the dummy variable  $k = i + 1$ , we have

$$P(A_0 \cap \dots \cap A_n) = \left[ \sum_{i=0}^{n-1} \binom{n-1}{i} (-1)^i p_i \prod_{j=0}^{i-1} \bar{p}_j \right] - \left[ \sum_{k=1}^n \binom{n-1}{k-1} (-1)^{k-1} p_k \prod_{j=0}^{k-1} \bar{p}_j \right] \quad (\text{A.26})$$

Substituting  $i = k$ , we have

$$\begin{aligned} P(A_0 \cap \dots \cap A_n) &= \left[ \sum_{i=0}^{n-1} \binom{n-1}{i} (-1)^i p_i \prod_{j=0}^{i-1} \bar{p}_j \right] - \left[ \sum_{i=1}^n \binom{n-1}{i-1} (-1)^{i-1} p_i \prod_{j=0}^{i-1} \bar{p}_j \right] \\ &= \left[ \sum_{i=0}^{n-1} \binom{n-1}{i} (-1)^i p_i \prod_{j=0}^{i-1} \bar{p}_j \right] + \left[ \sum_{i=1}^n \binom{n-1}{i-1} (-1)^i p_i \prod_{j=0}^{i-1} \bar{p}_j \right] \\ &= \left[ \sum_{i=1}^{n-1} \left[ \binom{n-1}{i} + \binom{n-1}{i-1} \right] (-1)^i p_i \prod_{j=0}^{i-1} \bar{p}_j \right] + \binom{n-1}{0} p_0 \\ &\quad + \binom{n-1}{n-1} (-1)^n p_n \prod_{j=0}^{n-1} \bar{p}_j \end{aligned} \quad (\text{A.27})$$

Since  $\binom{n-1}{i} + \binom{n-1}{i-1} = \binom{n}{i}$ ,  $\binom{n-1}{0} = \binom{n}{0}$ , and  $\binom{n-1}{n-1} = \binom{n}{n}$ ,

$$\begin{aligned} P(A_0 \cap \dots \cap A_n) &= \left[ \sum_{i=1}^{n-1} \binom{n}{i} (-1)^i p_i \prod_{j=0}^{i-1} \bar{p}_j \right] + \binom{n}{0} p_0 + \binom{n}{n} (-1)^n p_n \prod_{j=0}^{n-1} \bar{p}_j \\ &= \sum_{i=0}^n \binom{n}{i} (-1)^i p_i \prod_{j=0}^{i-1} \bar{p}_j \end{aligned} \quad (\text{A.28})$$

□

Therefore, from (A.10),

$$P(\rho = L) = P(A_0 \cap \dots \cap A_{L-1}) = \sum_{i=0}^{L-1} \binom{L-1}{i} (-1)^i p_i \prod_{j=0}^{i-1} \bar{p}_j. \quad (\text{A.29})$$

Since it is hard to obtain a closed form for the above expression, we will approximate it in the next section.

### A.2.1 Binomial Approximation

From (A.14)

$$h_n = \frac{L}{M-n} = \frac{L/M}{1-n/M} = \frac{h_0}{1-n/M}$$

with  $h_n > h_{n-1}$ . For small values of  $h_0 = L/M$ ,

$$h_L = \frac{h_0}{1-L/M} = h_0(1-h_0)^{-1} \approx h_0(1+h_0) = h_0 + h_0^2 \approx h_0. \quad (\text{A.30})$$

Therefore, for small  $h_0$ ,  $h_n \approx h_0$  for  $0 < n \leq L-1$  as well. This leads to  $p_n \approx p_0$ ,  $0 < n \leq L-1$  in (A.16), which, upon substitution in (A.29) yields

$$P(\rho = L) \approx p_0^L. \quad (\text{A.31})$$

### A.3 Derivation of the Global Constrained Detector

The optimization problem in (3.15) involves the minimization of a convex function over a convex constraint set. Hence, it has a unique minimum which can be determined using the gradient descent algorithm. Since (3.15) has a single constraint, there is only one dual variable. Thus, a simpler iterative algorithm can be found by solving for the dual problem as outlined below.

The objective function in (3.15) can be expanded in terms of  $\mathbf{y} = \mathbf{S}^H \mathbf{r}$  as

$$\|\mathbf{r} - \mathbf{S}\mathbf{A}\mathbf{x}\|^2 = \mathbf{r}^H \mathbf{r} - 2\text{Re}[\mathbf{y}^H \mathbf{A}\mathbf{x}] + \mathbf{x}^H \mathbf{T}\mathbf{x} \quad (\text{A.32})$$

where  $\mathbf{T} = \mathbf{A}\mathbf{R}\mathbf{A}$ . The Lagrangian dual function can be expressed as

$$\mathcal{L}(\mathbf{x}, \lambda) = \mathbf{x}^H \mathbf{T} \mathbf{x} - 2\text{Re}[\mathbf{y}^H \mathbf{A} \mathbf{x}] + \lambda(\mathbf{x}^H \mathbf{x} - K) \quad (\text{A.33})$$

which is to be maximized over  $\mathbf{x}$  and  $\lambda \geq 0$ . Equating  $\nabla \mathcal{L}(\hat{\mathbf{x}}(\lambda), \lambda) = 0$  and solving for  $\hat{\mathbf{x}}(\lambda)$  in terms of  $\lambda$ , we get

$$\hat{\mathbf{x}}(\lambda) = (\mathbf{T} + \lambda \mathbf{I})^{-1} \mathbf{A} \mathbf{y}. \quad (\text{A.34})$$

On substituting back into (A.33), we arrive at:

$$\max_{\lambda \geq 0} \mathcal{L}(\lambda) = -\mathbf{y}^H \mathbf{A} (\mathbf{T} + \lambda \mathbf{I})^{-1} \mathbf{A} \mathbf{y} - \lambda K \quad (\text{A.35})$$

which is a one-dimensional optimization problem and can be solved using a variety of iterative algorithms [65]. A simple unconstrained gradient descent algorithm is guaranteed to converge for a small enough step-size  $\mu$ , which can then be projected onto the positive axis [12]. Such an algorithm is

$$\bar{\lambda}(t+1) = \bar{\lambda}(t) - \mu [\nabla \mathcal{L}(\hat{\mathbf{x}}(\lambda), \lambda)] \quad (\text{A.36})$$

$$= \bar{\lambda}(t) - \mu \left[ \mathbf{y}^H \mathbf{A} (\mathbf{T} + \bar{\lambda}(t) \mathbf{I})^{-2} \mathbf{A} \mathbf{y} - K \right] \quad (\text{A.37})$$

which converges to  $\bar{\lambda}$ . The maximizer of (A.35) is given by  $\lambda^* = \max(0, \bar{\lambda})$ . Then, from (A.34), the unique minimizer of (3.15) can be re-written as

$$\hat{\mathbf{x}} = \mathbf{A}^{-1} (\mathbf{R} + \lambda^* \mathbf{A}^{-2})^{-1} \mathbf{y}. \quad (\text{A.38})$$

#### A.4 Derivation of the Local Constrained Detector

Here, we derive the solution to the optimization problem in (3.17). The objective function in (3.17) can be expanded as in (A.32). Since (3.17) involves the minimization of a convex function over a convex set, it has a unique minimum over this constraint set which can be found using a variety of iterative algorithms, e.g., the gradient descent algorithm [65]. In addition, the convex duality theorem [65] ensures that no duality gap

exists and one can solve for the dual problem instead. Since (3.17) has  $K$  constraints, there are  $K$  dual variables. In terms of  $\mathbf{T}_{kj} = \mathbf{A}_k \mathbf{S}_k^H \mathbf{S}_j \mathbf{A}_j$ , the Lagrangian dual function of (A.32) can be expressed as

$$\mathcal{L}(\mathbf{x}, \boldsymbol{\lambda}) = \mathbf{x}^H \mathbf{T} \mathbf{x} - 2 \operatorname{Re}[\mathbf{y}^H \mathbf{A} \mathbf{x}] + \sum_{i=1}^K \lambda_i (\mathbf{x}_i^H \mathbf{x}_i - 1) \quad (\text{A.39})$$

$$= \sum_{i=1}^K \sum_{j=1}^K \mathbf{x}_i^H \mathbf{T}_{ij} \mathbf{x}_j - 2 \operatorname{Re} \left[ \sum_{i=1}^K \mathbf{y}_i^H \mathbf{A}_i \mathbf{x}_i \right] + \sum_{i=1}^K \lambda_i (\mathbf{x}_i^H \mathbf{x}_i - 1) \quad (\text{A.40})$$

which is to be maximized over  $\mathbf{x}$  and  $\boldsymbol{\lambda} \geq 0$ , where  $\boldsymbol{\lambda} = [\lambda_1 \cdots \lambda_K]^T$ . The gradient vector associated with  $\mathcal{L}(\mathbf{x}, \boldsymbol{\lambda})$  is  $\nabla \mathcal{L}(\mathbf{x}, \boldsymbol{\lambda}) = [\nabla_{\mathbf{x}_1}^T \mathcal{L}(\mathbf{x}, \boldsymbol{\lambda}) \cdots \nabla_{\mathbf{x}_K}^T \mathcal{L}(\mathbf{x}, \boldsymbol{\lambda})]^T$ , where

$$\nabla_{\mathbf{x}_k} \mathcal{L}(\mathbf{x}, \boldsymbol{\lambda}) = 2 \left( \sum_{j=1}^K \mathbf{T}_{kj} \mathbf{x}_j - \mathbf{A}_k \mathbf{y}_k + \lambda_k \mathbf{x}_k \right). \quad (\text{A.41})$$

Consequently,

$$\nabla \mathcal{L}(\mathbf{x}, \boldsymbol{\lambda}) = 2 (\mathbf{T} \mathbf{x} - \mathbf{A} \mathbf{y} + \boldsymbol{\Lambda} \mathbf{x}) \quad (\text{A.42})$$

where

$$\boldsymbol{\Lambda} = \operatorname{diag}[\underbrace{\lambda_1, \dots, \lambda_1}_{M \text{ terms}}, \dots, \underbrace{\lambda_K, \dots, \lambda_K}_{M \text{ terms}}]$$

is an  $MK \times MK$  diagonal matrix. Let  $\hat{\mathbf{x}}(\boldsymbol{\lambda})$  be the solution to  $\nabla \mathcal{L}(\hat{\mathbf{x}}(\boldsymbol{\lambda}), \boldsymbol{\lambda}) = 0$ . Solving for  $\hat{\mathbf{x}}(\boldsymbol{\lambda})$ , we get

$$\hat{\mathbf{x}}(\boldsymbol{\lambda}) = (\mathbf{T} + \boldsymbol{\Lambda})^{-1} \mathbf{A} \mathbf{y} \quad (\text{A.43})$$

where  $\hat{\mathbf{x}}(\boldsymbol{\lambda}) = [\hat{\mathbf{x}}_1^T(\lambda_1) \cdots \hat{\mathbf{x}}_K^T(\lambda_K)]^T$ . On substituting  $\hat{\mathbf{x}}(\boldsymbol{\lambda})$  back into (A.39), we arrive at

$$\max_{\boldsymbol{\lambda} \geq \mathbf{0}} \mathcal{L}(\hat{\mathbf{x}}(\boldsymbol{\lambda}), \boldsymbol{\lambda}) = \hat{\mathbf{x}}(\boldsymbol{\lambda})^H \mathbf{T} \hat{\mathbf{x}}(\boldsymbol{\lambda}) - 2 \operatorname{Re}[\mathbf{y}^H \mathbf{A} \hat{\mathbf{x}}(\boldsymbol{\lambda})] + \sum_{i=1}^K \lambda_i (\hat{\mathbf{x}}_i(\lambda_i)^H \hat{\mathbf{x}}_i(\lambda_i) - 1). \quad (\text{A.44})$$

Simple unconstrained gradient descent algorithms can be used to iteratively determine each element of  $\boldsymbol{\lambda}$  as follows

$$\bar{\lambda}_k(t+1) = \bar{\lambda}_k(t) - \mu_k [\nabla_{\lambda_k} \mathcal{L}(\hat{\mathbf{x}}(\boldsymbol{\lambda}), \boldsymbol{\lambda})] \quad (\text{A.45})$$

which converges to  $\bar{\lambda}_k$ . The maximizer of (A.44) is given by  $\boldsymbol{\lambda}^* = [\lambda_1^* \cdots \lambda_K^*]^T$  where  $\lambda_k^* = \max(0, \bar{\lambda}_k)$ . Then, from (A.43), the unique minimizer of (3.17) can be re-written

as

$$\hat{\mathbf{x}}(\lambda^*) = \mathbf{A}^{-1}(\mathbf{R} + \Lambda^* \mathbf{A}^{-2})^{-1} \mathbf{y}. \quad (\text{A.46})$$

## A.5 Serial Soft-IC

From the matched-filter output in (3.8), the element of  $\mathbf{y}$  corresponding to message  $k$  of user  $m$  can be written as

$$y_{k,m} = \sum_{i=1}^K \sum_{j=1}^M \mathbf{s}_{k,m}^H \mathbf{s}_{i,j} A_{i,j} x_{i,j} + \mathbf{s}_{k,m}^H \mathbf{n}. \quad (\text{A.47})$$

Decomposing (A.47) to isolate the terms containing the  $k$ th user's messages, we have

$$y_{k,m} = \sum_{i=1}^{k-1} \sum_{j=1}^M \mathbf{s}_{k,m}^H \mathbf{s}_{i,j} A_{i,j} x_{i,j} + \sum_{j=1}^M \mathbf{s}_{k,m}^H \mathbf{s}_{k,j} A_{k,j} x_{k,j} + \sum_{i=k+1}^K \sum_{j=1}^M \mathbf{s}_{k,m}^H \mathbf{s}_{i,j} A_{i,j} x_{i,j} + \mathbf{s}_{k,m}^H \mathbf{n}. \quad (\text{A.48})$$

Note that the second term on the right side of (A.48) can be decomposed further to isolate the term representing the current message  $x_{k,m}$  as

$$\sum_{j=1}^M \mathbf{s}_{k,m}^H \mathbf{s}_{k,j} A_{k,j} x_{k,j} = \sum_{j=1}^{m-1} \mathbf{s}_{k,m}^H \mathbf{s}_{k,j} A_{k,j} x_{k,j} + \mathbf{s}_{k,m}^H \mathbf{s}_{k,m} A_{k,m} x_{k,m} + \sum_{j=m+1}^M \mathbf{s}_{k,m}^H \mathbf{s}_{k,j} A_{k,j} x_{k,j}. \quad (\text{A.49})$$

Since the signatures have unit norm,  $\mathbf{s}_{k,m}^H \mathbf{s}_{k,m} = 1$ , substituting (A.49) in (A.48) and solving for  $x_{k,m}$  yields

$$\begin{aligned} x_{k,m} = \frac{y_{k,m}}{A_{k,m}} & - \frac{1}{A_{k,m}} \sum_{i=1}^{k-1} \sum_{j=1}^M \mathbf{s}_{k,m}^H \mathbf{s}_{i,j} A_{i,j} x_{i,j} - \frac{1}{A_{k,m}} \sum_{j=1}^{m-1} \mathbf{s}_{k,m}^H \mathbf{s}_{k,j} A_{k,j} x_{k,j} \\ & - \frac{1}{A_{k,m}} \sum_{j=m+1}^M \mathbf{s}_{k,m}^H \mathbf{s}_{k,j} A_{k,j} x_{k,j} - \frac{1}{A_{k,m}} \sum_{i=k+1}^K \sum_{j=1}^M \mathbf{s}_{k,m}^H \mathbf{s}_{i,j} A_{i,j} x_{i,j}. \end{aligned} \quad (\text{A.50})$$

In the *serial* soft-IC, the current message estimate  $\tilde{x}_{k,m}$  is determined using the previous decisions to reconstruct the interference which is then subtracted from the matched filter output  $x_{k,m}$ . By rewriting the right side of (A.50) to distinguish those  $x_{k,m}$  which have already been estimated, we obtain (3.19).

## A.6 Optimum Decision Rule for the Selective Decorrelator

In this section, we seek the optimum decision rule based on  $\mathbf{v}$  (3.28). Let the covariance matrix of  $\bar{\eta}$  be  $\sigma^2\mathbf{Q}$ , where

$$\sigma^2 Q(i, j) = E[\bar{\eta}_i(1)\bar{\eta}_j^*(1)]. \quad (\text{A.51})$$

The covariance of  $\bar{\eta}_i$  and  $\bar{\eta}_j$  may be written as

$$E[\bar{\eta}_i\bar{\eta}_j^H] = \sigma^2\mathbf{G}_{ij} \quad (\text{A.52})$$

where

$$\mathbf{G}_{ij} = \bar{\mathbf{R}}_i^{-1}\bar{\mathbf{S}}_i^H\bar{\mathbf{S}}_j\bar{\mathbf{R}}_j^{-1} \quad (\text{A.53})$$

and hence,

$$E[\bar{\eta}_i(1)\bar{\eta}_j^*(1)] = \sigma^2 G_{ij}(1, 1). \quad (\text{A.54})$$

Consequently,  $Q(i, j) = G_{ij}(1, 1)$ .

We now follow the approach of [13] to derive the optimum decision rule. Let  $H_i$  denote the hypothesis that user 1 transmits the  $i$ th signal. If we assume equal *a priori* probabilities for the  $M$  signals, then the minimum error probability rule reduces to the ML test, leading to the optimum detector  $\phi^O$  (the superscript  $O$  stands for optimum),

$$\phi^O : \hat{i}^O = \arg \max_i \{f(\widehat{\mathbf{A}}_1\mathbf{x}_1 | H_i)\} \quad (\text{A.55})$$

with  $f$  being the conditional PDF (probability density function) of  $\widehat{\mathbf{A}}_1\mathbf{x}_1 | H_i$ . The term  $f(\widehat{\mathbf{A}}_1\mathbf{x}_1 | H_i)$  is evaluated by averaging out the conditional PDF  $f(\widehat{\mathbf{A}}_1\mathbf{x}_1 | H_i, \phi_{1,i})$  over the phase. Let

$$\mathbf{w} = \mathbf{U}\mathbf{S}\mathbf{A}\mathbf{x}. \quad (\text{A.56})$$

Then, in terms of  $\mathbf{P} = \mathbf{Q}^{-1}$ ,

$$\hat{i}^O = \arg \max_i \left\{ \frac{1}{\sqrt{(2\pi)^M |\mathbf{Q}|}} \int_0^{2\pi} e^{-(\mathbf{v}-\mathbf{w})^H \mathbf{P}(\mathbf{v}-\mathbf{w})/2\sigma^2} d\phi_{1,i} \right\} \quad (\text{A.57})$$

$$= \arg \max_i \left\{ \frac{1}{\sqrt{(2\pi)^M |\mathbf{Q}|}} \int_0^{2\pi} e^{-(\mathbf{v}^H \mathbf{P} \mathbf{v} + \mathbf{w}^H \mathbf{P} \mathbf{w} - 2\text{Re}[\mathbf{v}^H \mathbf{P} \mathbf{w}])/2\sigma^2} d\phi_{1,i} \right\} \quad (\text{A.58})$$

Given that user 1 transmits the  $i$ th message, from (3.28) and (A.56) we have

$$\mathbf{w} = \mathbf{U}\mathbf{s}_{1,i}A_{1,i}e^{-j\phi_{1,i}} \quad (\text{A.59})$$

$$\mathbf{w}^H\mathbf{P}\mathbf{w} = A_{1,i}^2\mathbf{s}_{1,i}^H\mathbf{U}^H\mathbf{P}\mathbf{U}\mathbf{s}_{1,i}. \quad (\text{A.60})$$

The term  $\mathbf{w}^H\mathbf{P}\mathbf{w}$  being independent of  $\phi_{1,i}$  can be brought out of the integral on the right side of (A.58), but it has to be retained for the final decision process due to its dependency on  $i$ . The term  $\mathbf{v}^H\mathbf{P}\mathbf{w}$  on the other hand, is completely independent of  $i$  and hence it can be excluded from the decision process entirely. Therefore, retaining only the terms relevant to the decision process, we have

$$\hat{i}^O = \arg \max_i \left\{ \frac{e^{-\mathbf{w}^H\mathbf{P}\mathbf{w}/2\sigma^2}}{2\pi} \int_0^{2\pi} e^{Re[\mathbf{v}^H\mathbf{P}\mathbf{w}]/\sigma^2} d\phi_{1,i} \right\} \quad (\text{A.61})$$

Also,

$$\mathbf{v}^H\mathbf{P}\mathbf{w} = A_{1,i}e^{-j\phi_{1,i}}\mathbf{v}^H\mathbf{P}\mathbf{U}\mathbf{s}_{1,i} \quad (\text{A.62})$$

$$= A_{1,i}e^{-j\phi_{1,i}}|\mathbf{v}^H\mathbf{P}\mathbf{U}\mathbf{s}_{1,i}|e^{-j\alpha} \quad (\text{A.63})$$

$$= A_{1,i}e^{-j(\phi_{1,i}+\alpha)}|\mathbf{v}^H\mathbf{P}\mathbf{U}\mathbf{s}_{1,i}|. \quad (\text{A.64})$$

Moreover, in terms of the modified Bessel function of order zero

$$I_0(x) = \frac{1}{2\pi} \int_0^{2\pi} e^{x\cos(\phi+\alpha)} d\phi \quad (\text{A.65})$$

the decision statistic is

$$\hat{i}^O = \arg \max_i \left\{ \frac{e^{-\mathbf{w}^H\mathbf{P}\mathbf{w}/2\sigma^2}}{2\pi} \int_0^{2\pi} e^{A_{1,i}|\mathbf{v}^H\mathbf{P}\mathbf{U}\mathbf{s}_{1,i}|\cos(\phi_{1,i}+\alpha)} d\phi_{1,i} \right\} \quad (\text{A.66})$$

$$= \arg \max_i \left\{ e^{-\mathbf{w}^H\mathbf{P}\mathbf{w}/2\sigma^2} I_0 \left( \frac{A_{1,i}|\mathbf{v}^H\mathbf{P}\mathbf{U}\mathbf{s}_{1,i}|}{\sigma^2} \right) \right\} \quad (\text{A.67})$$

Substituting for  $\mathbf{w}$ , and taking  $\ln(\cdot)$ , the decision statistic finally reduces to

$$\hat{i}^O = \arg \max_i \left\{ \frac{A_{1,i}^2\mathbf{s}_{1,i}^H\mathbf{U}^H\mathbf{P}\mathbf{U}\mathbf{s}_{1,i}}{2\sigma^2} + \ln I_0 \left( \frac{A_{1,i}|\mathbf{v}^H\mathbf{P}\mathbf{U}\mathbf{s}_{1,i}|}{\sigma^2} \right) \right\} \quad (\text{A.68})$$

## A.7 Union Bound for the Selective Decorrelator

In this section, we will derive an upper bound for the symbol error rate for user 1 using the MM based *selective* decorrelator. Therefore, given any hypothesis  $H_i$ , the decision statistic is  $\Lambda_i = |v(i)|^2$ , and an error occurs if for any  $j, j \neq i, \Lambda_i < \Lambda_j$ . Thus, the error probability can be union bounded as [1]

$$P_e \leq \frac{1}{M} \sum_{i=1}^M \sum_{\substack{j=1 \\ j \neq i}}^M P\{\Lambda_i < \Lambda_j\} \quad (\text{A.69})$$

$$\stackrel{\Delta}{=} \frac{1}{M} \sum_{i=1}^M \sum_{\substack{j=1 \\ j \neq i}}^M P_{H_i \rightarrow H_j} \quad (\text{A.70})$$

The probability of  $P_{H_i \rightarrow H_j}$  can be obtained from Appendix B of [1]. Given that user 1 transmits the  $i$ th message and that  $\bar{\eta}_m(1), m = 1, \dots, M$  in (3.28) is zero-mean, we have

$$E_i \stackrel{\Delta}{=} E[v(i)] = w(i) \quad (\text{A.71})$$

$$= \bar{\mathbf{R}}_i^{-1}(1, :) \bar{\mathbf{S}}_i^H \mathbf{S} \mathbf{A} \mathbf{x} \quad (\text{A.72})$$

$$= \mathbf{U}(i, :) \mathbf{s}_{1,i} A_{1,i} e^{-j\phi_{1,i}} \quad (\text{A.73})$$

$$E_j \stackrel{\Delta}{=} E[v(j)] = w(j) \quad (\text{A.74})$$

$$= \bar{\mathbf{R}}_j^{-1}(1, :) \bar{\mathbf{S}}_j^H \mathbf{S} \mathbf{A} \mathbf{x} \quad (\text{A.75})$$

$$= \mathbf{U}(j, :) \mathbf{s}_{1,i} A_{1,i} e^{-j\phi_{1,i}} \quad (\text{A.76})$$

$$\mu_{ij} \stackrel{\Delta}{=} \frac{1}{2} E[(v(i) - E_i)(v(j) - E_j)^*] \quad (\text{A.77})$$

$$= \frac{1}{2} (E[v(i)v^*(j)] - E_i E_j^*) \quad (\text{A.78})$$

$$= \frac{1}{2} (E_i E_j^* + E[\bar{\eta}_i(1)\bar{\eta}_j^*(1)] - E_i E_j^*) \quad (\text{A.79})$$

$$= \sigma^2 Q(i, j)/2 \quad (\text{A.80})$$

where the  $E[\cdot]$  are expectations conditioned on the phase. Adapting the definitions in [1] for our purposes, we have

$$\alpha_{ij} = 2(|E_i|^2 \mu_{jj} + |E_j|^2 \mu_{ii} - E_i^* E_j \mu_{ij} - E_i E_j^* \mu_{ij}^*) \quad (\text{A.81})$$

$$\beta_{ij} = |E_i|^2 - |E_j|^2 \quad (\text{A.82})$$

$$\omega = \frac{\mu_{ii} - \mu_{jj}}{4(\mu_{ii}\mu_{jj} - |\mu_{ij}|^2)} \quad (\text{A.83})$$

$$c_{ij} = \sqrt{\omega^2 + \frac{1}{4(\mu_{ii}\mu_{jj} - |\mu_{ij}|^2)}} - \omega \quad (\text{A.84})$$

$$d_{ij} = \sqrt{\omega^2 + \frac{1}{4(\mu_{ii}\mu_{jj} - |\mu_{ij}|^2)}} + \omega \quad (\text{A.85})$$

$$a_{ij} = \sqrt{\frac{2c_{ij}^2 d_{ij} (\alpha_{ij} d_{ij} - \beta_{ij})}{(c_{ij} + d_{ij})^2}} \quad (\text{A.86})$$

$$b_{ij} = \sqrt{\frac{2c_{ij} d_{ij}^2 (\alpha_{ij} c_{ij} + \beta_{ij})}{(c_{ij} + d_{ij})^2}} \quad (\text{A.87})$$

In terms of the above variables,

$$P_{H_i \rightarrow H_j} = Q(a_{ij}, b_{ij}) - \frac{d_{ij}}{c_{ij} + d_{ij}} I_0(a_{ij} b_{ij}) e^{-(a_{ij}^2 + b_{ij}^2)/2} \quad (\text{A.88})$$

where  $Q(\cdot, \cdot)$  is the Marcum  $Q$  function.

## References

- [1] J. Proakis. *Digital Communications*. McGraw Hill, 3rd edition, 1995.
- [2] L. J. Cimini. Analysis and simulation of a digital mobile channel using OFDM. *IEEE Transactions on Communications*, 33:665–675, July 1985.
- [3] R. W. Chang. Synthesis of band-limited orthogonal signals for multichannel data transmission. *Bell Systems Technical Journal*, 45:1775–1796, December 1966.
- [4] B. R. Saltzberg. Performance of an efficient parallel data transmission system. *IEEE Transactions on Communications Technology*, 15:805–813, December 1967.
- [5] S. B. Weinstein and P. M. Ebert. Data transmission by frequency division multiplexing using the discrete fourier transform. *IEEE Transactions on Communications Technology*, 19:628–634, October 1971.
- [6] V. K. Garg. *Wireless Network Evolution: 2G to 3G*. Prentice Hall PTR, 1st edition, 2001.
- [7] <http://grouper.ieee.org/groups/802/index.html>.
- [8] R. Sinha and R. D. Yates. Spread spectrum interference issues in the 900 MHz ISM band. Technical report, WINLAB, Rutgers University, 1996.
- [9] M. K. Simon, J. K. Omura, R. A. Scholtz, and B. K. Levitt. *Spread Spectrum Communications Handbook*. McGraw-Hill, revised edition, 1994.
- [10] S. Verdú. Computational complexity of multiuser detection. *Algorithmica*, 4(4):303–312, 1989.
- [11] S. Verdú. *Multiuser Detection*. Cambridge University Press, 1998.
- [12] A. Yener, R. D. Yates, and S. Ulukus. CDMA multiuser detection: A nonlinear programming approach. *IEEE Transactions on Communications*, 50(6), June 2002.
- [13] M. K. Varanasi and A. Russ. Noncoherent decorrelative detection for nonorthogonal multipulse modulation over the multiuser gaussian channel. *IEEE Transactions on Communications*, 46(12):1675–1684, December 1998.

- [14] A. Yener, R. D. Yates, and S. Ulukus. A nonlinear programming approach to CDMA multiuser detection. In *Proceedings of 33rd Asilomar Conference on Signals, Systems and Computers*, October 1999.
- [15] P. H. Tan, L. K. Larsmussen, and T. J. Lim. Constrained maximum-likelihood detection in CDMA. *IEEE Transactions on Communications*, 49(1):142–153, January 2001.
- [16] E. A. Geraniotis and M. B. Pursley. Error probabilities for slow frequency hopped spread-spectrum multiple access communications over fading channels. *IEEE Transactions on Communication*, 30(5):996–1099, May 1982.
- [17] E. A. Geraniotis. Multiple access capability of frequency hopped spread-spectrum revisited: An exact analysis of the effect of unequal power levels. *IEEE Transactions on Communications*, 38(7):1066–1077, July 1990.
- [18] K. Cheun and W. E. Stark. Probability of error in frequency-hop spread-spectrum multiple-access communication systems with noncoherent reception. *IEEE Transactions on Communications*, 39(9):1400–1410, Sept 1991.
- [19] D. J. Goodman, P. S. Henry, and V. K. Prabhu. Frequency-hopped multilevel FSK for mobile radio. *Bell Systems Technical Journal*, 59(7):1257–1275, September 1980.
- [20] G. Einarsson. Address assignment for a time-frequency coded, spread-spectrum system. *Bell Systems Technical Journal*, 59(7):1241–1255, September 1980.
- [21] U. Timor. Improved decoding scheme for frequency-hopped multilevel FSK sytem. *Bell Systems Technical Journal*, 59(10):1839–1855, December 1980.
- [22] O. C. Yue. Performance of frequency-hopping multiple-access multilevel FSK systems with hard-limited and linear combining. *IEEE Transactions on Communications*, 29(11):1687–1694, November 1981.
- [23] U.-C. Fiebig. On the efficiency of fast frequency hopping multiple-access systems. In *International Conference on Communications*, pages 302.2.1–302.2.5, 1992.
- [24] U.-C. Fiebig. On the potential of FFH/MFSK CDMA for mobile radio systems. In *ISSSTA*, pages 332–337, 1998.
- [25] M. K. Varanasi and D. Das. Noncoherent decision-feedback multiuser detection. *IEEE Transactions on Communications*, 48(2):259–269, February 2000.
- [26] A. Kapur, D. Das, and M. K. Varanasi. Noncoherent MMSE multiuser receivers and their blind adaptive implementations. *IEEE Transactions on Communications*, 50(3):503–513, March 2002.

- [27] M. L. McCloud and L. L. Scharf. Asymptotic analysis of the MMSE multiuser detector for non-orthogonal multipulse modulation. *IEEE Transactions on Communications*, 49(1):24–30, Jan 2001.
- [28] E. Visotsky and U. Madhow. Noncoherent multiuser detection for CDMA systems with nonlinear modulation: a non-Bayesian approach. *IEEE Transactions on Information Theory*, 47(4):1352–1367, May 2001.
- [29] R. Sinha, A. Yener, and R. D. Yates. Constrained detection for noncoherent nonlinear multiuser communications. In *Proceedings of 34th Asilomar Conference on Signals, Systems and Computers*, pages 1158–1162, October 2000.
- [30] R. Sinha, A. Yener, and R. D. Yates. Noncoherent multiuser communications: Multistage detection and selective filtering. *EURASIP Journal on Applied Signal Processing*, 2002(12):1415–1426, Dec 2002.
- [31] R. van Nee and R. Prasad. *OFDM for Wireless Multimedia Communications*. Artech House, 2000.
- [32] R. Sinha and R. D. Yates. An OFDM based multicarrier MFSK system. In *Proceedings of the 52nd Vehicular Technology Conference*, pages 257–264, September Fall 2000.
- [33] R. Sinha and R. D. Yates. Performance of multicarrier MFSK in fading channels. In *Proceedings of the 53rd Vehicular Technology Conference*, pages 1848–1851, October Fall 2001.
- [34] O. C. Yue. Maximum likelihood combining for noncoherent and differential coherent frequency-hopping multiple-access systems. *IEEE Transactions on Information Theory*, 28(4):631–639, July 1982.
- [35] G. Strang. *Linear Algebra and its Applications*. Harcourt Brace Jovanovich Inc., 3rd edition, 1988.
- [36] C. M. Keller and M. B. Pursley. Clipped diversity combining for channels with partial-band interference - part i: clipped-linear combining. *IEEE Transactions on Communications*, 35:1320–1328, Dec 1987.
- [37] C. M. Keller and M. B. Pursley. Clipped diversity combining for channels with partial-band interference - part ii: ratio-statistic combining. *IEEE Transactions on Communications*, 37:145–151, Feb 1989.
- [38] C. A. Ellement, A. K. Elhakeem, and J. F. Hayes. Error characteristics of soft limited fast frequency hopping multiaccess systems. In *Proceedings of GLOBE-COM*, pages 41.1.1–41.1.6, 1988.
- [39] T. A. Gulliver, E. B. Felstead, R. E. Ezers, and J. S. Wight. A unified approach to time diversity combining for fast frequency hopped NCMFSK. In *Proceedings of ISSSTA*, pages 303–308, 1994.

- [40] J. Chang and L. Lee. An exact performance analysis of the clipped diversity combining receiver for FH/MFSK systems against a band multitone jammer. *IEEE Transactions on Communications*, 42(2/3/4):700–710, Feb/March/April 1994.
- [41] C. P. Hung and Y. T. Su. Diversity combining considerations for incoherent frequency hopping multiple access systems. *IEEE Journal on Selected Areas in Communications*, 13(2):333–344, Feb 1995.
- [42] G. Li, Q. Wang, V. K. Bhargava, and L. J. Mason. Maximum-likelihood diversity combining in partial-band noise. *IEEE Transactions on Communications*, 46(12):1569–1574, Dec 1998.
- [43] J. F. Weng, G. Q. Xue, T. Le-Ngoc, and S. Tahar. Analysis of multilevel quantized soft-limiting detector for an FH-SSMA system. In *Proceedings of ICC*, pages 1380–1384, 2000.
- [44] J. M. Wozencraft and I. M. Jacobs. *Principles of Communication Engineering*. Waveland Press, reissued edition, 1990, ch. 7.
- [45] R. D. Yates and D. J. Goodman. *Probability and Stochastic Processes*. John Wiley & Sons, 1999.
- [46] H. L. Schneider. Data transmission with FSK permutation modulation. *Bell Systems Technical Journal*, 47(6):1131–1138, July-August 1968.
- [47] G. E. Atkin and H. P. Corrales. An efficient modulation/coding scheme for MFSK systems on bandwidth constrained channels. *IEEE Journal on Selected Areas in Communications*, 7(9):1396–1401, Dec 1989.
- [48] I. Ghareeb and A. Yongacoglu. Diversity achieved by multiple tone FSK over fading channels. In *Proceedings of URSI International Symposium on Signals, Systems, and Electronics*, pages 118–123, Sept 1998.
- [49] S. H. Kim and S. W. Kim. Frequency-hopped multiple-access communications with multicarrier on-off keying in rayleigh fading channels. *IEEE Transactions on Communications*, 48(10):1692–1701, Oct 2000.
- [50] M. K. Varanasi and B. Aazhang. Multistage detection in asynchronous CDMA communications. *IEEE Transactions on Communications*, 38(4):509–519, April 1990.
- [51] W. Ma, T. N. Davidson, K. M. Wong, Z. Q. Luo, and P. C. Ching. Efficient quasi-maximum-likelihood multiuser detection by semi-definite relaxation. In *IEEE International Conference on Communications*, pages 6–10, June 2001.
- [52] P. Spasojevic and A. Yener. Constrained slowest descent detectors for multiuser CDMA systems. In *IEEE International Symposium on Information Theory, ISIT'01*, June 2001.

- [53] R. Horn and C. Johnson. *Matrix Analysis*. Cambridge University Press, 1985.
- [54] U. Madhow and M. L. Honig. MMSE interference suppression for direct-sequence spread-spectrum CDMA. *IEEE Transactions on Communications*, 42(12):3178–3188, December 1994.
- [55] P. Hansen. Methods of nonlinear 0-1 programming. *Annals of Discrete Mathematics 5: Discrete Optimization II*. P.L. Hammer, E.L. Johnson and B.H. Korte, Eds. North Holland, 1979.
- [56] M. K. Varanasi and B. Aazhang. Near-optimum detection in synchronous CDMA systems. *IEEE Transactions on Communications*, 39(5):725–736, May 1991.
- [57] D. Divsalar, M. K. Simon, and D. Raphaeli. Improved parallel interference cancellation for CDMA. *IEEE Transactions on Communications*, 46(2):258–268, February 1998.
- [58] X. Zhang and D. Brady. Asymptotic multiuser efficiencies for decision-directed multiuser detectors. *IEEE Transactions on Information Theory*, 44(2):502–515, March 1998.
- [59] L. B. Nelson and H. V. Poor. Iterative multiuser receivers for CDMA channels: An EM-based approach. *IEEE Transactions on Communications*, 44(12):1700–1710, December 1996.
- [60] L. G. F. Trichard, J. S. Evans, and I. B. Collings. Large system analysis of parallel interference cancellation. In *IEEE International Conference on Communications*, pages 26–30, June 2001.
- [61] M. L. Honig, U. Madhow, and S. Verdu. Blind adaptive multiuser detection. *IEEE Transactions on Information Theory*, 41:994–960, July 1995.
- [62] X. Wang and V. Poor. Blind multiuser detection: A subspace approach. *IEEE Transactions on Information Theory*, 44(2):677–689, March 1998.
- [63] S. S. Haykin. *Adaptive Filter Theory*. Prentice Hall, 3rd edition, 1995.
- [64] P. Patel and J. Holtzman. Analysis of a simple successive interference cancellation scheme in a DS/CDMA system. *IEEE Journal on Selected Areas in Communications*, 12(5):796–807, June 1994.
- [65] S. G. Nash and A. Sofer. *Linear and Nonlinear Programming*. Preprint, 1995.

## Vita

### Rajnish Sinha

#### Education

- 1994** B.S. in Electrical and Computer Engineering, Rutgers University, Piscataway, NJ.
- 1997** M.S. in Electrical and Computer Engineering, Rutgers University, Piscataway, NJ.
- 2003** Ph.D. in Electrical and Computer Engineering, Rutgers University, Piscataway, NJ.

#### Employment

- 1992 - 1994** Undergraduate Student Researcher, WINLAB, Department of Electrical and Computer Engineering, Rutgers University, Piscataway, NJ.
- 1993** Summer Intern, Southwestern Bell Mobile Systems, Texas.
- 1994** Summer Intern, Bell Laboratories, Lucent Technologies, Whippany, NJ.
- 1994 - 1999** Teaching Assistant, Department of Electrical and Computer Engineering, Rutgers University, Piscataway, NJ.
- 1996** Summer Intern, Telcordia, Red Bank, NJ.
- 2001 - present** Member of Technical Staff, CDMA RF Performance Analysis Group, Lucent Technologies, Whippany, NJ.

#### Publications

- 1996** R. Sinha and R. D. Yates, "Spread Spectrum Interference Issues in the 900 MHz ISM Band," *WINLAB Technical Report 132*, Rutgers University, 1996.

- 2000** R. Sinha and R. D. Yates, "An OFDM Based Multicarrier MFSK System," Proceedings of the *52nd Vehicular Technology Conference*, September 2000, pp. 257-264.
- 2000** R. Sinha, A. Yener, and R. D. Yates, "Constrained Detection for Noncoherent Nonlinear Multiuser Communications," Proceedings of the *34th Asilomar Conference on Signals, Systems and Computers*, October 2000, pp. 1158-1162.
- 2001** R. Sinha and R. D. Yates, "Performance of Multicarrier MFSK in Fading Channels," Proceedings of the *53rd Vehicular Technology Conference*, October 2001, pp. 1848-1851.
- 2002** R. Sinha, A. Yener, and R. D. Yates, "Noncoherent Multiuser Communications: Multistage Detection and Selective Filtering," *EURASIP Journal on Applied Signal Processing*, Vol. 2002, No. 12, December 2002, pp. 1415-1426.